

Aus dem Institut BIH Center for Regenerative Therapies
der Medizinischen Fakultät Charité – Universitätsmedizin Berlin

DISSERTATION

**Application of mass spectrometry-based technology to discover spatial peptide
signatures in cancer research**

**Anwendung Massenspektrometrie basierter Technologie zur Entdeckung
räumlicher Peptidsignaturen in der Krebsforschung**

zur Erlangung des akademischen Grades
Doctor rerum medicinalium (Dr. rer. medic.)

vorgelegt der Medizinischen Fakultät
Charité – Universitätsmedizin Berlin

von

ZHIYANG WU
aus Jiangxi, Volksrepublik China

Datum der Promotion: 30.11.2023

Contents

1	Abstract.....	4
2	Introduction	6
2.1	Frontiers in Cancer research	6
2.2	Mass Spectrometry-based Technique for Clinical Proteomics Profiling.....	10
3	Methods.....	13
3.1	Sample Collection	13
3.1.1	Epithelial Ovarian Cancer Patient Cohort.....	13
3.1.2	Neuroblastoma Patient Cohort	14
3.2	Procedure of MALDI-MSI	15
3.3	Protein identification by nano-Liquid Chromatography Electrospray Ionization Tandem Mass Spectrometry	16
3.4	MALDI-MSI data processing for statistical analyses	18
3.4.1	Data Processing of the Project Epithelial Ovarian Cancer (46)	18
3.4.2	Data Processing of the Project Neuroblastoma	18
3.5	Statistical Analysis.....	19
3.5.1	Statistical Analysis of The Project Epithelial Ovarian Cancer (46).....	19
3.5.2	Statistical Analysis -Neuroblastoma	20
3.6	Tissue Immunohistochemistry.....	20
4	Results.....	22
4.1	Results from MALDI-MSI Data of Epithelial Ovarian Cancer	22
4.1.1	Discriminative Peptide Signatures for identification of different patient groups.....	22
4.1.2	Identification of Discriminative Proteins from MALDI-MSI primary data with complementary nano-liquid chromatography electrospray ionization tandem mass spectrometry	23
4.1.3	Relevance between Patients with RD and between Patients without RD.....	25
4.2	Results from MALDI-MSI Data of Neuroblastoma	26
4.2.1	Discriminative Peptide Signatures for identifying Different Tumor Features.....	26
4.2.2	Discriminative Proteins were identified from Neuroblastoma Tissue Sections based on MALDI-MSI Data by using nLC-ESI-MS/MS.....	29
5	Discussion	33
6	Abbreviations.....	38
7	References	39

8	Eidesstattliche Versicherung.....	46
9	Anteilerklärung an den erfolgten Publikationen.....	47
10	Publications and Journal Summary list	48
11	Curriculum Vitae	84
12	Complete list of publications	85
13	Acknowledgments.....	86

1 Abstract

English – Cancer is one of the leading causes of death worldwide, within the molecular and structure complexity of tumors are causal factors for disease progression and treatment standards. With the development of molecular biological techniques, physicians could use genetic variation or protein and metabolic expression profile besides histo-morphological evaluation to classify more accurate risk assessment and to guide treatment decisions. The biomarker-driven personalized therapies might improve clinical care, avoid unnecessary treatments and reduce the duration and costs for hospital stay. Therefore, there is a strong demand for more reliable molecular biomarker profiles. In this dissertation, a novel technique called imaging mass spectrometry (MADLI-MSI) is used to investigate the potential of spatially resolved peptide signatures (directly from tumor tissue; in situ) for (i) discrimination of subtypes of serous ovarian cancer (HGSOC) and (ii) risk assessment of neuroblastoma. Univariate and multivariate static methods were used to determine associated peptide signatures. Using complementary methods, liquid chromatography-based mass spectrometry the corresponding proteins to the peptides were identified and verified by immunohistology. Consequently, peptide signatures were identified to predict disease recurrence in early-stage HGSOC patients and to distinguish high-risk neuroblastoma patients from other risk groups. These results suggest that the MALDI-MSI technique is a promising analytical method that facilitates diagnosis and treatment decision-making. It has also provided new biological insights into tumor heterogeneity, that could benefit the development of molecular biomarker profiles. The data of this dissertation have been really published in Journal “Cancers (MDPI)” 2020 and 2021.

Deutsch – Onkologische Erkrankungen (Krebs) sind weltweit eine der häufigsten Todesursachen. Die molekulare und strukturelle Komplexität von Tumoren sind ursächlich für die Krankheitsprogression und Therapieanspruch. Mit der Entwicklung von neuen molekularbiologischen Verfahren könnten Ärzte neben der histo-morphologischen Bewertung auch genetische Variationen oder Protein- und Metabolit-Expressionsprofile nutzen, um eine genauere Risikobewertung vorzunehmen und die Behandlungsentscheidung zu treffen. Die personalisierten Therapien können die klinische

Versorgung verbessern durch Vermeidung unnötiger Behandlungen und verringerte Dauer und Kosten des Krankenhausaufenthalts. Daher besteht ein starker Bedarf an zuverlässigeren molekularen Biomarker Profilen. In dieser Dissertation wird ein neuartiges Verfahren, die sogenannten bildgebende Massenspektrometrie (MADLI-MSI) eingesetzt um das Potential von räumlich aufgelösten Peptide-Signaturen (direkt aus dem Tumorgewebe; *in situ*) für (i) die Diskriminierung von Subtypen des serösen Ovarialkarzinom (HGSOC) zu untersuchen und (ii) die Risikoabschätzung des Neuroblastomes. Dabei wurden univariate und multivariate statistischer Verfahren eingesetzt, um assoziierten Peptide-Signaturen zu bestimmen. Mittels komplementärer Verfahren, Flüssigkeitschromatographie basierte Massenspektrometrie wurden die korrespondierenden Proteine zu den Peptiden identifiziert und Immunhistologisch verifiziert. Folglich wurden Peptidsignaturen zur Vorhersage des Wiederauftretens der Krankheit bei HGSOC-Patienten im Frühstadium und zur Unterscheidung von Hochrisiko-Neuroblastom Patienten von anderen Risikogruppen identifiziert. Diese Ergebnisse deuten darauf hin, dass die MALDI-MSI-Technik eine vielversprechende Analysemethode ist, die die Diagnose und die Entscheidung über die Behandlung erleichtert. Außerdem hat sie neue biologische Erkenntnisse über die Heterogenität des Tumors geliefert, die der Entwicklung von molekularen Biomarker-Profilen zu Gute kommen könnten. Die Daten dieser Dissertation wurden in der Zeitschrift „Cancers (MDPI)“ 2020 und 2021 veröffentlicht.

2 Introduction

2.1 Frontiers in Cancer research

The diagnosis and therapeutic strategy are always the core cancer care procedure. The treatment decision must base on a series of diagnostic findings, such as patient characters like age, BMI value, living style etc., histopathological observations, and biochemical indicators in urine and blood etc. Following these the patients are often stratified into different risk groups before treatment decision making. The more precise classification, patient could better benefit from appropriate therapeutic strategy. This is also the concept of personalized therapy for cancer patients. This dissertation focuses on risk group stratification of patients with epithelial ovarian cancer (EOC) and neuroblastoma. For both cancer types there are unmet medical need for more reliable prediction of disease progression.

Epithelial ovarian cancer (EOC) is one of the most invasive gynecological cancers in the developed countries (reference statistically as <http://seer.cancer.gov>) and is commonly detected at an advanced stage due to a lack of specific symptoms (1). However, 25% of EOC patients may be diagnosed in the early stage, defined as FIGO stage I-II (International Federation of Gynecology and Obstetrics). The ICON1 (International Collaborative Ovarian Neoplasm 1) and ACTION (Adjuvant Chemotherapy In Ovarian Neoplasm) both trials showed that the efficiency of surgery alone or with platinum-based combinational chemotherapy was significant in the early stage (2, 3). The patients in the early stage have a better outcome after treatment, whose 5-year relative survival is between 80-90%. Nevertheless, a part of early-stage EOC could relapse and causes the death of about 20-30% of patients (4-6). Chan et al. have confirmed that older age, higher stage and grade, and malignant cytology predict independently increased risk of recurrence for early-stage EOC patients (7). In addition, the prognosis is also affected by the histological subtypes with high-grade serous ovarian cancer (HGSOC) that is the most frequently occurring ovarian carcinomas (8). Because of limited data, different standards of risk assessment for treatment decision making and the debate over fertility-sparing surgery for HGSOC patients are still existing. A preoperative screening method and comprehensive surgical staging for proper risk assessment can meet this need (9, 10). In this context, one-third of presumed stage I

ovarian cancers were upstaged due to the findings of dissemination in the peritoneal cavity (11). These high-risk patients in the early stage, who are defined as FIGO stage I with grade 3, FIGO stage IC, FIGO stage II or clear cell histological type, can benefit from adjuvant chemotherapy. After treatment, the relapse rate of EOC patients in FIGO stage IC decrease more than 60% (12). Thus, it is necessary at diagnosis to discriminate patients with high-risk disease from low-risk patients leading to further therapeutic strategy.

EOC is not a homogeneous disease. Based on histopathology, immunohistochemistry (IHC) and molecular genetic analysis, five tumor types are identified (13), their outcome and survival rate vary widely. Consequently, there is a medical need for biomarkers with high predictive value for risk of progression and therapy response at individual level in order to achieve a better benefit/risk/cost ratio. We aimed to prove the putative value of the application of mass spectrometry-based technology to discover spatial peptide signatures in this cancer entity.

Neuroblastoma is pediatric cancer with an overall incidence rate in Germany of 1 to 100,000 children under 15 years old (14). It is the most common malignant solid tumor occurring in infants with a median diagnosed age of 17 months (15). The tumor originates from neural crest cells of sympathoadrenal lineage, within about 65% of primary tumors that arises in the adrenal medulla or lumbar sympathetic ganglia and can spread in the whole sympathetic nervous system (16). Clinical behavior and outcome of this disease are highly diverse: low-risk tumors have a high possibility of spontaneous regression in all cancers, but high-risk tumors progress in treatment-refractory death or treatment-resistant recurrence despite aggressive multimodal therapies (17). Thus, treatment recommendations of neuroblastoma vary from simply mere observation or accompanying surgical resection alone to an elaborately therapeutic strategy such as high-dose chemotherapy, irradiation and immunotherapy (18). A common international staging and risk classification system (INSS/INRG) has been developed to stratify patients into different risk groups for treatment recommendation (19, 20). In Europe, patients have been stratified into three treatment risk groups according to GPOH (Gesellschaft für Pädiatrische Onkologie und Hämatologie)

guidelines described in Table 1 (18). The additional International Neuroblastoma Pathology Classification (INPC) criterion is exclusively used in the USA (21).

Table 1. “Treatment classification of neuroblastoma patients. INSS: International Neuroblastoma Staging System; INRG: International Neuroblastoma Risk Group (INRG) Staging System.” (Adapted from publication Wu. et al. Cancers, 2021) (22)

INSS / INRG Staging	Age at Diagnosis (months)	MYCN Status	Chromosome 1p Status	Treatment Risk Group
1		not amplified	normal	Low
		amplified		High
2			normal	Low
		not amplified	deletion / imbalance	intermediate
		amplified		High
3	< 24	not amplified	normal	Low
	≥ 24	not amplified	normal	intermediate
		not amplified	deletion / imbalance	
		amplified		High
4s / MS	< 18	not amplified	normal	Low
		amplified		High
4 / M	< 18	not amplified		intermediate
	≥ 18	amplified		High

The INSS/INRG stage, MYCN amplification, chromosome 1p abnormality and age play an important role in current disease risk assessment for the ongoing clinical trials in Germany. MYCN amplification as first identified, clinically relevant molecular marker (23) predicts an unfavorable outcome. The patients with young age and low stage have mostly favorable prognosis. However, a recent report from INRG (International Neuroblastoma Risk Group) revealed that the prognostic strength of MYCN amplification is strongly dependent on the context of clinical and biological features (24). Except the loss of heterozygosity at chromosome 1p, 11q and 17q gain the more expression-based prognostic markers in tumor continue to be further improved at the transcriptomic and genomic levels (25, 26). However, tumor progression is mainly influenced by tumor cell interactions and the surrounding microenvironment (27). Knowledge about the impact of high intratumoral heterogeneity and proteomic features in neuroblastoma on disease progression and treatment response remains limited (28). Therefore, there is an unmet need for a reliable classification of

neuroblastoma risk regarding the tumor microenvironment and inter- and intratumor heterogeneity.

Spatial molecular signatures based on protein expression could provide a new and helpful perspective to the current classification of treatment risk for neuroblastoma patients and potentially more reliably predict disease progression.

2.2 Mass Spectrometry-based Technique for Clinical Proteomics Profiling

Understanding the pathogenesis and improving therapeutic outcomes are always the challenges of human medicine. Since the Human Genome Project was completed in 2003, scientists have entered a new era in understanding and treating diseases. Especially the development of next-generation sequencing technology enhances discovering genetic disorders, infectious diseases, and diagnostic markers for cancers. Physicians and researchers have launched worldwide collaborative efforts to investigate large-scale analyses of genes in neurological disorders such as the Alzheimer's Disease Sequencing Project (ADSP), human autoimmune diseases (29) and tumors such as the Cancer Genome Atlas (TCGA) and the International Cancer Genome Consortium (ICGC) (30). This cooperation correlated the genomic abnormalities with disease phenotypes and suggested potential therapeutic targets and novel diagnostic tests. However, genomic disorders often insufficient in accurately predict proteins alterations and dynamics, which is also regulated by e.g., alternative splicing and post-translational modifications (PTMs). In fact, these proteins are effectors involved in cellular processes and signaling and can act as biomarkers or potential drug targets. Thus, access to protein activities and their interactions in the context of cancer can provide new insights into tumorigenesis and reveal potential pathways related to cancer progression (31, 32).

Recently, mass spectrometry (MS)-based proteomics approaches have become the favored tool for clinical proteomics application, it provides high-throughput, comprehensive and quantitative proteins inventories of tissue, serum, plasma, urine and cells etc. (33). Within Matrix-assisted laser desorption/ionization (MALDI) and electrospray ionization (ESI) are known for their soft ionization procedure of biomolecules such as peptides and proteins and mostly utilized for protein analysis. A special application technology is developed from MALDI-MS for direct tissue analysis, which demonstrates ion imaging of peptides and proteins with their spatial arrangement in tissue sections (34). Because a bottom-up proteomics approach is in the latter utilized to identify proteins and their PTMs, the sample is beforehand digested by endopeptidase trypsin. Then the tissue should be mounted on a

conductive glass slide and then fixed onto a MALDI target plate. This sample is mixed with an organic compound that acts as a matrix to facilitate ablation and ionization of analyte of interest, e.g. peptides in the sample. A UV laser in the mass spectrometer triggers ionization and desorption of molecules from the tissue section. To realize imaging a sample, the laser in this process performs a raster over the tissue surface in a pre-defined two-dimensional (2D) grid. The ionized analytes become protonated and give rise to $[M+H]^+$ ions that are subsequently measured according to their mass-to-charge ratio (m/z). In this study, we use a time-of-flight analyzer to measure m/z values of ions and generate a complete mass spectrum at each grid coordinate. Finally, these 2D ion density images/maps present individual m/z values with their corresponding intensities (35).

The other ESI technique is used in a (nano)LC-ESI-MS/MS system consisting of a nano high-performance liquid chromatography (nHPLC) device, electrospray ionization (ESI) chamber and mass spectrometer. Here we use a bottom-up proteomics approach, also known as shotgun proteomics, which is currently the most popular approach to identify proteins and their PTMs through analysis of corresponding proteolytic peptides (36). The sample is initially digested into peptides using proteolytic enzymes, e.g. trypsin. The resulting peptide mixture follows a sample preparation with a pipette tip filled with C18 media and then is separated through nHPLC. Subsequently, the sample solution enters the electrospray chamber maintaining an electric field through a stainless-steel hypodermic needle. At the needle tip, the surface of the emerging liquid is ionized and dispersed into a fine spray of charged droplets. Driven by the electric field, the charged droplets flow into the mass spectrometer via a capillary inlet (37). ESI tends to give multiply charged ions such as $[M + nH]^{n+}$ or $[M - nH]^{n-}$. "The charged peptides are detected and separated in the first mass analyzer and then fragmented and measured in the second mass analyzer. Finally, two types of spectra are collected: MS spectra depict the intensity and m/z for intact peptides; MS/MS spectra shows that one of the ions detected in the MS spectra is isolated, fragmented and measured in a high-throughput manner." (published by Kulyyassov et al., <https://biotechlink.org>, 3-2018) (38) "Using a database search engine, peptides are identified by searching their parent-ion masses and MS/MS spectra against a protein database, where each protein would perform

an in silico tryptic digest and generate a theoretical spectrum. The best match of experimental and theoretical spectra then identifies the protein.” (published by Griffiths and Wang, *Chem Soc Rev* 38(7): 1882-1896, 2009) (39)

A tumor is formed by many distinct cellular populations rather than a homogeneous cluster of identical cells. It presents histological, cellular and molecular heterogeneity and these heterogeneities play an essential role in tumors progression and treatment response (40). MALDI-MSI technology can take advantage to meet the challenge of tumor heterogeneity and obtain meaningful data from tissue sections frozen or formalin-fixed paraffin-embedded (FFPE). The analyzed molecules vary from peptides to lipids, proteins, glycans and even metabolites. The proteomics profiling on tissue section MALDI-MSI as described before, generates a peptide intensity map displaying the spatial relative molecule abundance in a predefined area. The dataset of position-correlated spectra is aligned with an optical image of the same tissue section (31, 41). Superior to antibody-based and fluorescent protein fusions spatial proteomics analysis, the priory knowledge of target protein is necessary. Moreover, the enormous and high-dimensional data derived by MALDI-MSI make automated computational analysis indispensable. Recently, cancer researchers have used MALDI-MSI for tumor histotype classification (42) and have identified some proteomic signatures for diagnostics (43, 44) and prognostic response to treatment (45). Therefore, this technology can interpret molecular tumor composition while preserving spatial morphology and provide critical mechanistic insights into tumor heterogeneity and its impact on tumor biology.

In the pilot studies presented in this dissertation, we aimed to investigate feasibility of MALDI-MSI technology to determine peptide signatures of two different tumor types, high grade serous ovarian carcinoma (HGSOC) and neuroblastoma, for therapy risk group classification. These discriminative peptides were identified by nLC-ESI-MS/MS technology. A peptide signature in each case was identified for predicting disease recurrence of early-stage HGSOC or for discriminating high-risk neuroblastoma from other risk groups. This finding could eventually improve fine-tuned risk assessment of clinical management of these patients.

3 Methods

3.1 Sample Collection

3.1.1 Epithelial Ovarian Cancer Patient Cohort

“All samples were collected at Charité, Department for Gynaecology at surgery after patients gave their informed consent and conserved in the local pathology departments as FFPE tissue blocks. Sample collection was permitted by the local ethics committee of the Charité Medical University Berlin (AVD-No. 2004-000034) and conducted according to the Declaration of Helsinki. All patients were of white Caucasian background and received an accurate staging via laparotomy, including lymph node sampling. An experienced gynaecological pathologist confirmed the diagnosis of the early stage of the high-grade serous subtype of EOC. Adjuvant chemotherapy regime was applied to all patients based on carboplatin in combination with paclitaxel. Detailed descriptions of clinicopathological parameters of patients are shown in Table 2. All samples were removed from FFPE tissue blocks using a 1.0-mm diameter hollow needle as tissue cores and arrayed in a recipient paraffin block forming tissue microarrays (TMAs).” (Published by Kulbe et al, Cancers, 2020) (46)

Table 2. Clinicopathological characteristics of patients. All patients received adjuvant chemotherapy for numbers of cycles as indicated in the table. Follow-ups of patients were performed for at least 5 years, if no relapse occurred, or till development of recurrent disease. (Adapted from publication Kulbe et al., Cancers, 2020) (46)

ID	Recurrent disease	Age	FIGO stage	Grade	Presence of ascites	Number of cycles	Recurrence (months)
1	-	68	IA	G3	<500 mL	6	NA
2	-	60	IC	G2	<500 mL	6	NA
3	-	68	IA	G3	<500 mL	4	NA
4	-	67	IC	G3	No	6	NA
5	+	44	IIB	G3	>500 mL	6	13
6	+	52	IIA	G3	No	9	12
7	+	67	IA	G3	No	6	54
8	+	57	IIA	G3	No	6	16

3.1.2 Neuroblastoma Patient Cohort

“All samples were collected from primary neuroblastoma (localized in the adrenal gland) for diagnostic purposes and preserved as FFPE tissue blocks in the local pathology department. An experienced reference pathologist confirmed the diagnosis of neuroblastoma, and patient risk classification by the National Neuroblastoma Study Group was based on the definitions of the German BFM-NB2004 study and the recommendations of the German Society of Pediatric Oncology and Hematology (GPOH). The comprehensive patient data set included gender, age, INSS stage of the tumor at diagnosis, presence of MYCN amplification in the diagnosed tumor sample (detected by FISH), INRG risk classification and outcome, especially diagnosed disease recurrence and death (Table 3). Patients in this cohort were followed up for at least four years or until the death of the disease. Pathologists identified tissue areas with >80% tumor cell content for collecting tissue cores to generate tissue microarrays analyzed by MALDI-MSI with section annotation.” (Published by Wu et al., *Cancers*, 2021) (22) Neuroblastoma samples from patients with low- and intermediate-risk groups were defined as other risk group (nHR group). High-risk groups were retained as high-risk group (HR group). Sample numbers 1-5 (high risk) and 10-13 (other risk groups, Table 3) were used for whole tissue section analysis (MALDI-MSI and immunohistochemistry). “Cores from samples numbers 4, 10, 12, and 13 were also used for tissue microarrays, together with tissue cores from six tumor samples from unrelated patients. Tumor cores were removed from the FFPE tissue blocks with a 1.0 mm diameter hollow needle and arranged a recipient paraffin block (Table 3)” (Published by Wu et al., *Cancers*, 2021) (22).

Table 3. Clinicopathological characteristics of patient cohort. (Adapted from publication Wu et al., *Cancers*, 2021) (22)

ID	Sex	Age [years]	INSS Stage	MYCN amplification	Risk classification (at diagnosis)	Disease recurrence	Death	Metastasis
1	F	0.3	3	+	high	-	-	No
2	M	0.6	2	+	high	-	-	No
3	M	1	3	+	high	-	+	No†
4	M	1.4	4	+	high	-	-	Yes

5	F	1.2	4	+	high	+	+	Yes
6	M	2.8	4	+	high	+	+	Yes
7	M	7.8	4	-	high	-	-	Yes
8	F	8	4	+	high	-	-	Yes
9 [†]	M	1.2	3	-	high	+	-	No [‡]
10	F	2.4	1	-	low	-	-	No
11	F	0.8	4	-	intermediate	-	-	Yes
12	M	0.1	4s	-	low	-	-	Yes
13	F	0.1	3	mosaic	low	-	-	No
14	F	5.9	3	-	intermediate	-	-	No
15	M	1.9	2	-	low	-	-	No

[†] Disease in this patient later metastasized and was upgraded to INSS stage 4.

[‡] This patient had multiple relapses after first-line therapy and was treated for high-risk disease in relapse therapy.

3.2 Procedure of MALDI-MSI

“All FFPE tissue sections (whole sections and tissue chips) were cut to a thickness of 6 μm using a slicer (HM325, Thermo Fisher Scientific, USA.) and mounted on conductive glass slides coated with indium tin oxide (Bruker Daltonik GmbH, Germany).” (Published by Wu et al., *Cancers*, 2021) (22) The sections were preheated to 80 °C for 15 min before deparaffinization and rehydration following Protocol 1. Thermally induced antigen re-extraction was performed in MilliQ water in a steamer for 20 min. Slides were dried for 10 min and then subjected to trypsin digestion. “16 layers of trypsin solution (Table 5) were applied onto the sections using an automated spraying device HTX TM-Sprayer (HTX Technologies LLC, ERC GmbH, Germany) at 30 °C. Tissue sections were incubated for 2 h at 50°C in a humidity chamber saturated with potassium sulfate solution, and then coated with 4 layers of matrix solution (Table 6) using a HTX TM sprayer at 75°C. MALDI imaging was performed on rapifleX® MALDI TissueTyper® (Bruker Daltonik GmbH, Germany) in reflector mode with a detection range of 800-3200 m/z, 500 lasers per spot, 1.25 GS/s sampling rate, and a grating width of 50 μm . FlexImaging 3.0 (EOC) / FlexImaging 5.1 (Neuroblastoma) and Flex-Control 3.0 software (Bruker Daltonik GmbH) coordinated MALDI imaging runs. External calibration was performed using peptide calibration standards. After MALDI imaging, the matrix was removed from the tissue sections with 70% ethanol and the sections were histologically stained with hematoxylin and eosin.” (Published by Wu et al.,

Cancers, 2021) (22) Tumor areas with >80% tumor cells were digitally annotated in SCiLS Cloud by a pathologist and transferred to SCiLS Lab software (EOC: Version 2015b Pro; Neuroblastoma: Version 2019c Pro, Bruker Daltonik GmbH).

Protocol 1: Rehydrate Sections

1. Immerse the slides in xylene 2 times for 5 minutes each.
2. Immerse the slides in isopropanol for 5 minutes.
3. Immerse the slides in 100% ethanol for 5 minutes.
4. Immerse the slides in 96% ethanol for 5 minutes.
5. Immerse the slides in 70% ethanol for 5 minutes.
6. Immerse the slides in 50% ethanol for 5 minutes.
7. Rinse the slides with Milli-Q pure water

Table 4. Digestion buffer

Reagent	CONC	Amount (µL)	Final CONC	Manufacturer
NH ₄ HCO ₃	100 mM	200	20mM	Sigma-Aldrich Co.
C ₃ H ₈ O ₃	1%	10	0.01%	Sigma-Aldrich Co.
Milli-Q water		790		Merck KGaA

Table 5. Trypsin solution

Reagent	Amount	Manufacturer
sequencing grade modified porcine trypsin	20 µg	Promega Co.
digestion buffer	800 µL	

Table 6. Matrix solution

Reagent	CONC	Amount	Final CONC	Manufacturer
HCCA		14 mg	7 mg/mL	Bruker Daltonik GmbH
C ₂ H ₅ N	100%	1.4 mL	70%	Sigma-Aldrich Co.
C ₂ H ₅ F ₃ O ₂	100%	20 µL	1%	ThermoFisher Scientific Inc.
Milli-Q water		580µL		Merck KGaA

3.3 Protein identification by nano-Liquid Chromatography Electrospray Ionization Tandem Mass Spectrometry

“Protein identification of m/z values was performed on sections of adjacent tissue (tumor cell-rich areas) using a bottom-up nano-liquid chromatography electrospray tandem mass

spectrometry method as previously described (47). Similar to MALDI-MSI preparation, sections were pre-heated to 80°C for 15 min before deparaffinisation. Paraffin removal, antigen retrieval and tryptic digest were carried out as for MAL-DI-MSI. After incubation for 2 hours at 50°C in a humidity chamber saturated with potassium sulphate solution, peptides were extracted from tumor cell-rich areas of each tissue section separately into 40 µL of 0.1% trifluoroacetic acid and incubated for 15 minutes at room temperature. The digests were filtered with ZipTip® C18 according to the manufacturer's instructions, the eluate was concentrated under vacuum (Eppendorf® Concentrator 5301, Eppendorf AG, Germany) and reconstituted in 20 µL of 0.1% trifluoroacetic acid, respectively, from which 2 µL were extracted into NanoHPLC (Dionex UltiMate 3000, Thermo Fisher Scientific) coupled to an ESI-QTOF ultra-high resolution mass spectrometer (Impact II™, Bruker Daltonic GmbH). The peptide mixture was loaded onto an Acclaim PepMap™ RSLC C18 column (100 µm × 2 cm, PN 164564, Thermo Fisher Scientific), calibrated with 10 mM sodium hypofluorite (flow rate 20 µL/h), and then separated on an Acclaim PepMap™ RSLC C18 column (75 µm × 50 cm, PN 164942, Thermo Fisher Scientific) with an increasing acetonitrile gradient of 2-35% in 0.1% formic acid (400 nL/min flow rate, 10-800 bar pressure range) for 90 min while the column was maintained at 60 °C. The released charged peptides were detected by a tandem mass spectrometer using a full mass scan (150-2200 m/z) with a resolution of 50,000 FWHM. The autoMS/MS InsantExpertise was used to select peaks for fragmentation by collision-induced dissociation. Raw MS/MS spectra obtained were converted to Mascot generic files (.mgf) for amino acid sequences using ProteoWizard software (48) and used to search the human Swiss-Prot database using the Mascot search engine (version 2.4, MatrixScience Inc. Boston, USA). The search parameters were set as following (I) A significance threshold of $p < 0.05$; (II) proteolytic enzyme is trypsin; (III) a maximum of 1 missed cleavage; (IV) 10 ppm peptide tolerance; (V) peptide charges of 2+, 3+ or 4+; (VI) oxidation allowed as variable modification; (VII) 0.8 Da MS/MS tolerance; (VIII) a MOWSE score >13 . MOWSE (for MOlecular Weight SEarch) is a method for identifying proteins from the molecular weight of peptides created by proteolytic digestion and measured with mass spectrometry (49). The probability-based MOWSE score formed the basis for the development of Mascot, a proprietary software for identifying proteins from mass spectrometry data. the results of

Mascot were exported as .csv files (Table S2: LC-MS reference list of ovarian cancer tissue (46) and Table S4: Protein identification by LC-MS of neuroblastoma whole tissue section (22)). To match the m/z values of MALDI-MSI to the peptides identified by LC-MS/MS, an EXCEL macro was developed in-house (File S1 (22)). This macro was applied taking into account the parameters previously described (50). Briefly, comparison of m/z values between MALDI-MSI and LC-MS/MS required the identification of >1 peptide (mass differences < 0.3 Da). Only peptides with the smallest mass difference in the mass window and a correlation ratio ≥ 0.30 were counted as matches. Peptides with the highest MOWSE score and the smallest mass difference between MALDI-MSI and LC-MS data were accepted as correctly identified.” (Published by Wu et al., Cancers, 2021) (22)

3.4 MALDI-MSI data processing for statistical analyses

3.4.1 Data Processing of the Project Epithelial Ovarian Cancer (46)

“The raw MALDI-MSI data were imported into the SCiLS Lab software version 2015b Pro (Bruker Daltonik GmbH) following settings preserving the total ion count (TIC) and convolution baseline removal with width of 20. All datasets were simultaneously pre-processed to ensure better comparability between sample sets. An attribute table was built for sample number, patient age, tumor FIGO stage, tumor cell-rich regions and whether the patient experienced disease recurrence. Attribute were used to divide a dataset into independent datasets from different spatial spectral regions in tissue sections, or samples with different tumor or patient characteristics for analysis. A standard segmentation pipeline was performed for peak finding and alignment in maximal interval processing mode with TIC normalization, medium noise reduction and no smoothing (Sigma: 0.75).” (51, 52) (Published by Kulbe et al, Cancers, 2020) (46)

3.4.2 Data Processing of the Project Neuroblastoma

“The raw MALDI-MSI data were imported into SCiLS Lab software version 2019c Pro (Bruker Daltonik GmbH) using settings to retain total ion counts (TIC) and not remove baselines and converted into SCiLS base data .sbd files and .slx files. An Attribute table was built for sample number, tumor cell-rich area, tumor INSS stage, *MYCN* amplification status in diagnostic

tumor sample, or risk group definition, and patient age, sex and whether the patient experienced disease recurrence. Attributes were used to divide a dataset into separate datasets from different spatial spectral regions in tissue sections, or samples with different tumor or patient characteristics, for analysis. A standard segmentation pipeline using TIC normalization, moderate noise reduction and no smoothing (Sigma: 0.75) in maximum interval processing mode was performed for Peak finding and alignment with an interval width of 0.3 Da (51, 52).” (Published by Wu et al., Cancers, 2021) (22)

3.5 Statistical Analysis

3.5.1 Statistical Analysis of The Project Epithelial Ovarian Cancer (46)

“Peaks were selected using the Orthogonal Matching Pursuit (OMP) algorithm (53). Top-down segmentation was performed using K-means clustering, interval width of ± 0.156 Da, mean interval processing and medium smoothing strength (51, 52). Two methods based on different principles were used: an unsupervised method, probabilistic latent semantic analysis (pLSA) to discriminate the two groups, and another supervised method, receiver operating characteristic (ROC) analysis, was used to detect characteristic peptide values.” (Published by Kulbe et al, Cancers, 2020) (46) The approach pLSA was applied to the whole MALDI-MSI dataset for definition of discriminative molecular features. The parameters were set such as interval width of 0.156 Da, single spectra and deterministic initialization (54). The approach ROC was used to assess all peaks (m/z values) within tumor cell-rich regions to discriminate recurrent and non-recurrent disease groups. 1500 spectra were randomly selected from each group, because the number of spectra from the participating group should be approximately same. “For those peaks with an AUC (the area under the ROC curve) >0.65 or <0.35 , a univariate hypothesis test (Wilcoxon rank sum test) was used to test the statistical significance of m/z values. Here we considered the peaks with AUC >0.7 or <0.3 ($p < 0.001$) as potential markers for predicting disease recurrence. All figures were created using SCiLS Lab software (Bruker Daltonik, Germany) and the R packages "ggplot2" and "ggbiplot".” (Published by Kulbe et al, Cancers, 2020) (46)

3.5.2 Statistical Analysis -Neuroblastoma

“Top-down segmentation using k-means cluster analysis was performed on the selected MALDI-MSI datasets from tissue sections and additionally only from regions with >80% tumor cells, as previously described (53), to define peptide signatures. Both analyses used settings for interval width of 0.3 Da, including all individual spectra, medium noise reduction and correlation distance. Discriminating m/z values from tumor cell-rich regions were identified using supervised ROC analysis on the selected datasets from tissue regions with >80% tumor cells. The AUC values vary between 0 and 1, where values close to 0 and 1 indicates peptides to be discriminatory and 0.5 indicates no discriminatory value. 35 000 m/z values were randomly selected per group. For those peptides with an AUC >0.7 or <0.3, an univariate hypothesis test (Wilcoxon rank sum test) was used to test the statistical significance of the m/z values. Peptides with p-values < 0.001 and a peak correlation ratio ≥ 0.30 were selected as candidate markers. Supervised principal component analysis (PCA) was performed to define characteristic peptide signatures differentiating tumor regions with >80% tumor cell content from high-risk or other risk groups. The data were scaled to PCA in a level scaling model. Only m/z values with AUC >0.8 or <0.2 and $p < 0.001$ were used as peak intervals for PCA using settings: five components, interval width of ± 0.3 Da maximum interval treatment mode, normalization to total ion number, and no noise reduction. ROC analysis was also used in validation experiments to identify discriminative m/z values (defined in data sets of whole-section) using MALDI-MSI data (2500 m/z values randomly selected per group) from arrayed tumor cores. The Wilcoxon rank sum test was used to test the statistical significance of the m/z values. Peptides with significant differences (p -value < 0.001) in the Wilcoxon test with a peak correlation ratio ≥ 0.30 were selected as candidate markers (significant correlations $p < 0.05$; Pearson's correlation analysis (55). All figures were created using the SCiLS Lab software (Bruker Daltonik GmbH).” (Published by Wu et al., Cancers, 2021) (22)

3.6 Tissue Immunohistochemistry

“FFPE tissue sections of neuroblastoma (whole sections) were dewaxed and subjected to a heat-induced epitope retrieval step. Endogenous peroxidase was blocked by hydrogen

peroxide prior to incubation with a monoclonal antibody against human CRMP1 (EP14521, Abcam, UK), followed by incubation with EnVision+ HRP-labeled polymer (Agilent Technologies Inc., USA) and visualization using the OPAL system (Akoya Biosciences Inc., USA) according to manufacturer's instructions. After protein inactivation, sections were incubated with a polyclonal antibody against human AHNAK (PA5-53890, Invitrogen, Thermo Fisher Scientific), followed by incubation with the EnVision+ polymer (Agilent Technologies Inc., USA) and visualization using the OPAL system. Nuclei were stained with 4',6-diamidino-2'-phenylindole dihydrochloride (DAPI; Merck KGaA, Germany) and slides were mounted in Fluoromount G (Southern Biotech, USA). Multispectral images were acquired using a Vectra® 3 imaging system (Akoya Biosciences Inc.)." (Published by Wu et al., *Cancers*, 2021) (22)

4 Results

4.1 Results from MALDI-MSI Data of Epithelial Ovarian Cancer

4.1.1 Discriminative Peptide Signatures for identification of different patient groups

In this retrospective study, the primary tumor tissue cores of early-stage HGSOC patients were arrayed in a recipient FFPE block and categorized as a recurrent disease (RD) (n=4) or non-recurrent disease (non-RD) (n=6) groups. MALDI-MSI data yielded 506 aligned m/z values in a mass range between m/z 600 and 3000 (Table S1, (46)). The unsupervised data analysis approach probabilistic latent semantic analysis (pLSA) was applied in the whole dataset to discriminate different patient groups. However, a subclass from the non-RD group was detected, which presented an individual pLSA component (Figure 1-A). The tissue samples of the subclass group were verified by an experienced gynecological pathologist that both did not match the criteria of HGSOC: one showed a mutated pattern of p53 and high expression of CD56 and synaptophysin via previous immunohistological staining, unlike typical HGSOC characters. Additionally, its morphological features indicated most likely an undifferentiated non-small cell neuroendocrine carcinoma (NSCNEC) of the ovary. Another was re-classified as pT2cG3 instead of HGSOC at early-stage. Therefore, these two exceptional cases were excluded for further analysis.

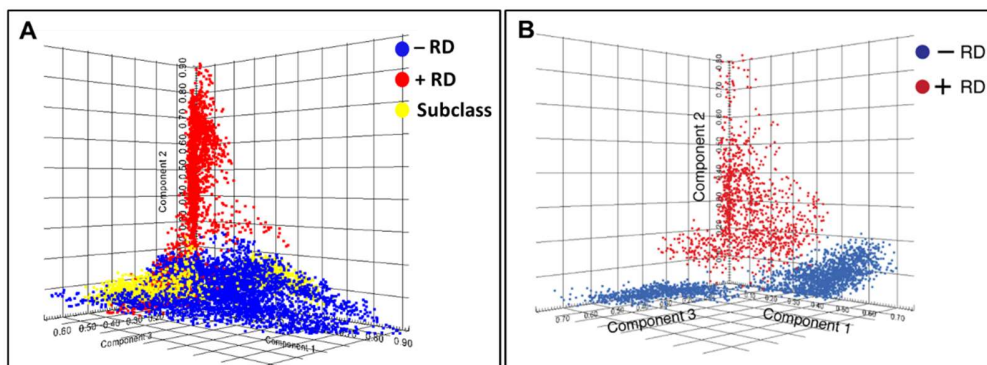


Figure 1: Discrimination of molecular signatures for the groups of HGSOC patients via probabilistic latent semantic analysis (pLSA). **(A)** Score plots of the first three components from MALDI-MSI spectra of primary tumors from patients without (- RD, in blue, n=4), recurrent disease (+ RD, in red, n=4) and a subclass (in yellow, n=2) are shown. **(B)** Score plots of the first three components from IMS spectra of primary tumors from patients without (- RD, in blue, n=4), and recurrent disease (+ RD, in red, n=4) are shown. (Adapted from publication Kulbe et al., *Cancers*, 2020) (46)

Furthermore, the tumor cell-rich region and microenvironment region of each tumor core tissue were separately evaluated using the software SCiLS Lab. Following an expertise annotation, MALDI-MSI of tumor cell-rich regions data yielded 612 m/z values in a mass range between m/z 800 and 3.500. To explore most discriminative peptide signatures to discriminate between RD and non-RD HGSOc patients, probabilistic latent semantic analysis (pLSA) was applied to the MALDI-MSI data of tumor cell-rich regions. The first three components show a clear difference between RD and non-RD groups in a score plots image. (Figure 1-B) This finding demonstrates that this unsupervised statistical approach is able to use MALDI-MSI data from tumor cell-rich regions to determine potentially peptide signatures for discriminating both distinct patient groups.

4.1.2 Identification of Discriminative Proteins from MALDI-MSI primary data with complementary nano-liquid chromatography electrospray ionization tandem mass spectrometry

A supervised statistical analysis, receiver operating characteristic (ROC) was applied to the 612 aligned m/z values from tumor cell-rich regions from RD and non-RD patient groups. This approach follows a paired comparison strategy to find the most discriminative peptide values (m/z values) between two participant groups. The ROC analysis resulted in 151 peptide values that were able to discriminate between patients with RD and non-RD (AUC > 0.6 or < 0.4; $p < 0.01$; Table S1(46)). "From these, we depict three peptides with the strongest discriminatory values in Figure 2 (46). Two peptides (m/z values 840.6 Da, 1138.5 Da) demonstrate significantly higher intensity distributions and one peptide with m/z value 1631.8 Da demonstrates significantly lower intensity distribution in tumor cores from RD patient group. To identify the proteins corresponding to the discriminative peptide values, we performed a bottom-up nano-liquid chromatography electrospray ionization tandem mass spectrometry (nLC-ESI-MS/MS) approach in an adjacent tissue section. The analysis assigned 49 of the 506 m/z values (Table S1 (46)), within 18 discriminative m/z values could be assigned to 13 proteins (AUC > 0.6 or AUC < 0.4, $p < 0.001$) (Table 7 (46))." (Published by Kulbe et al, Cancers, 2020) (46) Two peptides at least from proteins, KRT9, COL1A2 and ACTB were significantly higher expressed in RD patient group, but other proteins, CALD1,

APOA1, TUBB, HIST1H2BK, HIST1H4A and LMA (only single peptide) were higher expressed in non-RD patient group.

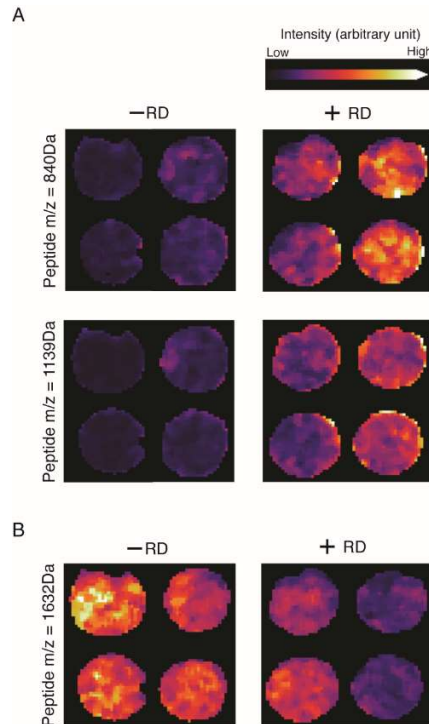


Figure 2: Exemplary representative cases for characteristic peptides for group of patients with disease recurrence and no recurrence discriminated via individual peak mass spectra intensity and spatial peak distribution. **(A)** The peptides 840.6 Da and 1138.5 Da show significantly higher spatial intensities (area under the curve (AUC) > 0.6; $p < 0.001$) in patients with recurrent disease (+RD) than patients without recurrence (-RD). **(B)** The peptide 1631.8 Da, as an example, exhibited significantly higher intensities (AUC < 0.4; $p < 0.001$) in no recurrence group. (Adapted from publication Kulbe et al., *Cancers*, 2020) (46)

Table 7: Receiver operating characteristic (ROC) curve analysis reveals a prognostic protein signature for early-stage HGSOC. Significantly differentially expressed proteins in primary tumors of patients with recurrent compared with no-recurrent disease are listed (overexpressed, AUC values > 0.6, and underrepresented < 0.4, $p < 0.0001$). (Adapted from publication Kulbe et al., *Cancers*, 2020) (46)

Centroid [m/z]	IMS Mr [m/z] [Da]	Tumor+R D VS -RD (AUC)	LC-MS Mr [Da]	Δ [Da]	Ascension	Protein	HGNC Symbol
2705.026	2704.0181	0.7547	2704.1538	0.1358	K1C9_HUMAN	Keratin, type I cytoskeletal 9	KRT9
1791.698	1790.6901	0.6250	1790.7204	0.0304	K1C9_HUMAN	Keratin, type I cytoskeletal 9	KRT9
644.336	643.3281	0.7470	643.3653	0.0373	ACTB_HUMAN	Actin, cytoplasmic 1	ACTB
840.564	839.5561	0.7407	839.4613	0.0947	CO1A2_HUMAN	Collagen alpha-2(I) chain	COL1A2
868.467	867.4591	0.7331	867.4563	0.0028	CO1A2_HUMAN	Collagen alpha-2(I) chain	COL1A2
2027.831	2026.8231	0.7008	2026.0093	0.8138	CO1A2_HUMAN	Collagen alpha-2(I) chain	COL1A2
1562.765	1561.7571	0.6930	1561.7849	0.0278	CO1A2_HUMAN	Collagen alpha-2(I) chain	COL1A2
1223.417	1222.4091	0.6262	1222.6054	0.1964	CO1A2_HUMAN	Collagen alpha-2(I) chain	COL1A2
700.444	699.4361	0.6388	699.4643	0.0282	RL37A_HUMAN	60S ribosomal protein L37a	RPL37A

1790.797	1789.7891	0.6253	1789.8846	0.0956	ACTB_HUMAN	Actin, cytoplasmic 1	ACTB
1743.691	1742.6831	0.6055	1742.8120	0.1290	H2B1N_HUMAN	Histone H2B type 1-N	HIST1H2BN
1550.764	1549.7561	0.6016	1549.8100	0.0540	ANXA1_HUMAN	Annexin A1	ANXA1
858.566	857.5581	0.3975	857.4607	0.0974	CALD1_HUMAN	Caldesmon	CALD1
1157.708	1156.7001	0.3782	1156.6200	0.0800	APOA1_HUMAN	Apolipoprotein A-I	APOA1
1631.775	1630.7671	0.3682	1630.8236	0.0566	TBB5_HUMAN	Tubulin beta chain	TUBB
1751.792	1750.7841	0.3554	1750.0353	0.7488	H2B1K_HUMAN	Histone H2B type 1-K	HIST1H2BK
1055.394	1054.3861	0.3460	1054.5196	0.1335	H4_HUMAN	Histone H4	HIST1H4A
1752.992	1751.9841	0.3159	1751.8551	0.1290	LMNA_HUMAN	Prelamin-A/C	LMNA

4.1.3 Relevance between Patients with RD and between Patients without RD

“The analysis was extended to apply the peptide signature (discriminant m/z values) to three additional patients with early-stage high-grade endometriosis ovarian cancer (HGEC), two of whom were RD; one was non-RD and showed similar peptide intensities in the sample of HGSOC patients. A principal component analysis (PCA) was performed to superimpose the effects of covariates onto the principal component space (Figure 3 (46)). PCA confirmed a closer relevance between RD patients and non-RD patients. The inclusion of three patients with early HGSC showed a similar relevance. Variable markers were clustered in two groups, indicating the variables of interest. The higher associated group peptides, 1223.4, 1790.8, 1550.8 and 2705.0 Da, concentrate in the RD patient group, but another peptide, 1631.8 Da is partial to the non-RD patient group.” (Published by Kulbe et al, Cancers, 2020) (46)

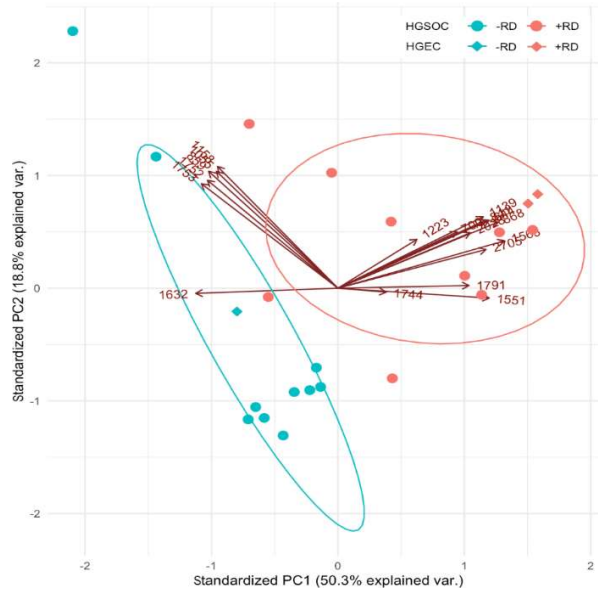


Figure 3: A biplot showing included eight samples of early-stage HGSOC patients as points. Additionally, three patients with high-grade endometrioid ovarian cancer (HGEC) were included in the analysis and marked with diamonds. Biplot axes indicate the influence of each peptide in the principal component space. The principal component analysis (PCA) shows a discrimination of patients with (+RD) and without recurrent disease (-RD). (Adapted from publication Kulbe et al., *Cancers*, 2020) (46)

4.2 Results from MALDI-MSI Data of Neuroblastoma

4.2.1 Discriminative Peptide Signatures for identifying Different Tumor Features

“Here, we assessed the technical feasibility of MALDI-MSI to identify potentially discriminatory protein signatures from formalin-fixed, paraffin-embedded (FFPE) tissue sections of more aggressive neuroblastomas (high risk). Tissue samples were diagnostic biopsies from primary neuroblastoma classified as high risk (n = 5) or other risk groups (low or moderate risk, n = 4). Peptide signatures extracted from the analyzed tissue samples yielded 501 aligned m/z values in the mass range m/z 800-3200. Neuroblastoma cell-rich tumor regions yielded 397 aligned m/z values (Table S1 (22)). The MALDI-MSI data from tissue sections were characterized using bisecting k-means clustering, an unsupervised multivariate segmentation analysis, to determine the peptide signature of different tissue regions. The segmentation analysis created two clusters, shown as segmentation maps (Figure 4), that corresponded well to tissue regions in the tumor that were either tumor cells rich (>80%) or poor (defined by a reference pathologist). Thus, peptide signatures obtained

from MALDI-MSI data can directly distinguish tumor regions with high tumor cell content from those with <80% tumor cell content from FFPE tissue sections. To determine whether signatures could be defined to distinguish high risk groups from other risk groups, we performed the same segmentation analysis across only those regions with >80% tumor cell content as defined by a pathologist. Unsupervised segmentation analysis of m/z values for these regions resulted in three segmentation groups with different peptide signatures in high-risk tumors, (contribution percentage of each peptide signature to the tumor cell-rich regions in Table S2 (22)), but only one segmentation group was classified as low risk in neuroblastoma (Figure 4). These data illustrate for the first time at the protein level the molecular intratumoral heterogeneity of high-risk tumors. Unsupervised clustering allows the extraction of peptide signatures from MALDI-MSI data, which can correctly identify tumor cell-rich regions in neuroblastoma and distinguish high-risk neuroblastomas from other risk groups.” (Published by Wu et al., *Cancers*, 2021) (22)

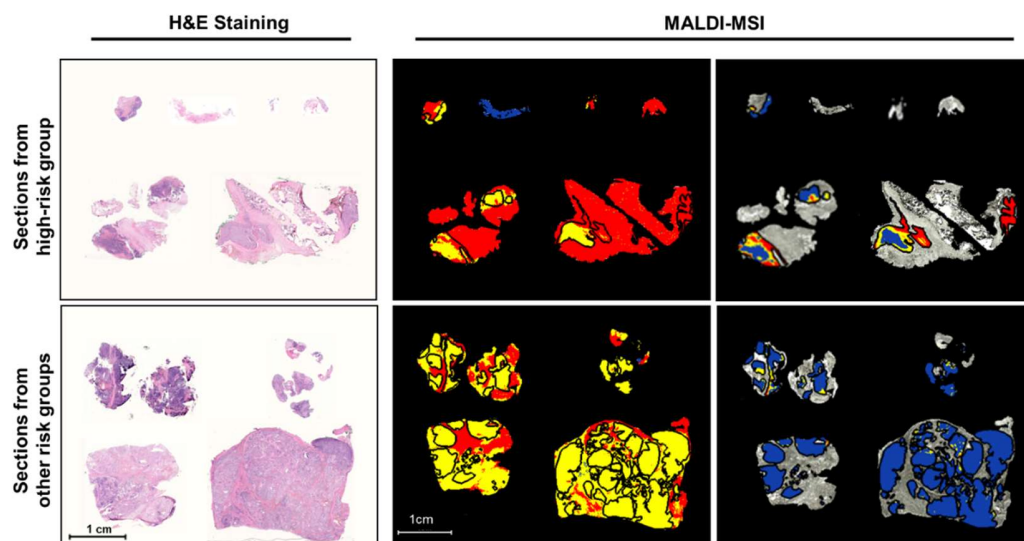


Figure 4: Exemplary cases for MALDI imaging identifying high-risk neuroblastomas by heterogeneous peptide signatures in tumor cell-rich regions. Sections from primary neuroblastomas with high or other risk classifications are shown with hematoxylin and eosin (H&E) staining for tissue section orientation in segmentation maps of MALDI-MSI analysis. Segments (indicated by different colors) represent different proteomic clusters generated by bisecting k-means clustering. Black lines surround tumor areas with >80% tumor cell content (annotated by the reference pathologist). Signatures derived from segmentation clustering across the whole tissue section are shown in the middle column and peptide signatures derived only across the tumor cell-rich areas in the sections shown on the right. Colors represent the same proteomic clusters in the 2 images in the middle column and the 2 images in the right column, but not between the middle and right

images. (22) Nine representative cases of nine total cases are shown. (Adapted from publication Wu et al., Cancers, 2021) (22)

“Univariate analysis of MALDI-MSI data has the potential to determine which single peptides are most discriminatory for neuroblastoma tissues from different risk groups. We performed ROC analysis on a total of 397 aligned m/z peaks in tumor cell-rich regions from the HR and non-HR neuroblastoma groups. The different spatial peptide intensity distributions in tissue samples from the two risk groups determined the discriminatory power of individual peptides. The Wilcoxon rank sum test was applied to the 397 aligned m/z peaks, yielding 206 statistically significant m/z values (AUC values >0.8 or <0.2 ; $p<0.001$). From these results, we show in Figure 5 the five peptides with the most potent discriminatory value. In the tumor cell-enriched region of high-risk neuroblastoma tissue sections, three peptides (m/z values: 1707.68, 1775.79 and 1832.79 Da) had a significantly higher intensity distribution, and two peptides (m/z values: 766.48 and 1178.73 Da) had a significantly lower intensity distribution. To explore the potential of the most discriminatory peptides in the peptide signatures to distinguish HR groups from other risk groups, PCA was performed on 206 statistically significant m/z values (AUC values >0.8 or <0.2 ; $p<0.001$). Principle component 1 (PC-1) primarily captured differences within tumor cell-rich regions across risk groups and showed an increased intensity distribution of tumor cell-rich regions in HR neuroblastoma (Figure 5). As the first principal component explained 62% of the variance (Figure S2), these findings suggest that both unsupervised and supervised statistical methods using MAL-DI-MSI data from neuroblastoma tissue sections can provide a discriminatory peptide signature for the identification of HR or other risks neuroblastomas.” (Published by Wu et al., Cancers, 2021) (22)

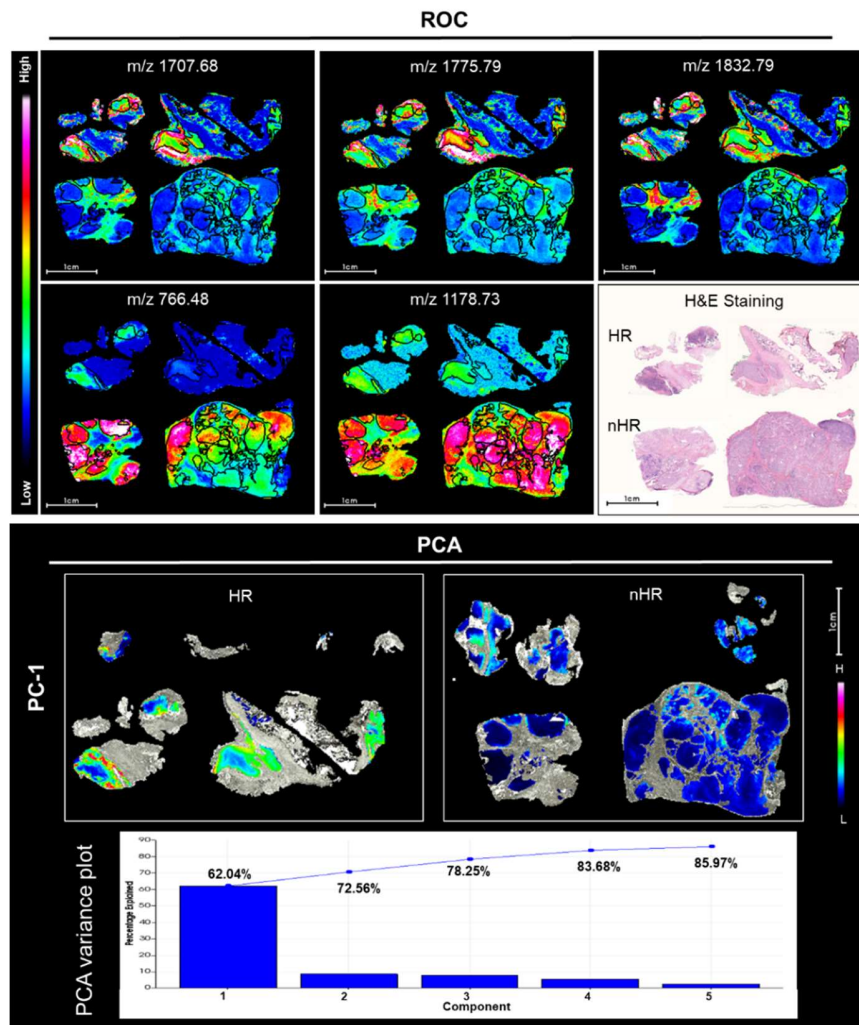


Figure 5: Discriminative peptide signatures in tumor cell-rich regions for discrimination between high-risk (HR) and other risks (nHR) groups (n=9). Based on MALDI-MSI data, ROC analysis resulted in significantly discriminative m/z values, whose differential ion intensity distributions were depicted in tumor cell-rich regions of HR and nHR neuroblastoma tissue sections. Relative peptide expression was scaled in the colour bar. The m/z values with the highest area under the curve (AUC) values ($AUC > 0.85$, $p < 0.001$) were shown in the top row and the m/z values with the lowest AUC values ($AUC < 0.3$, $p < 0.001$) were shown in the bottom row. Black lines surround tumor areas with $>80\%$ tumor cell content (annotated by the reference pathologist). Haematoxylin and eosin (H&E) staining in sections is shown for orientation. Based on MALDI-MSI data PCA analysis was applied to statistically significant m/z values obtained from ROC analysis to explore potential peptide signatures for discriminating HR and nHR neuroblastoma cell-rich regions. The ion intensity of the first principal component (PC-1) is scaled in HR and nHR neuroblastoma tissue sections. PCA variance plot indicates that 62% of variance is explained by PC-1. (Adapted from publication Wu et al., *Cancers*, 2021) (22)

4.2.2 Discriminative Proteins were identified from Neuroblastoma Tissue Sections based on MALDI-MSI Data by using nLC-ESI-MS/MS

"We performed an approach, nLC-ESI-MS/MS, in adjacent tissue sections to identify the proteins corresponding to the discriminatory peptide values. This analysis assigned 147 of

the 206 m/z values shown in the ROC analysis (Table S3 (Wu, Hundsdoerfer et al. 2021)) (AUC>0.7 or AUC<0.3, p<0.001). According to the guidelines, proteins corresponding to m/z values were correctly identified when the validation method (in this case nLC-ESI-MS/MS; Supplementary Table S4 (22)) identified at least two peptides that were detected by MALDI-MSI from the same protein with similar intensity of spatial difference and correlated within the same tissue region that was evaluated by correlation coefficient (50). These criteria were met in eight proteins that corresponded to 18 MALDI-MSI m/z values (Table 8 (22)). The differential intensity distributions of m/z values for six of these eight proteins (14 m/z values) were validated using MALDI-MSI data from 10 array cores from neuroblastoma tissue regions with >80% tumor cell content. Two peptides (m/z values are shown in Table S3 (22)) from these proteins, COL1A2, COL6A3, HSPA5, HIST1H2BC, KRT9, AHNAK and NID2, expressed significantly higher in the tumor cell-rich region of high-risk neuroblastoma.” (Published by Wu et al., Cancers, 2021) (22)

“This group was enriched for extracellular matrix components (COL1A2, COL6A3 and NID2) and proteins associated with or regulating cytoskeletal proteins (AHNAK) and a cytoskeletal protein (KRT9). The two peptides assigned to CRMP1 were significantly less expressed in tumor cell-rich regions of high-risk neuroblastoma than other risk group. We selected two representative proteins from the identified proteins and validated them in adjacent neuroblastoma tissue sections using immunohistochemistry. Expression of AHNAK was higher in the tumor cell-rich region of high-risk neuroblastoma. In contrast, CRMP1 expression was higher in other risk neuroblastoma (Figure 6 (22)). Our data suggest that the 1832.79 m/z peak obtained by MALDI-MSI in the tumor cell-enriched region of high-risk neuroblastoma is a tryptic peptide from AHNAK, an approximately 700 kD scaffolding protein that has not been previously published in the context of neuroblastoma. It was initially reported relating to neuroblast differentiation that was reviewed by Davis et al. in 2014 (56), but recent studies have also pointed to its important role in promoting cell proliferation, migration, and epithelial-mesenchymal transition (EMT), leading to short disease-free survival time and poor outcomes in aggressive cancers, including pancreatic ductal adenocarcinoma (57). Similarly, the relatively higher intensity of 922.50 m/z peak in MALDI-MSI of other risk neuroblastoma is a tryptic peptide from CRMP1, a marker for neuronal

differentiation associated with neuronal growth and guidance. It has previously been used in mRNA panels for detecting minimal residual disease of neuroblastoma and tumor initiation cells (58-61). These findings confirmed the potential to correctly identify 18 tryptic peptides obtained by MALDI-MSI from FFPE neuroblastoma tissue sections corresponding to the eight proteins and validated AHNAK and CRMP1 as discriminatory protein markers with potentially interesting and plausible biological roles.” (Published by Wu et al., Cancers, 2021) (22)

Table 8: Differential intensity distributions of peptides (MALDI-MSI) and their corresponding proteins in tissue sections from neuroblastomas in high or other risk groups. (Adapted from publication Wu et al., Cancers, 2021) (22)

MALDI-MSI m/z value	ROC [AUC] for HR versus nHR*	ROC [AUC] HR/nHR TMA †	Significance rating-WRS	LC-MS/MS [Mr + H ⁺ cal.]	MOWSE Scores§	Deviation [Da]	Correlation Coefficient	HGNC Symbol	Protein
868.49	0.85	0.73	<0.001	868.46	48.1	0.03	0.38		
1562.77	0.91	0.74	<0.001	1562.79	127.0	0.02	0.64	COL1A2	Collagen type I alpha 2 chain
2026.91	0.86	0.73	<0.001	2027.02	65.8	0.11	0.36		
1459.85	0.72	0.66	<0.001	1459.86	40.5	0.01	0.38	COL6A3	Collagen type VI alpha 3 chain
2056.92	0.88	0.63	<0.001	2057.04	59.4	0.12	0.32		
766.48	0.08	0.28	<0.001	766.46	21.7	0.02	0.44	CRMP1	Collapsin response mediator protein 1
922.50	0.14	0.34	<0.001	922.51	22.3	0.01	0.40		
1833.99	0.87	0.67	<0.001	1833.91	65.1	0.08	0.40	HSPA5	Heat shock protein family A (Hsp70) member 5
2042.22	0.85	0.73	<0.001	2042.05	25.6	0.17	0.32		
1477.86	0.90	0.75	<0.001	1477.79	28.1	0.07	0.41		
1743.68	0.82	0.58	<0.001	1743.82	96.2	0.14	0.58	HIST1H2BC	H2B clustered histone 4
1775.79	0.90	0.70	<0.001	1775.81	123.0	0.02	0.55		
1586.77	0.90	0.74	<0.001	1586.77	89.4	0.00	0.47	KRT9	Keratin 9
2705.28	0.86	0.78	<0.001	2705.16	67.9	0.12	0.44		
1267.50	0.87	0.74	<0.001	1267.65	63.9	0.15	0.38		
1832.79	0.92	0.70	<0.001	1832.88	44.7	0.09	0.39	AHNAK	AHNAK nucleoprotein
1706.78	0.87	0.74	<0.001	1706.78	31.2	0.00	0.31		
2455.36	0.79	0.72	<0.001	2455.17	34.9	0.19	0.33	NID2	Nidogen 2

* Calculated from data obtained from regions in whole tissue sections with >80% tumor cell content.

† TMA = tissue microarray (arrayed neuroblastoma tissue cores from areas with >80% cell content).

§ MOlecular Weight Search score (49)

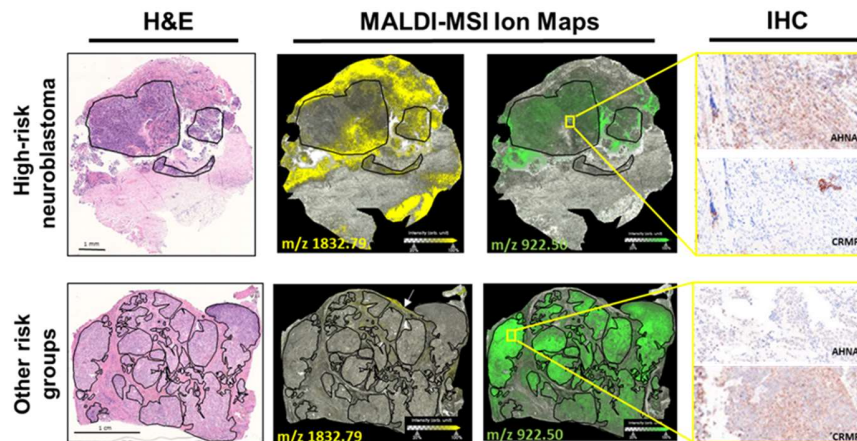


Figure 6: Validation of two discriminative protein markers for neuroblastoma risk in tissue sections. Two exemplary representative samples each from high-risk (HR) and other risk groups (nHR) neuroblastoma were shown. MALDI-MSI ion maps for one peptide (m/z 1832.79 Da) assigned to AHNAK and one peptide (m/z 922.50 Da) assigned to CRMP1 are shown next to the corresponding sections stained with haematoxylin and eosin (H&E) for orientation. Black lines border areas included $>80\%$ tumor cell content. Immunohistochemical (IHC) detection of AHNAK and CRMP1 is shown for the regions surrounded by the yellow squares in the expanded image ($400\times$ magnification). (Adapted from publication Wu et al., *Cancers*, 2021) (22)

“In summary, MALDI-MSI is feasible for investigating the molecular features in histologically homogenous areas of high-risk neuroblastoma. Our method exposed the existing intra-heterogeneity of tumor cells and identified discriminative peptide signatures for high-risk and other risk neuroblastoma. Eighteen peptides of the discriminatory peptides could be assigned to eight proteins, and then the differential expression of AHNAK and CRMP1 was verified in tissue sections using immunohistochemistry. AHNAK showed intense staining in tumor cell-rich areas of high-risk neuroblastoma compared to other risk groups with slight staining. However, staining for CRMP1 shows mostly intense in tumor cell-rich regions of other risk-classified neuroblastomas and slight in the high-risk group. A further validation analysis for their biological roles in neuroblastoma is necessary.” (Published by Wu et al., *Cancers*, 2021) (22)

5 Discussion

Tumors do not seem a simple mass of invasive cancer cells, and they are actually a mixture of different types and structures of cancer cells, including malignant cells, extracellular matrix, microenvironmental factors, blood vessels and cellular immune components. In addition, the distribution of these cells varies in density and protein expression within tumor tissue. (62) This diversity of cellular and molecular composition leads to intratumor heterogeneity and is an essential factor involved in treatment failure, drug resistance and recurrence (63). Many researchers have applied LC-MS based proteomics approach to tumor fluid and tissue homogenates to explore cancer biomarkers for diagnostic and therapeutic purposes. Previously, 51 proteins in ovarian tumor fluid have been identified by LC-MS/MS associated with the invasive state of malignant cells (64) and a large scale up-or down-regulated proteins of neuroblastomas defined by the same method relate in high-risk disease or tumor regression (65, 66). However, information about protein alterations cannot be correlated to the corresponding morphological structures through this method. In this dissertation, we have chosen another mass spectrometric technique, MALDI-MSI, to decipher comprehensive proteomic information of tumor tissue, including composition, location, and relative quantity. This procedure needs neither labels nor prior knowledge of molecular targets following relatively automated and straightforward sample preparation. The proteome screening analysis is performed in full equivalence covering high tumor cell-rich regions and stroma (microenvironment) on the surface of tumor tissue. A large number of investigations confirmed that neighboring cells and/or proteomic changes in the tumor stroma could affect tumor transformation, progress, and metastases (67). Therefore, deep proteomic profiling in tumor stroma is just as crucial to understanding tumorigenesis and growth as in cancer cells themselves. For example, other cancer researchers have reported that "AHNAK was also occasionally upregulated in tumor stroma. Because of the barriers posed by natural structures such as connective tissue, fibroblasts, immune cells and vasculature, the common mass spectrometry methods are limited in their ability to reveal the molecular composition of the stromal compartment. Nevertheless, MALDI-MSI can map protein changes in both regions, clearly demonstrating the intercellular interactions between malignant cancer cells and their environment. This ability provides new insights into understanding neuroblastoma

tumorigenesis and progression.” (Published by Wu et al., *Cancers*, 2021) (22) Another advantage of this technique is that the tissue under the MALDI-matrix layer (about 3-4 μm) is intact. After the removal, the same tissue section could be used for further studies, such as chemical staining for morphological assessment, immunochemical analysis, transcriptomics profiling and sequencing technology (68, 69). The evaluation of analysis combinations offers more precise and comprehensive molecular profiles. Additionally, some of them are already utilized as standard clinicopathological assessments. Integration of the MALDI-MSI technique could not only act as a method of cross-validation but also enhance precision cancer medicine learning. Just as our data identified a higher intensity distribution of CRMP1 in low- and intermediate-risk neuroblastomas. This same finding is well reported that CRMP1 has been used as a gene marker for prognosis and diagnosis in neuroblastoma gene expression panels (70).

Due to cellular and molecular heterogeneous distribution across a tumor tissue section, the accuracy and reproducibility of TMAs application in cancer research should be questioned, although this technique has a tremendous advantage when applied to large amounts of samples within a short investigation time (42). We applied MALDI-MSI data derived from neuroblastoma TMA to validate discriminative peptide values obtained from whole tissue sections and found that “not all peptides detected by MALDI-MSI in whole sections could be detected in cores of TMA (Figure 7, (22))” (Published by Wu et al., *Cancers*, 2021) (22). This suggests that the detection of tumor heterogeneity using tissue microarrays has significant limitations compared to MALDI-MSI using whole tissue sections, “a more comprehensive and precise, new diagnostic method. The present study emphasizes that the investigation of whole tissue sections is a promising way to investigate the molecular heterogeneity of tumors directly.” (Published by Wu et al., *Cancers*, 2021) (22) Different regions of tumor tissue may be morphologically homogeneous but contain differences in molecular composition (71, 72).

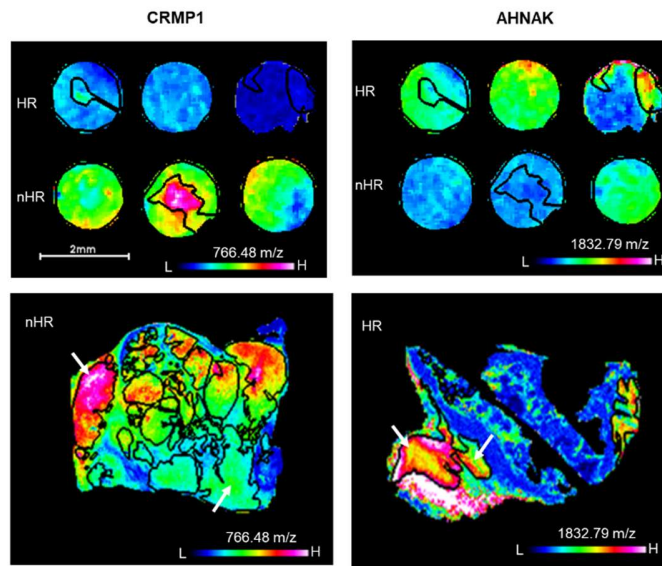


Figure 7: Ion maps of m/z values for CRMP1 and AHNAK in whole neuroblastoma sections and their validation in selected cores from the tissue microarray. Intensity distributions of one peptide from CRMP1 (m/z value 766.48 Da) and one peptide from AHNAK (m/z value 1832.79 Da) are shown in selected tumor cores from the neuroblastoma tissue microarray (upper images) and whole tissue sections (lower images) from neuroblastomas designated high-risk (HR) or in other risk groups (nHR). White arrows point out areas of heterogenic ion distribution in the whole tumor sections. (Adapted from publication Wu et al., *Cancers*, 2021) (22)

corresponding to proteins rather than applied MALDI tandem mass spectrometry (MALDI-MS/MS) for direct identification of protein markers. Firstly, the approach MALDI-MS/MS cannot select and fragment all the precursor peaks because of signal depletion in a single pixel. Secondly, the major peaks belong to the most abundant proteins, and many peaks corresponding to less abundant proteins are not detected due to the ion suppression and the complexity of the samples. Moreover, the whole tumor tissue section is too complex, the searching database scores would not be sufficient to confirm the protein IDs when performing directly region-specific targeted MS/MS (50). Indeed, there are other mass spectrometry imaging approaches, such as nano desorption electrospray ionization (DESI) mass spectrometry and secondary ion mass spectrometry (SIMS), that offer higher spatial resolution and better MS/MS opportunities than MALDI-TOF. However, both methods are not well suitable for high-throughput and large cohort clinical investigation due to more lowly limited mass range and extreme high time-consuming. Time is an essential factor in the methodology proposed for potential clinical use since this must be applied in real-time for

disease decisions. Therefore, high-resolution mass spectrometry technologies were not considered for the POC study design and would be unsuitable for large-scale imaging analysis studies using whole tissue sections or clinical application. Undeniably, the presented MALDI-TOF instrument suffers from a mass accuracy that makes it more susceptible to false protein assignments. Thus, we have examined the matching between “selected m/z values and their source proteins, whether the differential peptide signature from biologically feasible proteins in neuroblastoma and validated their differential expression in tumor sections using immunohistochemistry.” (Published by Wu et al., *Cancers*, 2021) (22) The intensive IHC staining of AHNAK in tumor cell-rich regions of high-risk neuroblastoma conforms to disease-related biological plausibility.

Using MALDI-MSI, we have observed high expression of tryptic peptides from cytoskeleton, cytoplasm, cytosol, and extracellular matrix proteins invasive and malignant tumor regions. For instance, the primary tumors from early-stage HGSOV patients with recurrence disease presented the intense distribution of particular peptides corresponding to Keratin type 1, Actin, Cytoplasmic 1 and Collagen alpha-2(I) in tumor cell-rich regions. These peptide values indicated strong prognostic potential (AUC > 0.7). “A published reference database of MALDI-IMS-derived peptide and protein values (73) can support our findings. The expression of collagen production by ovarian cancer cells, including Collagen alpha-2(I), Actin and Cytoplasmic 1, could increase drug resistance by inhibiting the penetration of the drug into the cancer tissue as well as increase resistance to apoptosis (74)” (Published by Kulbe et al, *Cancers*, 2020) (46) that was also confirmed in MALDI-MSI studies of lung tumor biopsies (75). Keratins, the epithelial-predominant members of the intermediate filament superfamily, regulates various signaling pathways in cancer cells to influence a series of processes in tumor progression (76). Similarly, we identified AHNAK as a marker protein highly expressed in tumor cell-rich regions of high-risk neuroblastoma tissue sections. AHNAK has not previously been linked to neuroblastoma but is involved in several cancer-related cellular functions and is listed as “one of six putative cancer genes involved in the evolution of nine different cancers in 3000 cancer genomes (77). However, the role of AHNAK in cancer appears to be tissue-specific, with other reports pointing to a possible role as a tumor suppressor in gliomas (78) and breast cancer (79).” (Published by Wu et al.,

Cancers, 2021) (22) The reason is maybe that AHNAK is a large protein, which mitigates the function of multiprotein complexes by acting as a scaffold to link activities either in the nucleus or at the plasma membrane and alters interactivity and intracellular localization through its own phosphorylation sites (56).

A profound understanding of the biological roles of identified discriminative proteins in early-stage HGSOV and neuroblastomas might improve risk assessment at diagnostics and eventually develop new therapeutic strategies, but for it more comprehensive molecular characterization supported by transcriptome and DNA analysis and more precise proteomics data from micro-dissected malignant tumor areas and adjacent stroma compartments are required in future. Furthermore, the identified peptides signature should be validated in a larger cohort of patient samples. Generally, this dissertation has confirmed the technical feasibility of MALDI-MSI to explore molecular changes on tumor tissues on the protein level, to identify new spatially characteristic peptides signature for tumor diagnosing and prognosis through the combination with the nLC-ESI-MS/MS.

6 Abbreviations

2D	two-dimensional
AUC	the area under the curve
CONC	concentration
DESI	nano desorption electrospray ionisation
EMT	epithelial-mesenchymal transition
EOC	epithelial ovarian cancer
ESI-LC-MS	electrospray ionization liquid chromatography mass spectrometry
FFPE	formalin-fixed paraffin embedded
FIGO	international federation of gynaecology and obstetrics
HCCA	α -cyano-4-hydroxycinnamic acid
HGEC	high-grade endometriosis ovarian cancer
HGSOC	high-grade serous ovarian cancer
HR	high-risk
IHC	immunohistochemistry
LC-MS/MS	liquid chromatography tandem mass spectrometry
MALDI	matrix-assisted laser desorption/ionization
MALDI-MS/MS	MALDI tandem mass spectrometry
MS	mass spectrometry
MSI	mass spectrometry imaging
nHPLC	nano high-performance liquid chromatography
nHR	other risk group
nLC-ESI-MS/MS	nano-liquid chromatography electrospray ionization tandem mass spectrometry
NSCNEC	non-small cell neuroendocrine carcinoma
PCA	principal component analysis
pLSA	probabilistic latent semantic analysis
POC	principal-of-concept
PTMs	post-translational modifications
ROC	receiver operating characteristic analysis
SIMS	secondary ion mass spectrometry
TIC	total ion count
TMA	tissue microarrays
TOF	time of flight

7 References

1. Vaughan S, Coward JI, Bast RC, Jr., Berchuck A, Berek JS, Brenton JD, Coukos G, Crum CC, Drapkin R, Etemadmoghadam D, Friedlander M, Gabra H, Kaye SB, Lord CJ, Lengyel E, Levine DA, McNeish IA, Menon U, Mills GB, Nephew KP, Oza AM, Sood AK, Stronach EA, Walczak H, Bowtell DD, Balkwill FR. Rethinking ovarian cancer: recommendations for improving outcomes. *Nat Rev Cancer*. 2011;11(10):719-25.
2. Prat J, Oncology FCoG. Staging classification for cancer of the ovary, fallopian tube, and peritoneum. *Int J Gynaecol Obstet*. 2014;124(1):1-5.
3. Trimbos JB, Parmar M, Vergote I, Guthrie D, Bolis G, Colombo N, Vermorken JB, Torri V, Mangioni C, Pecorelli S, Lissoni A, Swart AM. International Collaborative Ovarian Neoplasm trial 1 and Adjuvant ChemoTherapy In Ovarian Neoplasm trial: two parallel randomized phase III trials of adjuvant chemotherapy in patients with early-stage ovarian carcinoma. *J Natl Cancer Inst*. 2003;95(2):105-12.
4. Ahmed FY, Wiltshaw E, A'Hern RP, Nicol B, Shepherd J, Blake P, Fisher C, Gore ME. Natural history and prognosis of untreated stage I epithelial ovarian carcinoma. *J Clin Oncol*. 1996;14(11):2968-75.
5. Duggan MA, Anderson WF, Altekruse S, Penberthy L, Sherman ME. The Surveillance, Epidemiology, and End Results (SEER) Program and Pathology: Toward Strengthening the Critical Relationship. *Am J Surg Pathol*. 2016;40(12):e94-e102.
6. Hoskins PJ, Swenerton KD, Manji M, Wong F, O'Reilly SE, McMurtrie EJ, Le N, Acker B, Le Richer J. 'Moderate-risk' ovarian cancer (stage I, grade 2; stage II, grade 1 or 2) treated with cisplatin chemotherapy (single agent or combination) and pelvi-abdominal irradiation. *Int J Gynecol Cancer*. 1994;4(4):272-8.
7. Chan JK, Tian C, Monk BJ, Herzog T, Kapp DS, Bell J, Young RC, Gynecologic Oncology G. Prognostic factors for high-risk early-stage epithelial ovarian cancer: a Gynecologic Oncology Group study. *Cancer*. 2008;112(10):2202-10.
8. Colombo N, Peiretti M, Parma G, Lapresa M, Mancari R, Carinelli S, Sessa C, Castiglione M. Newly diagnosed and relapsed epithelial ovarian carcinoma: ESMO Clinical Practice Guidelines for diagnosis, treatment and follow-up. *Ann Oncol*. 2010;21 Suppl 5:v23-30.
9. Lee CL, Kusunoki S, Huang CY, Wu KY, Lee PS, Huang KG. Surgical and survival outcomes of laparoscopic staging surgery for patients with stage I ovarian cancer. *Taiwan J Obstet Gynecol*. 2018;57(1):7-12.
10. Wei W, Li N, Sun Y, Li B, Xu L, Wu L. Clinical outcome and prognostic factors of patients with early-stage epithelial ovarian cancer. *Oncotarget*. 2017;8(14):23862-70.
11. Leblanc E, Querleu D, Narducci F, Chauvet MP, Chevalier A, Lesoin A, Vennin P, Taieb S. Surgical staging of early invasive epithelial ovarian tumors. *Semin Surg Oncol*. 2000;19(1):36-41.
12. Collinson F, Qian W, Fossati R, Lissoni A, Williams C, Parmar M, Ledermann J, Colombo N, Swart A. Optimal treatment of early-stage ovarian cancer. *Ann Oncol*. 2014;25(6):1165-71.
13. Prat J. New insights into ovarian cancer pathology. *Annals of Oncology*. 2012;23:x111-x7.

14. Husmann G, Kaatsch P, Katalinic A, Bertz J, Haberland J, Kraywinkel K, Wolf U. Krebs in Deutschland 2005/2006 - Häufigkeiten und Trends. Robert Koch-Institut; 2010.
15. Maris JM. Recent advances in neuroblastoma. *N Engl J Med.* 2010;362(23):2202-11.
16. Cheung NK, Dyer MA. Neuroblastoma: developmental biology, cancer genomics and immunotherapy. *Nat Rev Cancer.* 2013;13(6):397-411.
17. Maris JM, Hogarty MD, Bagatell R, Cohn SL. Neuroblastoma. *Lancet.* 2007;369(9579):2106-20.
18. Simon T, Hero B, Schulte JH, Deubzer H, Hundsdoerfer P, von Schweinitz D, Fuchs J, Schmidt M, Prasad V, Krug B, Timmermann B, Leuschner I, Fischer M, Langer T, Astrahantseff K, Berthold F, Lode H, Eggert A. 2017 GPOH Guidelines for Diagnosis and Treatment of Patients with Neuroblastic Tumors. *Klin Padiatr.* 2017;229(3):147-67.
19. Cohn SL, Pearson AD, London WB, Monclair T, Ambros PF, Brodeur GM, Faldum A, Hero B, Iehara T, Machin D, Mosseri V, Simon T, Garaventa A, Castel V, Matthay KK, Force IT. The International Neuroblastoma Risk Group (INRG) classification system: an INRG Task Force report. *J Clin Oncol.* 2009;27(2):289-97.
20. Liang WH, Federico SM, London WB, Naranjo A, Irwin MS, Volchenbom SL, Cohn SL. Tailoring Therapy for Children With Neuroblastoma on the Basis of Risk Group Classification: Past, Present, and Future. *JCO Clin Cancer Inform.* 2020;4:895-905.
21. Ora I, Eggert A. Progress in treatment and risk stratification of neuroblastoma: impact on future clinical and basic research. *Semin Cancer Biol.* 2011;21(4):217-28.
22. Wu Z, Hundsdoerfer P, Schulte JH, Astrahantseff K, Boral S, Schmelz K, Eggert A, Klein O. Discovery of Spatial Peptide Signatures for Neuroblastoma Risk Assessment by MALDI Mass Spectrometry Imaging. *Cancers (Basel).* 2021;13(13).
23. Brodeur GM, Seeger RC, Schwab M, Varmus HE, Bishop JM. Amplification of N-myc in untreated human neuroblastomas correlates with advanced disease stage. *Science.* 1984;224(4653):1121-4.
24. Campbell K, Gastier-Foster JM, Mann M, Naranjo AH, Van Ryn C, Bagatell R, Matthay KK, London WB, Irwin MS, Shimada H, Granger MM, Hogarty MD, Park JR, DuBois SG. Association of MYCN copy number with clinical features, tumor biology, and outcomes in neuroblastoma: A report from the Children's Oncology Group. *Cancer.* 2017;123(21):4224-35.
25. Oberthuer A, Juraeva D, Hero B, Volland R, Sterz C, Schmidt R, Faldum A, Kahlert Y, Engesser A, Asgharzadeh S, Seeger R, Ohira M, Nakagawara A, Scaruffi P, Tonini GP, Janoueix-Lerosey I, Delattre O, Schleiermacher G, Vandesompele J, Speleman F, Noguera R, Piqueras M, Benard J, Valent A, Avigad S, Yaniv I, Grundy RG, Ortmann M, Shao C, Schwab M, Eils R, Simon T, Theissen J, Berthold F, Westermann F, Brors B, Fischer M. Revised risk estimation and treatment stratification of low- and intermediate-risk neuroblastoma patients by integrating clinical and molecular prognostic markers. *Clin Cancer Res.* 2015;21(8):1904-15.
26. Ackermann S, Cartolano M, Hero B, Welte A, Kahlert Y, Roderwieser A, Bartenhagen C, Walter E, Gecht J, Kerschke L, Volland R, Menon R, Heuckmann JM, Gartlgruber M, Hartlieb S, Henrich KO, Okonechnikov K, Altmüller J, Nurnberg P, Lefever S, de Wilde B, Sand F, Ikram F, Rosswog C, Fischer J, Theissen J, Hertwig F, Singhi AD, Simon T, Vogel W, Perner S, Krug B, Schmidt M, Rahmann S, Achter V, Lang U, Vokuhl C, Ortmann M, Buttner R, Eggert A, Speleman F, O'Sullivan RJ, Thomas RK, Berthold F, Vandesompele J,

- Schramm A, Westermann F, Schulte JH, Peifer M, Fischer M. A mechanistic classification of clinical phenotypes in neuroblastoma. *Science*. 2018;362(6419):1165-70.
27. de Sousa VML, Carvalho L. Heterogeneity in Lung Cancer. *Pathobiology*. 2018;85(1-2):96-107.
28. Ngan ES. Heterogeneity of neuroblastoma. *Oncoscience*. 2015;2(10):837-8.
29. Lessard CJ, Ice JA, Adrianto I, Wiley GB, Kelly JA, Gaffney PM, Montgomery CG, Moser KL. The genomics of autoimmune disease in the era of genome-wide association studies and beyond. *Autoimmun Rev*. 2012;11(4):267-75.
30. International Cancer Genome C, Hudson TJ, Anderson W, Artez A, Barker AD, Bell C, Bernabé RR, Bhan MK, Calvo F, Eerola I, Gerhard DS, Guttmacher A, Guyer M, Hemsley FM, Jennings JL, Kerr D, Klatt P, Kolar P, Kusada J, Lane DP, Laplace F, Youyong L, Nettekoven G, Ozenberger B, Peterson J, Rao TS, Remale J, Schafer AJ, Shibata T, Stratton MR, Vockley JG, Watanabe K, Yang H, Yuen MMF, Knoppers BM, Bobrow M, Cambon-Thomsen A, Dressler LG, Dyke SOM, Joly Y, Kato K, Kennedy KL, Nicolás P, Parker MJ, Rial-Sebbag E, Romeo-Casabona CM, Shaw KM, Wallace S, Wiesner GL, Zeps N, Lichter P, Biankin AV, Chabannon C, Chin L, Clément B, de Alava E, Degos F, Ferguson ML, Geary P, Hayes DN, Hudson TJ, Johns AL, Kasprzyk A, Nakagawa H, Penny R, Piris MA, Sarin R, Scarpa A, Shibata T, van de Vijver M, Futreal PA, Aburatani H, Bayés M, Botwell DDL, Campbell PJ, Estivill X, Gerhard DS, Grimmond SM, Gut I, Hirst M, López-Otín C, Majumder P, Marra M, McPherson JD, Nakagawa H, Ning Z, Puente XS, Ruan Y, Shibata T, Stratton MR, Stunnenberg HG, Swerdlow H, Velculescu VE, Wilson RK, Xue HH, Yang L, Spellman PT, Bader GD, Boutros PC, Campbell PJ, Flicek P, Getz G, Guigó R, Guo G, Haussler D, Heath S, Hubbard TJ, Jiang T, Jones SM, Li Q, López-Bigas N, Luo R, Muthuswamy L, Ouellette BFF, Pearson JV, Puente XS, Quesada V, Raphael BJ, Sander C, Shibata T, Speed TP, Stein LD, Stuart JM, Teague JW, Totoki Y, Tsunoda T, Valencia A, Wheeler DA, Wu H, Zhao S, Zhou G, Stein LD, Guigó R, Hubbard TJ, Joly Y, Jones SM, Kasprzyk A, Lathrop M, López-Bigas N, Ouellette BFF, Spellman PT, Teague JW, Thomas G, Valencia A, Yoshida T, Kennedy KL, Axton M, Dyke SOM, Futreal PA, Gerhard DS, Gunter C, Guyer M, Hudson TJ, McPherson JD, Miller LJ, Ozenberger B, Shaw KM, Kasprzyk A, Stein LD, Zhang J, Haider SA, Wang J, Yung CK, Cros A, Liang Y, Gnaneshan S, Guberman J, Hsu J, Bobrow M, Chalmers DRC, Hasel KW, Joly Y, Kaan TSH, Kennedy KL, Knoppers BM, Lowrance WW, Masui T, Nicolás P, Rial-Sebbag E, Rodriguez LL, Vergely C, Yoshida T, Grimmond SM, Biankin AV, Bowtell DDL, Cloonan N, deFazio A, Eshleman JR, Etemadmoghadam D, Gardiner BB, Kench JG, Scarpa A, Sutherland RL, Tempero MA, Waddell NJ, Wilson PJ, McPherson JD, Gallinger S, Tsao M-S, Shaw PA, Petersen GM, Mukhopadhyay D, Chin L, DePinho RA, Thayer S, Muthuswamy L, Shazand K, Beck T, Sam M, Timms L, Ballin V, Lu Y, Ji J, Zhang X, Chen F, Hu X, Zhou G, Yang Q, Tian G, Zhang L, Xing X, Li X, Zhu Z, Yu Y, Yu J, Yang H, Lathrop M, Tost J, Brennan P, Holcatova I, Zaridze D, Brazma A, Egevard L, Prokhortchouk E, Banks RE, Uhlén M, Cambon-Thomsen A, Viksna J, Ponten F, Skryabin K, Stratton MR, Futreal PA, Birney E, Borg A, Børresen-Dale A-L, Caldas C, Foekens JA, Martin S, Reis-Filho JS, Richardson AL, Sotiriou C, Stunnenberg HG, Thoms G, van de Vijver M, van't Veer L, Calvo F, Birnbaum D, Blanche H, Boucher P, Boyault S, Chabannon C, Gut I, Masson-Jacquemier JD, Lathrop M, Pauporté I, Pivot X, Vincent-Salomon A, Tabone E, Theillet C, Thomas G, Tost J, Treilleux I, Calvo F, Bioulac-Sage P, Clément B, Decaens T, Degos F, Franco D, Gut I, Gut M, Heath S, Lathrop M,

- Samuel D, Thomas G, Zucman-Rossi J, Lichter P, Eils R, Brors B, Korbel JO, Korshunov A, Landgraf P, Lehrach H, Pfister S, Radlwimmer B, Reifemberger G, Taylor MD, von Kalle C, Majumder PP, Sarin R, Rao TS, Bhan MK, Scarpa A, Pederzoli P, Lawlor RA, Delledonne M, Bardelli A, Biankin AV, Grimmond SM, Gress T, Klimstra D, Zamboni G, Shibata T, Nakamura Y, Nakagawa H, Kusada J, Tsunoda T, Miyano S, Aburatani H, Kato K, Fujimoto A, Yoshida T, Campo E, López-Otín C, Estivill X, Guigó R, de Sanjosé S, Piris MA, Montserrat E, González-Díaz M, Puente XS, Jares P, Valencia A, Himmelbauer H, Quesada V, Bea S, Stratton MR, Futreal PA, Campbell PJ, Vincent-Salomon A, Richardson AL, Reis-Filho JS, van de Vijver M, Thomas G, Masson-Jacquemier JD, Aparicio S, Borg A, Børresen-Dale A-L, Caldas C, Foekens JA, Stunnenberg HG, van't Veer L, Easton DF, Spellman PT, Martin S, Barker AD, Chin L, Collins FS, Compton CC, Ferguson ML, Gerhard DS, Getz G, Gunter C, Guttmacher A, Guyer M, Hayes DN, Lander ES, Ozenberger B, Penny R, Peterson J, Sander C, Shaw KM, Speed TP, Spellman PT, Vockley JG, Wheeler DA, Wilson RK, Hudson TJ, Chin L, Knoppers BM, Lander ES, Lichter P, Stein LD, Stratton MR, Anderson W, Barker AD, Bell C, Bobrow M, Burke W, Collins FS, Compton CC, DePinho RA, Easton DF, Futreal PA, Gerhard DS, Green AR, Guyer M, Hamilton SR, Hubbard TJ, Kallioniemi OP, Kennedy KL, Ley TJ, Liu ET, Lu Y, Majumder P, Marra M, Ozenberger B, Peterson J, Schafer AJ, Spellman PT, Stunnenberg HG, Wainwright BJ, Wilson RK, Yang H. International network of cancer genome projects. *Nature*. 2010;464(7291):993-8.
31. Berghmans E, Boonen K, Maes E, Mertens I, Pauwels P, Baggerman G. Implementation of MALDI Mass Spectrometry Imaging in Cancer Proteomics Research: Applications and Challenges. *J Pers Med*. 2020;10(2).
32. Lorentzian A, Uzozie A, Lange PF. Origins and clinical relevance of proteoforms in pediatric malignancies. *Expert Rev Proteomics*. 2019;16(3):185-200.
33. Jimenez CR, Verheul HM. Mass spectrometry-based proteomics: from cancer biology to protein biomarkers, drug targets, and clinical applications. *Am Soc Clin Oncol Educ Book*. 2014:e504-10.
34. Caprioli RM, Farmer TB, Gile J. Molecular imaging of biological samples: localization of peptides and proteins using MALDI-TOF MS. *Anal Chem*. 1997;69(23):4751-60.
35. Herring KD, Oppenheimer SR, Caprioli RM. Direct tissue analysis by matrix-assisted laser desorption ionization mass spectrometry: application to kidney biology. *Semin Nephrol*. 2007;27(6):597-608.
36. Bensimon A, Heck AJ, Aebersold R. Mass spectrometry-based proteomics and network biology. *Annu Rev Biochem*. 2012;81:379-405.
37. Fenn JB, Mann M, Meng CK, Wong SF, Whitehouse CM. Electrospray ionization for mass spectrometry of large biomolecules. *Science*. 1989;246(4926):64-71.
38. Kulyyassov A.T. RYM. APPLICATIONS OF THE IMPACT II HIGH RESOLUTION QUADRUPOLE TIME-OF-FLIGHT (QTOF) INSTRUMENT FOR SHOTGUN PROTEOMICS. <https://biotechlink.org>. 2018;3-2018.
39. Griffiths WJ, Wang Y. Mass spectrometry: from proteomics to metabolomics and lipidomics. *Chem Soc Rev*. 2009;38(7):1882-96.
40. El-Sayes N, Vito A, Mossman K. Tumor Heterogeneity: A Great Barrier in the Age of Cancer Immunotherapy. *Cancers (Basel)*. 2021;13(4).

41. McDonnell LA, Corthals GL, Willems SM, van Remoortere A, van Zeijl RJ, Deelder AM. Peptide and protein imaging mass spectrometry in cancer research. *J Proteomics*. 2010;73(10):1921-44.
42. Klein O, Kanter F, Kulbe H, Jank P, Denkert C, Nebrich G, Schmitt WD, Wu Z, Kunze CA, Sehoul J, Darb-Esfahani S, Braicu I, Lellmann J, Thiele H, Taube ET. MALDI-Imaging for Classification of Epithelial Ovarian Cancer Histotypes from a Tissue Microarray Using Machine Learning Methods. *Proteomics Clin Appl*. 2019;13(1):e1700181.
43. Schwamborn K, Krieg RC, Jirak P, Ott G, Knuchel R, Rosenwald A, Wellmann A. Application of MALDI imaging for the diagnosis of classical Hodgkin lymphoma. *J Cancer Res Clin Oncol*. 2010;136(11):1651-5.
44. Rauser S, Marquardt C, Balluff B, Deininger SO, Albers C, Belau E, Hartmer R, Suckau D, Specht K, Ebert MP, Schmitt M, Aubele M, Hofler H, Walch A. Classification of HER2 receptor status in breast cancer tissues by MALDI imaging mass spectrometry. *J Proteome Res*. 2010;9(4):1854-63.
45. Balluff B, Rauser S, Meding S, Elsner M, Schone C, Feuchtinger A, Schuhmacher C, Novotny A, Jutting U, Maccarrone G, Sarioglu H, Ueffing M, Braselmann H, Zitzelsberger H, Schmid RM, Hofler H, Ebert MP, Walch A. MALDI imaging identifies prognostic seven-protein signature of novel tissue markers in intestinal-type gastric cancer. *Am J Pathol*. 2011;179(6):2720-9.
46. Kulbe H, Klein O, Wu Z, Taube ET, Kassuhn W, Horst D, Darb-Esfahani S, Jank P, Abobaker S, Ringel F, du Bois A, Heitz F, Sehoul J, Braicu EI. Discovery of Prognostic Markers for Early-Stage High-Grade Serous Ovarian Cancer by Maldi-Imaging. *Cancers (Basel)*. 2020;12(8).
47. Klein O, Strohschein K, Nebrich G, Oetjen J, Trede D, Thiele H, Alexandrov T, Giavalisco P, Duda GN, von Roth P, Geissler S, Klose J, Winkler T. MALDI imaging mass spectrometry: discrimination of pathophysiological regions in traumatized skeletal muscle by characteristic peptide signatures. *Proteomics*. 2014;14(20):2249-60.
48. Chambers MC, Maclean B, Burke R, Amodei D, Ruderman DL, Neumann S, Gatto L, Fischer B, Pratt B, Egertson J, Hoff K, Kessner D, Tasman N, Shulman N, Frewen B, Baker TA, Brusniak MY, Paulse C, Creasy D, Flashner L, Kani K, Moulding C, Seymour SL, Nuwaysir LM, Lefebvre B, Kuhlmann F, Roark J, Rainer P, Detlev S, Hemenway T, Huhmer A, Langridge J, Connolly B, Chadick T, Holly K, Eckels J, Deutsch EW, Moritz RL, Katz JE, Agus DB, MacCoss M, Tabb DL, Mallick P. A cross-platform toolkit for mass spectrometry and proteomics. *Nat Biotechnol*. 2012;30(10):918-20.
49. Pappin DJ, Hojrup P, Bleasby AJ. Rapid identification of proteins by peptide-mass fingerprinting. *Curr Biol*. 1993;3(6):327-32.
50. Cillero-Pastor B, Heeren RM. Matrix-assisted laser desorption ionization mass spectrometry imaging for peptide and protein analyses: a critical review of on-tissue digestion. *J Proteome Res*. 2014;13(2):325-35.
51. Alexandrov T, Becker M, Deininger SO, Ernst G, Wehder L, Grasmair M, von Eggeling F, Thiele H, Maass P. Spatial segmentation of imaging mass spectrometry data with edge-preserving image denoising and clustering. *J Proteome Res*. 2010;9(12):6535-46.
52. Alexandrov T, Becker M, Guntinas-Lichius O, Ernst G, von Eggeling F. MALDI-imaging segmentation is a powerful tool for spatial functional proteomic analysis of human larynx carcinoma. *J Cancer Res Clin Oncol*. 2013;139(1):85-95.

53. Trede D, Schiffler S, Becker M, Wirtz S, Steinhorst K, Strehlow J, Aichler M, Kobarg JH, Oetjen J, Dyatlov A, Heldmann S, Walch A, Thiele H, Maass P, Alexandrov T. Exploring three-dimensional matrix-assisted laser desorption/ionization imaging mass spectrometry data: three-dimensional spatial segmentation of mouse kidney. *Anal Chem.* 2012;84(14):6079-87.
54. Hanselmann M, Kirchner M, Renard BY, Amstalden ER, Glunde K, Heeren RM, Hamprecht FA. Concise representation of mass spectrometry images by probabilistic latent semantic analysis. *Anal Chem.* 2008;80(24):9649-58.
55. McDonnell LA, van Remoortere A, van Zeijl RJM, Deelder AM. Mass spectrometry image correlation: Quantifying colocalization. *J Proteome Res.* 2008;7(8):3619-27.
56. Davis TA, Loos B, Engelbrecht AM. AHNAK: the giant jack of all trades. *Cell Signal.* 2014;26(12):2683-93.
57. Zhang Z, Liu X, Huang R, Liu X, Liang Z, Liu T. Upregulation of nucleoprotein AHNAK is associated with poor outcome of pancreatic ductal adenocarcinoma prognosis via mediating epithelial-mesenchymal transition. *J Cancer.* 2019;10(16):3860-70.
58. Hirase S, Saitoh A, Hartomo TB, Kozaki A, Yanai T, Hasegawa D, Kawasaki K, Kosaka Y, Matsuo M, Yamamoto N, Mori T, Hayakawa A, Iijima K, Nishio H, Nishimura N. Early detection of tumor relapse/regrowth by consecutive minimal residual disease monitoring in high-risk neuroblastoma patients. *Oncol Lett.* 2016;12(2):1119-23.
59. Yamamoto N, Kozaki A, Hartomo TB, Yanai T, Hasegawa D, Kawasaki K, Kosaka Y, Matsuo M, Hirase S, Mori T, Hayakawa A, Iijima K, Nishio H, Nishimura N. Differential expression of minimal residual disease markers in peripheral blood and bone marrow samples from high-risk neuroblastoma patients. *Oncol Lett.* 2015;10(5):3228-32.
60. Hartomo TB, Kozaki A, Hasegawa D, Van Huyen Pham T, Yamamoto N, Saitoh A, Ishida T, Kawasaki K, Kosaka Y, Ohashi H, Yamamoto T, Morikawa S, Hirase S, Kubokawa I, Mori T, Yanai T, Hayakawa A, Takeshima Y, Iijima K, Matsuo M, Nishio H, Nishimura N. Minimal residual disease monitoring in neuroblastoma patients based on the expression of a set of real-time RT-PCR markers in tumor-initiating cells. *Oncol Rep.* 2013;29(4):1629-36.
61. Thwin KKM, Ishida T, Uemura S, Yamamoto N, Lin KS, Tamura A, Kozaki A, Saito A, Kishimoto K, Mori T, Hasegawa D, Kosaka Y, Nino N, Takafuji S, Iijima K, Nishimura N. Level of Seven Neuroblastoma-Associated mRNAs Detected by Droplet Digital PCR Is Associated with Tumor Relapse/Regrowth of High-Risk Neuroblastoma Patients. *J Mol Diagn.* 2020;22(2):236-46.
62. Schöne C, Höfler H, Walch A. MALDI imaging mass spectrometry in cancer research: Combining proteomic profiling and histological evaluation. *Clinical Biochemistry.* 2013;46(6):539-45.
63. McGranahan N, Swanton C. Clonal Heterogeneity and Tumor Evolution: Past, Present, and the Future. *Cell.* 2017;168(4):613-28.
64. Poersch A, Grassi ML, Carvalho VP, Lanfredi GP, Palma CS, Greene LJ, de Sousa CB, Carrara HHA, Candido Dos Reis FJ, Faça VM. A proteomic signature of ovarian cancer tumor fluid identified by highthroughput and verified by targeted proteomics. *J Proteomics.* 2016;145:226-36.
65. Chen QR, Song YK, Yu LR, Wei JS, Chung JY, Hewitt SM, Veenstra TD, Khan J. Global genomic and proteomic analysis identifies biological pathways related to high-risk neuroblastoma. *J Proteome Res.* 2010;9(1):373-82.

66. Yu F, Zhu X, Feng C, Wang T, Hong Q, Liu Z, Tang S. Proteomics-based identification of spontaneous regression-associated proteins in neuroblastoma. *J Pediatr Surg*. 2011;46(10):1948-55.
67. Boyle ST, Mittal P, Kaur G, Hoffmann P, Samuel MS, Klingler-Hoffmann M. Uncovering tumor-stroma inter-relationships using MALDI Mass spectrometry imaging. *J Proteome Res*. 2020.
68. Maccarrone G, Nischwitz S, Deininger SO, Hornung J, König FB, Stadelmann C, Turck CW, Weber F. MALDI imaging mass spectrometry analysis-A new approach for protein mapping in multiple sclerosis brain lesions. *J Chromatogr B Analyt Technol Biomed Life Sci*. 2017;1047:131-40.
69. DeLaney K, Hu M, Hellenbrand T, Dickinson PS, Nusbaum MP, Li L. Mass Spectrometry Quantification, Localization, and Discovery of Feeding-Related Neuropeptides in Cancer borealis. *ACS Chem Neurosci*. 2021;12(4):782-98.
70. Tan F, Thiele CJ, Li Z. Collapsin response mediator proteins: Potential diagnostic and prognostic biomarkers in cancers (Review). *Oncol Lett*. 2014;7(5):1333-40.
71. Giordano S, Zucchetti M, Decio A, Cesca M, Fuso Nerini I, Maiezza M, Ferrari M, Licandro SA, Frapolli R, Giavazzi R, Maurizio D, Davoli E, Morosi L. Heterogeneity of paclitaxel distribution in different tumor models assessed by MALDI mass spectrometry imaging. *Sci Rep*. 2016;6:39284.
72. Longuespee R, Baiwir D, Mazzucchelli G, Smargiasso N, De Pauw E. Laser Microdissection-Based Microproteomics of Formalin-Fixed and Paraffin-Embedded (FFPE) Tissues. *Methods Mol Biol*. 2018;1723:19-31.
73. Meding S, Martin K, Gustafsson OJ, Eddes JS, Hack S, Oehler MK, Hoffmann P. Tryptic peptide reference data sets for MALDI imaging mass spectrometry on formalin-fixed ovarian cancer tissues. *J Proteome Res*. 2013;12(1):308-15.
74. Januchowski R, Świerczewska M, Sterzyńska K, Wojtowicz K, Nowicki M, Zabel M. Increased Expression of Several Collagen Genes is Associated with Drug Resistance in Ovarian Cancer Cell Lines. *J Cancer*. 2016;7(10):1295-310.
75. Groseclose MR, Massion PP, Chaurand P, Caprioli RM. High-throughput proteomic analysis of formalin-fixed paraffin-embedded tissue microarrays using MALDI imaging mass spectrometry. *Proteomics*. 2008;8(18):3715-24.
76. Dmello C, Srivastava SS, Tiwari R, Chaudhari PR, Sawant S, Vaidya MM. Multifaceted role of keratins in epithelial cell differentiation and transformation. *J Biosci*. 2019;44(2).
77. Cheng F, Liu C, Lin CC, Zhao J, Jia P, Li WH, Zhao Z. A Gene Gravity Model for the Evolution of Cancer Genomes: A Study of 3,000 Cancer Genomes across 9 Cancer Types. *PLoS Comput Biol*. 2015;11(9):e1004497.
78. Zhao Z, Xiao S, Yuan X, Yuan J, Zhang C, Li H, Su J, Wang X, Liu Q. AHNAK as a Prognosis Factor Suppresses the Tumor Progression in Glioma. *J Cancer*. 2017;8(15):2924-32.
79. Cimas FJ, Manzano A, Baliu-Pique M, Garcia-Gil E, Perez-Segura P, Nagy A, Pandiella A, Gyorffy B, Ocana A. Genomic Mapping Identifies Mutations in RYR2 and AHNAK as Associated with Favorable Outcome in Basal-Like Breast Tumors Expressing PD1/PD-L1. *Cancers (Basel)*. 2020;12(8).

8 Eidesstattliche Versicherung

„Ich, ZHIYANG WU, versichere an Eides statt durch meine eigenhändige Unterschrift, dass ich die vorgelegte Dissertation mit dem Thema: Anwendung Massenspektrometrie basierter Technologie zur Entdeckung räumlicher Peptidsignaturen in der Krebsforschung / Application of mass spectrometry-based technology to discover spatial peptide signatures in cancer research selbstständig und ohne nicht offengelegte Hilfe Dritter verfasst und keine anderen als die angegebenen Quellen und Hilfsmittel genutzt habe.

Alle Stellen, die wörtlich oder dem Sinne nach auf Publikationen oder Vorträgen anderer Autoren/innen beruhen, sind als solche in korrekter Zitierung kenntlich gemacht. Die Abschnitte zu Methodik (insbesondere praktische Arbeiten, Laborbestimmungen, statistische Aufarbeitung) und Resultaten (insbesondere Abbildungen, Graphiken und Tabellen) werden von mir verantwortet.

Ich versichere ferner, dass ich die in Zusammenarbeit mit anderen Personen generierten Daten, Datenauswertungen und Schlussfolgerungen korrekt gekennzeichnet und meinen eigenen Beitrag sowie die Beiträge anderer Personen korrekt kenntlich gemacht habe (siehe Anteilserklärung). Texte oder Textteile, die gemeinsam mit anderen erstellt oder verwendet wurden, habe ich korrekt kenntlich gemacht.

Meine Anteile an etwaigen Publikationen zu dieser Dissertation entsprechen denen, die in der untenstehenden gemeinsamen Erklärung mit dem/der Erstbetreuer/in, angegeben sind. Für sämtliche im Rahmen der Dissertation entstandenen Publikationen wurden die Richtlinien des ICMJE (International Committee of Medical Journal Editors; www.icmje.org) zur Autorenschaft eingehalten. Ich erkläre ferner, dass ich mich zur Einhaltung der Satzung der Charité – Universitätsmedizin Berlin zur Sicherung Guter Wissenschaftlicher Praxis verpflichte.

Weiterhin versichere ich, dass ich diese Dissertation weder in gleicher noch in ähnlicher Form bereits an einer anderen Fakultät eingereicht habe.

Die Bedeutung dieser eidesstattlichen Versicherung und die strafrechtlichen Folgen einer unwahren eidesstattlichen Versicherung (§§ 156, 161 des Strafgesetzbuches) sind mir bekannt und bewusst.“

Datum

Unterschrift

9 Anteilserklärung an den erfolgten Publikationen

Zhiyang Wu hatte folgenden Anteil an den folgenden Publikationen:

Publication 1: Wu Z (alleinige Erstautorin), Hundsdoerfer P, Schulte JH, Astrahantseff K, Boral S, Schmelz K, Eggert A, Klein O. Discovery of Spatial Peptide Signatures for Neuroblastoma Risk Assessment by MALDI Mass Spectrometry Imaging. Cancers (Basel). 2021

IF: 6.126, Platz 37/244 Journal Summary List "ONCOLOGY" (2019)

I (Zhiyang Wu) performed all MS-associated experiments, chemical staining, image digitalization; programmed the excel macro linking MALDI-MS results to LC-MS/MS results; analyzed and interpreted the data such as MS-based data analysis, statistical analysis, data presentation, and wrote the manuscript. Figure 1, 2, Table 2, and supplementary Figure S1, S2, S3 and Table S1, S2, S3 result from my statistical analysis and data interpretation. Supplementary File S1 was encoded alone by me for linking MALDI-MSI data and LC-MS/MS data. Supplementary Table S4 result from application of encoded supplementary File 1 and my statistical analysis. The immunohistochemical staining was performed by iPath.Berlin and Figure 3 was graphically depicted by me. The patient samples and information were provided by Dr. Patrick Hundsdoerfer, Prof. Angelika Eggert and Prof. JH Shulte and Table 3 was composed by me. The original manuscript was written by me and revised by Dr. Oliver Klein, Dr. Kathy Astrahantseff and Prof. Angelika Eggert.

Publication 2: Kulbe H, Klein O, Wu Z, Taube ET, Kassuhn W, Horst D, Darb-Esfahani S, Jank P, Abobaker S, Ringel F, du Bois A, Heitz F, Sehouli J, Braicu EI. Discovery of Prognostic Markers for Early-Stage High-Grade Serous Ovarian Cancer by Maldi-Imaging. Cancers (Basel). 2020

IF: 6.162, Platz 31/229 Journal Summary List "ONCOLOGY" (2018)

I (Zhiyang Wu) performed all MS-associated experiments, hematoxylin and eosin stain, image digitalization, analyzed and interpreted MS-based data (portion about 30%). Figure 1, 2, 3 and Table 1 result from my statistical analysis and data interpretation. Supplementary Figure S1, Table S1 and S2 result from my statistical analysis.

Unterschrift des Doktoranden/der Doktorandin

10 Publications and Journal Summary list

Based on the extract from the ISI Web of Knowledge (https://intranet.charite.de/medbib/impact_faktoren_2019_fuer_zeitschriften_nach_fachgebieten/), the journal "Cancers" ranked 37 out of 244 journals in the category "Oncology" with impact factor 6.126 (2019).

Journal Data Filtered By: **Selected JCR Year: 2019** Selected Editions: SCIE,SSCI
 Selected Categories: **"ONCOLOGY"** Selected Category Scheme: WoS
Gesamtanzahl: 244 Journale

Rank	Full Journal Title	Total Cites	Journal Impact Factor	Eigenfactor Score
1	CA-A CANCER JOURNAL FOR CLINICIANS	39.917	292,278	0.093460
2	Nature Reviews Clinical Oncology	12.384	53,276	0.035980
3	NATURE REVIEWS CANCER	52.053	53,030	0.066030
4	LANCET ONCOLOGY	53.592	33,752	0.143420
5	JOURNAL OF CLINICAL ONCOLOGY	155.297	32,956	0.261940
6	Cancer Discovery	18.093	29,497	0.069280
7	CANCER CELL	41.064	26,602	0.095430
8	JAMA Oncology	13.794	24,799	0.064650
9	ANNALS OF ONCOLOGY	45.813	18,274	0.107060
10	Molecular Cancer	15.448	15,302	0.023990
11	Journal of Thoracic Oncology	18.136	13,357	0.038200
12	JNCI-Journal of the National Cancer Institute	36.018	11,577	0.045450
13	Trends in Cancer	2.351	11,093	0.010140
14	SEMINARS IN CANCER BIOLOGY	8.310	11,090	0.011730
15	Journal of Hematology & Oncology	6.732	11,059	0.015550
16	NEURO-ONCOLOGY	12.950	10,247	0.029050
17	CLINICAL CANCER RESEARCH	85.288	10,107	0.131520
18	Journal for ImmunoTherapy of Cancer	4.557	9,913	0.016030
19	CANCER RESEARCH	135.753	9,727	0.118680
20	Liver Cancer	1.131	9,720	0.002660
21	Journal of the National Comprehensive Cancer Network	6.912	9,316	0.020020

22	CANCER TREATMENT REVIEWS	9.427	8,885	0.017800
23	Cancer Immunology Research	6.969	8,728	0.026440
24	LEUKEMIA	25.819	8,665	0.048640
25	Blood Cancer Journal	2.800	8,023	0.010400
26	ONCOGENE	66.303	7,971	0.068320
27	Clinical and Translational Medicine	1.349	7,919	0.003280
28	npj Precision Oncology	500	7,717	0.001520
29	BIOCHIMICA ET BIOPHYSICA ACTA- REVIEWS ON CANCER	5.650	7,365	0.007800
30	CANCER LETTERS	34.162	7,360	0.044450
31	EUROPEAN JOURNAL OF CANCER	32.241	7,275	0.048170
32	Gastric Cancer	5.525	7,088	0.010730
33	JOURNAL OF EXPERIMENTAL & CLINICAL CANCER RESEARCH	9.316	7,068	0.014540
34	Therapeutic Advances in Medical Oncology	1.894	6,852	0.004260
35	Molecular Oncology	6.378	6,574	0.013820
36	CANCER AND METASTASIS REVIEWS	6.247	6,400	0.005940
37	Cancers	10.442	6,126	0.018740
38	Oncogenesis	2.775	6,119	0.007750

Article

Discovery of Spatial Peptide Signatures for Neuroblastoma Risk Assessment by MALDI Mass Spectrometry Imaging

Zhiyang Wu ¹, Patrick Hundsdoerfer ², Johannes H. Schulte ^{3,4,5}, Kathy Astrahantseff ³, Senguel Boral ⁶, Karin Schmelz ^{3,4,5}, Angelika Eggert ^{3,4,5,7} and Oliver Klein ^{1,7,*}

- ¹ BIH Center for Regenerative Therapies BCRT, Charité—Universitätsmedizin Berlin, 13353 Berlin, Germany; zhiyang.wu@charite.de
 - ² Department of Pediatric Oncology, Helios Klinikum Berlin-Buch, 13125 Berlin, Germany; patrick.hundsdoerfer@helios-gesundheit.de
 - ³ Department of Pediatric Oncology & Hematology, Charité—Universitätsmedizin Berlin, 13353 Berlin, Germany; johannes.schulte@charite.de (J.H.S.); kathy.astrahantseff@charite.de (K.A.); karin.schmelz@charite.de (K.S.); angelika.eggert@charite.de (A.E.)
 - ⁴ Partner Site Berlin, The German Cancer Consortium (DKTK), 10117 Berlin, Germany
 - ⁵ The German Cancer Research Center (DKFZ), 69120 Heidelberg, Germany
 - ⁶ Institute of Pathology, Charité—Universitätsmedizin Berlin, 10117 Berlin, Germany; senguel.boral@charite.de
 - ⁷ Berlin Institute of Health, Charité—Universitätsmedizin Berlin (BIH), 10178 Berlin, Germany
- * Correspondence: oliver.klein@charite.de; Tel.: +49-(0)30-450566143



Citation: Wu, Z.; Hundsdoerfer, P.; Schulte, J.H.; Astrahantseff, K.; Boral, S.; Schmelz, K.; Eggert, A.; Klein, O. Discovery of Spatial Peptide Signatures for Neuroblastoma Risk Assessment by MALDI Mass Spectrometry Imaging. *Cancers* **2021**, *13*, 3184. <https://doi.org/10.3390/cancers13133184>

Academic Editors: Fabio Pagni, Stefania Galimberti and Maria Valeria Corrias

Received: 23 April 2021

Accepted: 22 June 2021

Published: 25 June 2021

Publisher's Note: MDPI stays neutral with regard to jurisdictional claims in published maps and institutional affiliations.



Copyright: © 2021 by the authors. Licensee MDPI, Basel, Switzerland. This article is an open access article distributed under the terms and conditions of the Creative Commons Attribution (CC BY) license (<https://creativecommons.org/licenses/by/4.0/>).

Simple Summary: The childhood tumor, neuroblastoma, has a broad clinical presentation. Risk assessment at diagnosis is particularly difficult in molecularly heterogeneous high-risk cases. Here we investigate the potential of imaging mass spectrometry to directly detect intratumor heterogeneity on the protein level in tissue sections. We show that this approach can produce discriminatory peptide signatures separating high- from low- and intermediate-risk tumors, identify 8 proteins associated with these signatures and validate two marker proteins using tissue immunostaining that have promise for further basic and translational research in neuroblastoma. We provide proof-of-concept that mass spectrometry-based technology could assist early risk assessment in neuroblastoma and provide insights into peptide signature-based detection of intratumor heterogeneity.

Abstract: Risk classification plays a crucial role in clinical management and therapy decisions in children with neuroblastoma. Risk assessment is currently based on patient criteria and molecular factors in single tumor biopsies at diagnosis. Growing evidence of extensive neuroblastoma intratumor heterogeneity drives the need for novel diagnostics to assess molecular profiles more comprehensively in spatial resolution to better predict risk for tumor progression and therapy resistance. We present a pilot study investigating the feasibility and potential of matrix-assisted laser desorption/ionization mass spectrometry imaging (MALDI-MSI) to identify spatial peptide heterogeneity in neuroblastoma tissues of divergent current risk classification: high versus low/intermediate risk. Univariate (receiver operating characteristic analysis) and multivariate (segmentation, principal component analysis) statistical strategies identified spatially discriminative risk-associated MALDI-based peptide signatures. The AHNK nucleoprotein and collapsin response mediator protein 1 (CRMP1) were identified as proteins associated with these peptide signatures, and their differential expression in the neuroblastomas of divergent risk was immunohistochemically validated. This proof-of-concept study demonstrates that MALDI-MSI combined with univariate and multivariate analysis strategies can identify spatially discriminative risk-associated peptide signatures in neuroblastoma tissues. These results suggest a promising new analytical strategy improving risk classification and providing new biological insights into neuroblastoma intratumor heterogeneity.

Keywords: neuroblastoma; risk assessment; intratumor heterogeneity; peptide signatures; MALDI-MSI

toma with distinct evolutionary patterns that impact clinical behavior [14]. Previous extensive next-generation sequencing efforts by the global neuroblastoma community to catalog genetic aberrations in neuroblastoma [12,14–21] used primarily single diagnostic biopsies, and identified a low number of recurrent point mutations and translocations even in high-risk and relapsed neuroblastomas. One of these studies also included matched diagnostic and relapse samples from five patients, corroborating evidence of the genetic evolution of disease [20]. The demonstration of intratumor genetic heterogeneity and its evolution over disease course have assisted an expansion of tissue sample collection accompanying patient treatment and trials worldwide. In-depth analysis and further interpretation with respect to potential clinical implications will achieve a better grasp of the extent of intratumor heterogeneity in neuroblastoma to improve personalized patient treatment. Knowledge remains limited about the influence of both high intratumor heterogeneity and peptide signatures in neuroblastomas on disease progression and response to treatment. Tumor progression, in general, is known to be affected by tumor cellular interplay and the surrounding microenvironment [22]. Taken together, there is unmet need for reliable neuroblastoma risk classification that takes the tumor microenvironment and spatial heterogeneity into account.

Matrix-assisted laser desorption/ionization mass spectrometry imaging (MALDI-MSI) innovative technology combines the comprehensive mass spectrometric technique with a conventional histological evaluation. It allows unsupervised (unlabelled) analysis of molecules (e.g., metabolites, proteins, peptide, lipids and glycans) directly on a single tissue section, preserving their spatial coordinates and generating a molecular intensity map displaying the spatial relative molecule abundance [23–26]. MALDI-MSI has several advantages over other techniques, such as nano-desorption electrospray ionization (DESI), secondary ion mass spectrometry (SIMS) and liquid extraction surface analysis. MALDI-MSI requires less time to perform measurements, and provides better spatial resolution for a larger mass range, which are all important prerequisites for potential clinical application. The mass range of DESI and SIMS are limited to 2000 Da and 1000 Da, respectively. Spatial resolution of DESI and LESA are much lower than MALDI-MSI. In the present study, tryptic peptides ranging from 600 to 3500 Da were analyzed with 50 μm resolution, which could not have been achieved by the other techniques [27]. Direct identification of proteins, from which the peptides (acquired by MALDI-MSI) stem, remains limited to only a few abundant proteins. Several studies have recently demonstrated that high-resolution MSI data combined with microproteomics (high-resolution mass spectrometry) from microdissected tissue sections enables retention of an aspect of spatial specificity and accurate protein assignment (high mass accuracy) [28–30]. This is a promising strategy to explore potential disease-relevant protein markers in small patient collectives, but is not well suited for large-scale studies because of the longer processing time both for microdissection and mass spectrometry and the higher cost. In contrast, spatially distinct signatures of peptide spectra, such as those extracted from MALDI tissue imaging data, can be obtained in high-throughput in a clinically feasible time frame at a lower cost, and could provide a new dimension to the current classification of distinct patient subgroups, and potentially assist prediction of disease progression and/or resistance development [31–34]. Therefore, MALDI imaging is a promising technology to aid histopathology tissue assessment in routinely used large-scale formats. MALDI-MSI has been used to classify tumor types [35], to predict a therapeutic strategy [36,37] and to act as a biomarker for indicating response to treatment [38,39]. This technology can interpret molecular tumor composition while preserving spatial morphology, providing important insights into tumor heterogeneity and its impact on tumor biology.

In this pilot study, we investigated the feasibility and potential of MALDI-MSI combined with uni- and multivariate statistical strategies to (1) determine discriminative peptide signatures for neuroblastomas designated as high or lower risk groups as a starting point for subsequent more fine-tuned comparisons in the same patient subgroup and (2) to explore neuroblastoma intratumor heterogeneity for the first time on the protein level. Our aim was to reach an initial proof-of-concept that peptide signatures are capable of adding

1. Introduction

Neuroblastoma is a pediatric cancer arising in approximately 1 of 100,000 children under 15 years of age in Germany [1]. It is the most common malignant solid tumor diagnosed in infants with a median age at diagnosis of 17 months [2]. The tumor derives from neural crest cells of sympathoadrenal lineage, and can develop anywhere in the sympathetic nervous system. About 65% of primary tumors arise in the adrenal medulla or lumbar sympathetic ganglia, while the rest arise in the neck, chest and pelvis. Clinical behavior and outcome is highly diverse, ranging from low-risk disease with the highest rate of spontaneous regression in all cancers to treatment-refractory lethal disease progression or treatment-resistant relapse occurring in high-risk disease despite aggressive multimodal treatment [3,4]. Consequentially, neuroblastoma treatment recommendations range from mere observation or surgical resection alone to very aggressive therapy protocols including high-dose chemotherapy, irradiation and immunotherapy [5]. To address the issue of appropriate therapy intensity, a common international staging and risk classification system (INSS/INRG) has been developed [6,7]. In Europe, patients have been classified into three risk groups following the criteria described in Table 1 [5]. The additional International Neuroblastoma Pathology Classification (INPC) criterion is exclusively used in the USA [8]. Neuroblastoma samples from patients with low and intermediate risk (INSS/INRG) were grouped together for this retrospective study and high-risk patients were defined as in Table 1 (Stage 4 > 18 months plus all *MYCN*-amplified cases).

Table 1. Treatment classification of neuroblastoma patients.

INSS/INRG Staging	Age at Diagnosis (Months)	<i>MYCN</i> Status	Chromosome 1p Status	Treatment Risk Group
1		not amplified	normal	Low
		amplified		High
2		not amplified	normal	Low
			deletion/imbalance	intermediate
		amplified		High
		3	<24	not amplified
≥24	not amplified		normal	intermediate
	not amplified		deletion/imbalance	
		amplified		High
4s/MS	<18	not amplified	normal	Low
		amplified		High
4/M	<18	not amplified		intermediate
		≥18	amplified	High

INSS = International Neuroblastoma Staging System. INRG = International Neuroblastoma Risk Group (INRG) Staging System.

MYCN amplification was the first identified clinically relevant molecular biomarker for neuroblastoma [9], and remains a strong single predictor for unfavorable outcome. However, a recent report from the INRG revealed that the prognostic impact of *MYCN* amplification is greatly dependent on the context of clinical and biological features [10]. In Germany, current risk stratification for the ongoing clinical trials is based on patient age, stage, *MYCN* amplification and the result of an mRNA-based molecular classifier [11] that is continuously further improved on transcriptomic and genomic levels [12]. We previously demonstrated spatial intratumor genetic heterogeneity and first evidence of branched evolution in neuroblastoma by bulk sequencing of paired diagnostic and relapse tumor samples [13]. A more recent sequencing effort has demonstrated extensive genetic intratumour heterogeneity in neuroblas-

toma with distinct evolutionary patterns that impact clinical behavior [14]. Previous extensive next-generation sequencing efforts by the global neuroblastoma community to catalog genetic aberrations in neuroblastoma [12,14–21] used primarily single diagnostic biopsies, and identified a low number of recurrent point mutations and translocations even in high-risk and relapsed neuroblastomas. One of these studies also included matched diagnostic and relapse samples from five patients, corroborating evidence of the genetic evolution of disease [20]. The demonstration of intratumor genetic heterogeneity and its evolution over disease course have assisted an expansion of tissue sample collection accompanying patient treatment and trials worldwide. In-depth analysis and further interpretation with respect to potential clinical implications will achieve a better grasp of the extent of intratumor heterogeneity in neuroblastoma to improve personalized patient treatment. Knowledge remains limited about the influence of both high intratumor heterogeneity and peptide signatures in neuroblastomas on disease progression and response to treatment. Tumor progression, in general, is known to be affected by tumor cellular interplay and the surrounding microenvironment [22]. Taken together, there is unmet need for reliable neuroblastoma risk classification that takes the tumor microenvironment and spatial heterogeneity into account.

Matrix-assisted laser desorption/ionization mass spectrometry imaging (MALDI-MSI) innovative technology combines the comprehensive mass spectrometric technique with a conventional histological evaluation. It allows unsupervised (unlabelled) analysis of molecules (e.g., metabolites, proteins, peptide, lipids and glycans) directly on a single tissue section, preserving their spatial coordinates and generating a molecular intensity map displaying the spatial relative molecule abundance [23–26]. MALDI-MSI has several advantages over other techniques, such as nano-desorption electrospray ionization (DESI), secondary ion mass spectrometry (SIMS) and liquid extraction surface analysis. MALDI-MSI requires less time to perform measurements, and provides better spatial resolution for a larger mass range, which are all important prerequisites for potential clinical application. The mass range of DESI and SIMS are limited to 2000 Da and 1000 Da, respectively. Spatial resolution of DESI and LESA are much lower than MALDI-MSI. In the present study, tryptic peptides ranging from 600 to 3500 Da were analyzed with 50 μm resolution, which could not have been achieved by the other techniques [27]. Direct identification of proteins, from which the peptides (acquired by MALDI-MSI) stem, remains limited to only a few abundant proteins. Several studies have recently demonstrated that high-resolution MSI data combined with microproteomics (high-resolution mass spectrometry) from microdissected tissue sections enables retention of an aspect of spatial specificity and accurate protein assignment (high mass accuracy) [28–30]. This is a promising strategy to explore potential disease-relevant protein markers in small patient collectives, but is not well suited for large-scale studies because of the longer processing time both for microdissection and mass spectrometry and the higher cost. In contrast, spatially distinct signatures of peptide spectra, such as those extracted from MALDI tissue imaging data, can be obtained in high-throughput in a clinically feasible time frame at a lower cost, and could provide a new dimension to the current classification of distinct patient subgroups, and potentially assist prediction of disease progression and/or resistance development [31–34]. Therefore, MALDI imaging is a promising technology to aid histopathology tissue assessment in routinely used large-scale formats. MALDI-MSI has been used to classify tumor types [35], to predict a therapeutic strategy [36,37] and to act as a biomarker for indicating response to treatment [38,39]. This technology can interpret molecular tumor composition while preserving spatial morphology, providing important insights into tumor heterogeneity and its impact on tumor biology.

In this pilot study, we investigated the feasibility and potential of MALDI-MSI combined with uni- and multivariate statistical strategies to (1) determine discriminative peptide signatures for neuroblastomas designated as high or lower risk groups as a starting point for subsequent more fine-tuned comparisons in the same patient subgroup and (2) to explore neuroblastoma intratumor heterogeneity for the first time on the protein level. Our aim was to reach an initial proof-of-concept that peptide signatures are capable of adding

a new useful dimension of novel information to current clinical and transcriptomic risk classification schemes for neuroblastoma.

2. Results

2.1. Discriminative Peptide Signatures Can Be Derived from MALDI-MSI Data to Identify Different Tumor Features

Here we evaluated the technical feasibility of MALDI-MSI to identify potential discriminative protein features of more aggressive neuroblastomas (high-risk) from formalin-fixed, paraffin-embedded (FFPE) tissue sections. Tissue samples were diagnostic biopsies from primary neuroblastomas categorized as high ($n = 5$) or other risk groups (low or intermediate risk, $n = 4$). Peptide signatures extracted from the analyzed tissue samples yielded 501 aligned m/z values in a mass range for tryptic peptides (m/z value range: 800–3200). Neuroblastoma cell-rich tumor regions yielded 397 aligned m/z values (Table S1). Representative average spectra of whole sections are shown in Figure S1. Peptide signatures were identified that characterized different tissue regions using bisecting k-means clustering, an unsupervised multivariate segmentation analysis, conducted on MALDI-MSI data from the tissue sections. Segmentation analysis produced two clusters shown as segmentation maps (Figure 1) that corresponded well to tissue areas in the tumors that were either tumor cell rich (>80%) or poor (defined by the reference pathologist). Consequently, peptide signatures obtained from MALDI-MSI data can distinguish tumor regions with a high tumor cell content from those with <80% tumor cell content directly from fixed tissue sections. To determine whether signatures could be defined to discriminate high from other risk groups, we performed a segmentation analysis (bisecting k-means) across only the regions with >80% tumor cell content, as defined by the pathologist. Unsupervised segmentation analysis of m/z values from these areas produced three segment clusters with different peptide signatures in high-risk tumors, (percentage of each peptide signature contributing to the tumor cell-rich region in Table S2), but only a single segment cluster in neuroblastomas were classified as lower risk (Figure 1). These data illustrate molecular intratumor heterogeneity for the first time on the protein level in high-risk tumors. Peptide signatures can be extracted from MALDI-MSI data by unsupervised clustering that correctly identify tumor cell-rich regions in neuroblastomas and discriminate high-risk neuroblastomas from lower risk groups.

Univariate analysis of MALDI-MSI data has the potential to determine which single peptides are the most discriminative between neuroblastoma tissues from different risk groups. We applied receiver operator characteristic (ROC) analysis to the total 397 aligned m/z peaks from tumor cell-rich areas in paired comparisons of tissue sections from high or other neuroblastoma risk groups. Differential spatial peptide intensity distributions in tissue samples from the two risk groupings determined the discriminatory power of individual peptides. Wilcoxon rank sum testing was applied to the total 397 aligned m/z peaks, resulting in 206 statistically significant m/z values (AUC values of >0.8 or <0.2; $p < 0.001$). From these, we show the five peptides with the strongest discriminatory values in Figure 2. Three peptides (m/z values: 1707.68, 1775.79 and 1832.79 Da) had significantly higher intensity distributions and two peptides (m/z values: 766.48 and 1178.73 Da) had significantly lower intensity distributions in tumor cell-rich regions from high-risk neuroblastoma tissue sections. To explore the potential of the most discriminatory peptides in the peptide signatures to discriminate high from other risk groups, principle component analysis was applied to the 206 statistically significant m/z values (AUC values of >0.8 or <0.2; $p < 0.001$). Principal component 1 (PC-1) mainly captured the differences within the tumor cell-rich regions in tumors from different risk groups and shows an increased intensity distribution in cell-rich tumor regions in high-risk neuroblastomas (Figure S2). Since 62% of the variance was explained by the first principal component (Figure S2), these findings demonstrate that both unsupervised and supervised statistical approaches result in discriminatory peptide signatures for high or other risk designations using MALDI-MSI data from neuroblastoma tissue sections.

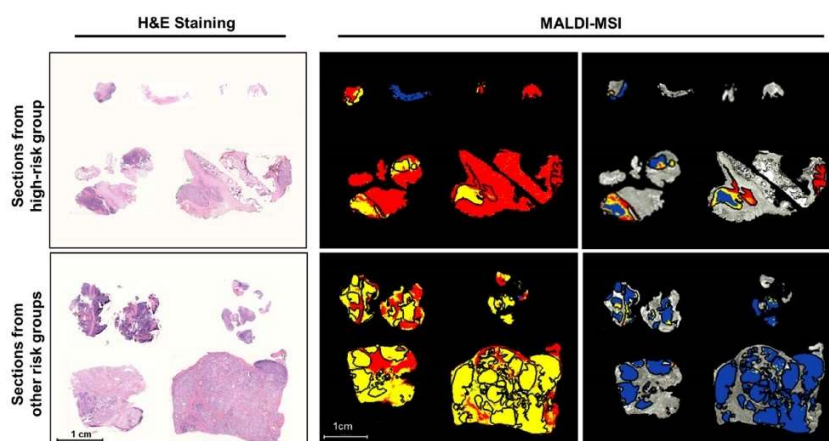


Figure 1. MALDI imaging identifies high-risk neuroblastomas by heterogeneous peptide signatures in tumor cell-rich regions. Sections from primary neuroblastomas with high or other risk classifications are shown with hematoxylin and eosin (H&E) staining for tissue section orientation in segmentation maps of MALDI-MSI analysis. Segments (indicated by different colors) represent different proteomic clusters generated by bisecting k-means clustering. Black lines surround tumor areas with >80% tumor cell content (annotated by the reference pathologist). Signatures derived from segmentation clustering across the whole tissue section are shown in the middle column and peptide signatures derived only across the tumor cell-rich areas in the sections shown on the right. Colors represent the same proteomic clusters in the 2 images in the middle column and the 2 images in the right column, but not between the middle and right images.

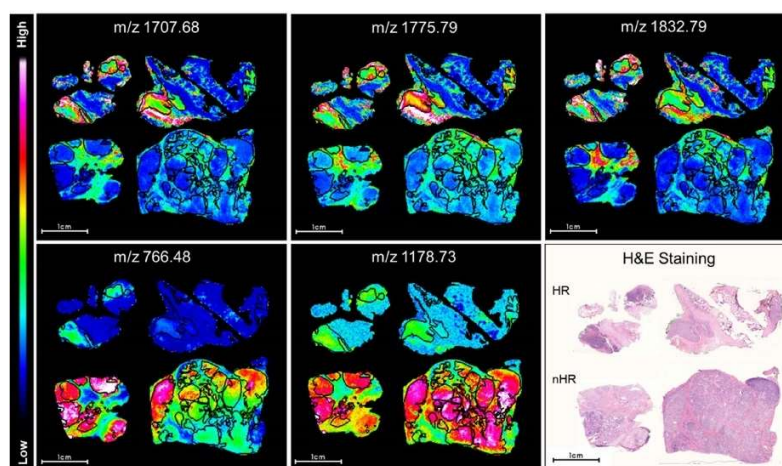


Figure 2. Selected peptides have differential intensity distributions in neuroblastoma cell-rich tumor regions between high and other risk groups. Relative peptide expression (color bar) is shown for MALDI m/z ion peaks with the highest significant area under the curve (AUC values >0.85 , $p < 0.001$, top row) in receiver operator characteristic (ROC) analysis and the lowest AUC values (AUC < 0.3 , $p < 0.001$, bottom MALDI images). MALDI-MSI ion images are shown for the same set of neuroblastoma tissue sections categorized either as high (HR) or other risk groups (nHR) in each image. Black lines surround tumor areas with >80% tumor cell content (annotated by the reference pathologist). Hematoxylin and eosin (H&E) staining in sections is shown for orientation.

2.2. Discriminative Proteins Were Identified from Neuroblastoma Tissue Sections Based on MALDI-MSI Data

To identify the proteins corresponding to the discriminatory tryptic peptide fragments, we used a bottom-up nanoliquid chromatography-tandem mass spectrometry (nanoLC-MS/MS) approach in adjacent tissue sections. This analysis assigned 147 of the 206 m/z values (Table S3) shown to be discriminative in ROC analysis ($AUC > 0.7$ or $AUC < 0.3$, $p < 0.001$) to peptides corresponding to proteins identified by nanoLC-MS/MS. According to guidelines, corresponding proteins to m/z values are correctly identified when the validating approach (nanoLC-MS/MS in this case; Table S4) identifies at least two peptides (detected in MALDI-MSI) from the same protein, whose spatial differential intensities are similar and correlated in the same tissue region (correlation coefficients) [40]. These guidelines were fulfilled for 8 proteins (Table 2) that corresponded to 18 MALDI-MSI m/z values. Of these 8 proteins, differential intensity distributions for m/z values from 6 (14 m/z values) proteins were verified using MALDI-MSI data obtained from 10 arrayed cores from neuroblastoma tissue areas having $>80\%$ tumor cell content (Table 2; selected ion intensity maps from TMA shown in Figure S2). Two peptides (m/z values in Table S3) from the proteins, COL1A2, COL6A3, HSPA5, HIST1H2BC, KRT9, AHNAK and NID2, were present at significantly higher intensities in tumor cell-rich areas in high-risk neuroblastomas.

This group is enriched for extracellular matrix components (COL1A2, COL6A3 and NID2) and proteins associating with or regulating cytoskeletal proteins (AHNAK) as well as a cytoskeletal protein (KRT9). The two peptides assigned to CRMP1 had significantly lower intensities in tumor cell-rich areas from high-risk neuroblastomas compared to lower risk classifications. We selected two representative proteins from those identified for validation in adjacent neuroblastoma tissue sections using immunohistochemistry. AHNAK expression was higher in tumor cell-rich areas in high-risk neuroblastomas than in the lower risk groups (Figure 3). Reciprocally, CRMP1 expression was lower in high-risk neuroblastomas compared with lower risk groups (Figure 3), validating our MALDI-MSI profiling results. Our data strongly support that the 1832.79 m/z peak captured by MALDI-MSI have a higher intensity in tumor cell-rich regions of high-risk neuroblastomas is a tryptic peptide from AHNAK, an approximately 700 kD scaffold protein not previously published in the context of neuroblastoma. It was initially reported to be associated with neuroblast differentiation (reviewed in Davis2014) [41], but more recent studies have also pointed to an important role in promoting cellular proliferation, migration and epithelial-mesenchymal transition (EMT), processes leading to a short disease-free survival time and poor outcome of aggressive cancers including pancreatic ductal adenocarcinoma [42]. Likewise, the relatively low intensity 922.50 m/z peak in MALDI-MSI of high-risk neuroblastomas is a tryptic peptide from CRMP1, a marker for neuronal differentiation that is involved in neuronal outgrowth and guidance. It has been previously used in mRNA panels for neuroblastoma MRD and tumor-initiating cells [43–46]. These findings strongly support the correct identification of these 8 proteins as sources for 18 tryptic peptides detected by MALDI-MSI in FFPE neuroblastoma tissue sections and validate AHNAK and CRMP1 as discriminatory protein markers with potentially interesting and plausible biological roles.

Table 2. Differential intensity distributions of peptides (MALDI-MSI) and their corresponding proteins in tissue sections from neuroblastomas in high or other risk groups.

MALDI IMS m/z Value	ROC [AUC] for High Versus other Risk *	ROC [AUC] HR/nHR TMA †	Significance Rating-WRS	LC-MS/MS [Mr + H+ cal.]	Scores §	Deviation [Da]	Correlation Coefficient	Protein Symbol	Protein
868.4930	0.85	0.73	<0.001	868.46	48.1	0.03	0.38		
1562.7700	0.91	0.74	<0.001	1562.79	127.	0.02	0.64	COL1A2	Collagen type I alpha 2 chain
2026.9100	0.86	0.73	<0.001	2027.02	65.8	0.11	0.36		
1459.8500	0.72	0.66	<0.001	1459.86	40.5	0.01	0.38	COL6A3	Collagen type VI alpha 3 chain
2056.9200	0.88	0.63	<0.001	2057.04	59.4	0.12	0.32		
766.4820	0.08	0.28	<0.001	766.46	21.7	0.03	0.44	CRMP1	Collapsin response mediator protein 1
922.4990	0.14	0.34	<0.001	922.51	22.3	0.02	0.40	HSPA5	Heat shock protein family A (Hsp70) member 5
1833.9900	0.87	0.67	<0.001	1833.91	65.1	0.08	0.40		
2042.2200	0.85	0.73	<0.001	2042.05	25.6	0.17	0.32		
1477.8600	0.90	0.75	<0.001	1477.79	28.1	0.07	0.41		
1743.6800	0.82	0.58	<0.001	1743.82	96.2	0.14	0.58	HIST1H2BC	H2B clustered histone 4
1775.7900	0.90	0.70	<0.001	1775.81	123.	0.02	0.55		
1586.7700	0.90	0.74	<0.001	1586.77	89.4	0.00	0.47	KRT9	Keratin 9
2705.2800	0.86	0.78	<0.001	2705.16	67.9	0.12	0.44		
1267.5000	0.87	0.74	<0.001	1267.65	63.9	0.12	0.38	AHNAK	AHNAK nucleoprotein
1832.7900	0.92	0.70	<0.001	1832.88	44.7	0.09	0.39		
1706.7800	0.87	0.74	<0.001	1706.78	31.2	0.00	0.31	NID2	Nidogen 2
2455.3600	0.79	0.72	<0.001	2455.17	34.9	0.19	0.33		

* Calculated from data obtained from regions in whole tissue sections with >80% tumor cell content. † TMA = tissue microarray (arrayed neuroblastom tissue cores from areas with >80% tumor cell content). § M(Olecular Weight Search score [47].

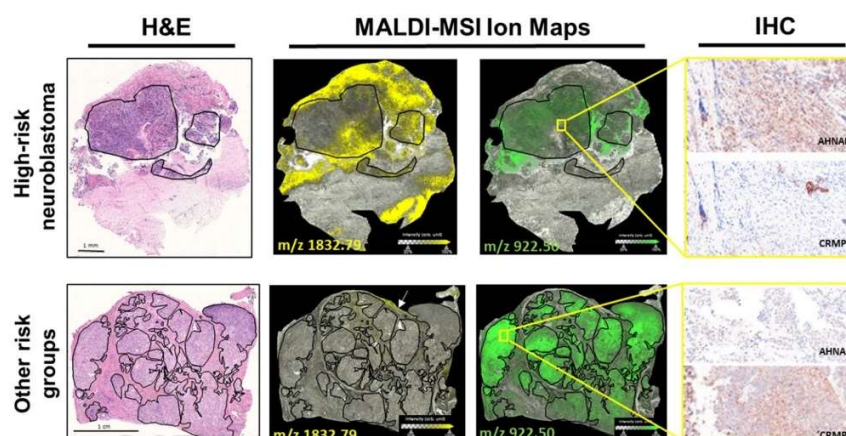


Figure 3. Validation of two discriminative protein markers for neuroblastoma risk in tissue sections. Shown are representative tissue sections from neuroblastoma designated high-risk (HR) and as other risk groups (nHR). MALDI-MSI ion maps for one peptide (m/z 1832.79 Da) assigned to AHNAK and one peptide (m/z 922.50 Da) assigned to CRMP1 are shown next to the corresponding sections stained with hematoxylin and eosin (H&E) for orientation. Black lines border areas with $>80\%$ tumor cell content. Immunohistochemical (IHC) detection of AHNAK and CRMP1 is shown for the regions surrounded by the yellow squares in the expanded image ($400\times$ magnification).

Taken together, MALDI-MSI is feasible for the investigation of molecular cell phenotypes in histologically homogeneous appearing areas of high-risk neuroblastoma. Our data show these cells to be molecularly heterogeneous, and we identified discriminatory peptide signatures for high-risk neuroblastoma. From the discriminatory peptides, 18 could be assigned to 8 proteins, and differential AHNAK and CRMP1 expression was immunohistochemically validated in tissue sections. AHNAK shows intense and distinct staining in the tumor cell-rich regions in high-risk neuroblastomas in comparison to other risk groups (slight staining). In contrast, CRMP1 staining is intense in tumor cell-rich regions of neuroblastomas with other risk designations and only exhibited slight staining in the high-risk group. A detailed analysis of their biological roles in neuroblastoma is warranted.

3. Discussion

MALDI-MSI is a unique mass spectrometric technique that combines spatial molecular analysis with conventional histological assessment. Neither labels nor prior knowledge of molecular targets is necessary to simultaneously analyze the distribution of hundreds of peptides within a tissue, and sample preparation is automated and relatively simple. These advantages make MALDI-MSI an optimal tool to identify biomarkers and explore tumor complexity. We have previously used MALDI-MSI on epithelial ovarian cancer samples to discriminate among four different histotypes [48] and identify a proteomic signature in early-stage disease that is a prognostic marker for recurrence [49]. Here, we applied this technique to expose spatially resolved proteomic changes directly on intact neuroblastoma FFPE tissue sections. The acquired spatial peptide signatures resulted in 11 identified proteins, most of which are associated with the extracellular matrix and cytoskeleton, which enabled us to distinguish high-risk neuroblastomas from the tissue sections independently of conventional histology. Differential expression of the identified discriminative proteins, AHNAK and CRMP1, was immunohistochemically confirmed in sections, and discriminative spatial intensities of m/z peaks were validated in microarrayed tissue cores from tumor cell-rich regions in neuroblastomas. Importantly, we show

that MALDI-MSI is capable of detecting molecular heterogeneity on the protein level in neuroblastoma tissue sections.

Due to their heterogeneous distribution throughout the whole tissue sections, not all peptides detected by MALDI-MSI in the whole sections were detected in cores in the tissue microarray (Figure S3). Depending on the area of the entire tumor from which the core is obtained, this information can be lost, pointing to significant limitations in the use of tissue microarrays to detect tumor heterogeneity in comparison to MALDI-MSI on whole tissue sections as a new, more comprehensive and precise diagnostic option. Several studies demonstrate that MALDI-MSI is a powerful tool to aid pathology for different cancer types [26,50,51]. Our study emphasizes that the investigation of whole tumor tissue sections are promising to directly explore molecular tumor heterogeneity. Different areas in a tumor section, while being homogeneous in morphological structure, can contain differences in molecular composition [52,53]. Previous studies demonstrate that MALDI-MSI is suitable to determine molecular subtypes in high-grade serous ovarian cancer [31,49] or to perform tumor classification. MALDI-MSI is shown here to be suitable to acquire spatial peptide signatures with potential as tools to directly examine molecular heterogeneity from diagnostic neuroblastoma tissue sections and potentially assist discrimination of high- or ultrahigh-risk disease after testing in a larger patient cohort.

International risk classification of neuroblastoma, based on clinical criteria plus *MYCN* amplification and recently complemented by transcriptomic parameters, has proven its usefulness for making therapy decisions and for disease management. Adding diagnostic information on the protein level might have the potential to further improve fine-tuning and the precision of current risk classification approaches. With this paper, we provide the proof-of-concept for the technical feasibility of this approach. Even more important is the consideration of tumor heterogeneity for the future selection of reliable prognostic or predicative biomarkers and signatures.

Tumors are complex tissues interposing cancer cells with distinct cell types and structures including extracellular matrix, stromal cells, blood vessels and cellular immune components. Neighboring cells in the tumor stroma, best described by combining proteomic profiling with histological evaluation, also influence tumor actions and phenotypes [54]. This diversity of cellular and molecular composition results in intratumor heterogeneity as a key factor contributing to therapeutic failure, drug resistance and recurrence [55]. Neuroblastoma proteomes have been previously studied using tandem LC-MS in bulk tissue homogenates from each tumor sample, and have defined large-scale, up- or down-regulated proteins associated with high risk [56,57]. The most commonly used (LC-MS, 2-dimensional electrophoresis) proteomic methods use tissue homogenates and cannot assign protein alterations to morphological structures. Due to the high intratumor heterogeneity, information about protein alterations may be lost.

In addition to providing proof-of-concept for the technical feasibility of MALDI-MSI, the potential risk classification-relevant peptide signatures of neuroblastoma are described to open new avenues to assess tumor heterogeneity. Our data also identified two specific proteins with potentially important roles in neuroblastoma biology and disease course. Our data showed a lower intensity distribution of CRMP1 in high-risk neuroblastomas and reciprocally higher intensity distribution in low- and intermediate-risk neuroblastomas. This is well in line with the reported role of CRMP1 in neuronal differentiation and its previous use as a marker gene in neuroblastoma gene expression panels as well as its usefulness as a prognostic and diagnostic marker in other cancers [58]. A detailed functional assessment of the biological role of CRMP1 in neuroblastoma is warranted in subsequent studies, but is beyond the scope of this paper. The lower mass accuracy of the presented workflow makes it more susceptible to false-positive protein assignments. Consequently, selected *m/z* values were matched to their source proteins to examine whether the differential peptide signature includes peptides from biologically feasible proteins in neuroblastoma, and subsequently validated their differential expression in tumor sections using immunohistochemistry. High- or ultrahigh-resolution mass spectrometry

combined with microproteomics from microdissected regions in consecutive tissue sections is a promising technology for accurate extensive spatial proteomic characterization and quantification [28,29]. However, its use in high-throughput workflows, such as for large sample cohorts, is limited. This is an important prerequisite to explore potential clinical applications for alternative or improved risk assessment in a large tumor sample cohort.

We identified AHNAK as a marker protein highly expressed in high-risk neuroblastoma, from which tryptic peptides have high intensity distributions in tumor cell-rich regions of sections analyzed by MALDI-MSI. AHNAK has not been previously associated with neuroblastoma, but has been implicated in several cellular functions associated with cancer, including being listed one of six putative cancer genes involved in the evolution of nine cancer types across 3000 cancer genomes [59]. Most interestingly, AHNAK has been reported to be associated with enhanced proliferation and migration in rhabdomyosarcoma [60] among other cancers as well as supporting EMT in hepatoblastoma [61], endometrial [62] and lung [63] cancer cells as well as pancreatic ductal adenocarcinoma [42] and gastric cancer [64]. A similar role in neuroblastoma would be well in line with our previous observations that several signaling elements involved in EMT regulation are mutated in relapsed neuroblastomas [13]. However, the role of AHNAK in cancer appears to be tissue-specific, as other reports also point to a potential role as a tumor suppressor in glioma [65] and breast cancer [66]. This may be due to the fact that AHNAK achieves its breadth of activity by being a large protein that moderates multiprotein complex function by acting as a scaffold to tether activity either in the nucleus or at the plasma membrane and having its own phosphorylation sites that alters interactivity and intracellular localization [41]. The neuroblastoma-specific biological role of AHNAK has to be evaluated in subsequent detailed studies beyond the scope of this paper. Interestingly, AHNAK peptide intensity in MALDI imaging of low- and intermediate-risk neuroblastoma sections was also occasionally high in areas with <80% tumor cell content. While we can only speculate about the source of expression, these could represent subclones of molecularly evolving neuroblastoma cells or groups of neuroblastoma cells that are held back from evolving by influences of the surrounding stroma.

AHNAK was also occasionally upregulated in some area of the tumor stroma. Due to the barrier of natural structure including connective tissues, fibroblasts, immune cells and vasculature, common mass spectrometry methods are limited and cannot expose the molecular composition of the stromal compartment. MALDI-MSI is able to map protein changes in both areas that clearly exhibit the cellular interaction between malignant cancer cells and their environment and provides new insights for understanding neuroblastoma tumorigenesis and progression.

4. Materials and Methods

4.1. Patient and Sample Cohort

All samples were collected from primary neuroblastomas (located in the adrenal) for diagnostic purposes and were conserved in the local pathology departments as FFPE tissue blocks. Diagnosis of neuroblastoma was confirmed by an experienced reference pathologist and risk classification for patients, performed by the national neuroblastoma trial group, was based on definitions of the German BFM-NB2004 Trial and recommendations by the German Society for Pediatric Oncology and Hematology (GPOH). The comprehensive patient data set included sex, age, tumor INSS stage at diagnosis, presence or absence of *MYCN* amplification in the diagnostic tumor sample (detected by FISH), INRG risk classification and outcome, in particular diagnosis of relapse and death of disease (Table 3). Follow-up time for patients in this cohort was at least 4 years or until death of disease. Tissue areas with >80% tumor cell content were identified by the pathologist for both stancing tissue cores to create the tissue microarray and annotating sections analyzed by MALDI-MSI. Sample numbers 1–5 (high-risk) and 10–13 (other risk designations, Table 3) were used in an analyses of whole tissue sections (MALDI-MSI and immunohistochemistry). Cores from sample numbers 4, 10, 12 and 13 were also stanced for the tissue microarray together with tissue cores from 6

tumor samples from independent patients. Tumor cores were removed from FFPE tissue blocks using a 1.0-mm diameter hollow needle as tissue cores, which were arrayed in a recipient paraffin block (Table 3).

Table 3. Clinicopathological characteristics for our patient cohort.

ID	Sex	Age (Years)	INSS Stage	MYCN Amplification	Risk Classification (at Diagnosis)	Disease Recurrence	Death	Metastasis
1	F	0.3	3	+	high	-	-	No
2	M	0.6	2	+	high	-	-	No
3	M	1	3	+	high	-	+	No †
4	M	1.4	4	+	high	-	-	Yes
5	F	1.2	4	+	high	+	+	Yes
6	M	2.8	4	+	high	+	+	Yes
7	M	7.8	4	-	high	-	-	Yes
8	F	8	4	+	high	-	-	Yes
9 ‡	M	1.2	3	-	high	+	-	No ‡
10	F	2.4	1	-	low	-	-	No
11	F	0.8	4	-	intermediate	-	-	Yes
12	M	0.1	4s	-	low	-	-	Yes
13	F	0.1	3	mosaic	low	-	-	No
14	F	5.9	3	-	intermediate	-	-	No
15	M	1.9	2	-	low	-	-	No

† Disease in this patient later metastasized and was upgraded to INSS stage 4. ‡ This patient had multiple relapses after first-line therapy and was treated for high-risk disease in relapse therapy.

4.2. Tissue Immunohistochemistry

FFPE tissue sections (whole sections) were dewaxed and subjected to a heat-induced epitope retrieval step. Endogenous peroxidase was blocked by hydrogen peroxide prior to incubation with a monoclonal antibody against human CRMP1 (EP14521, Abcam, Cambridge, UK), followed by incubation with EnVision+ HRP-labeled polymer (Agilent Technologies Inc., Santa Clara, CA, USA) and visualization using the OPAL system (Akoya Biosciences Inc., Marlborough, MA, USA) according to manufacturer's instructions. After protein inactivation, sections were incubated with a polyclonal antibody against human AHNAK (PA5-53890, Invitrogen, Thermo Fisher Scientific, Waltham, MA, USA), followed by incubation with the EnVision+ polymer (Agilent Technologies Inc.) and visualization using the OPAL system. Nuclei were stained with 4',6-diamidino-2'-phenylindole dihydrochloride (DAPI; Merck KGaA, Darmstadt, Germany) and slides were mounted in Fluoromount G (Southern Biotech, Birmingham, AL, USA). Multispectral images were acquired using a Vectra® 3 imaging system (Akoya Biosciences Inc., Marlborough, MA, USA).

4.3. MALDI-MSI

All FFPE tissue sections (whole sections and tissue microarrays) were cut to 6- μ m thickness by microtome (HM325, Thermo Fisher Scientific, Waltham, MA, USA) and mounted onto conductive glass slides coated in indium tin oxide (Bruker Daltonik GmbH, Bremen, Germany). Sections were preheated to 80 °C for 15 min before deparaffinization. Paraffin was removed in xylene, and tissue sections were processed through 100% isopropanol and successive hydration steps of 100% ethanol followed by 96%, 70%, and 50% ethanol, each for 5 min. Sections were fully rehydrated in Milli-Q-purified water (Merck KGaA, Darmstadt, Germany). Heat-induced antigen retrieval was performed in MilliQ-water for 20 min in a steamer. After drying slides for 10 min, tryptic digestion was performed. An automated spraying device (HTX TM-Sprayer, HTX Technologies LLC, ERC GmbH, Riemerling, Germany) was used to deliver, onto each section, 16 layers of tryptic solution (20 μ g Promega® Sequencing Grade Modified Porcine Trypsin in 800 μ L digestion buffer-20 mM ammonium bicarbonate with 0.01% glycerol) at 30 °C. Tissue

sections were incubated for 2 h at 50 °C in a humidity chamber saturated with potassium sulfate solution, then the HTX™ Sprayer applied 4 layers of the matrix solution (7 g/L *α*-cyano-4-hydroxycinnamic acid in 70% acetonitrile and 1% trifluoroacetic acid) at 75 °C. MALDI imaging was conducted on the rapifleX® MALDI TissueTyper® (Bruker Daltonik GmbH, Bremen, Germany) in reflector mode with the detection range of 800–3200 *m/z*, 500 laser shots per spot, a 1.25 GS/s sampling rate and raster width of 50 μm. FlexImaging 5.1 and flexControl 3.0 software (Bruker Daltonik GmbH) coordinated the MALDI imaging run. External calibration was performed using a peptide calibration standard (Bruker Daltonik GmbH). The matrix was removed from tissue sections with 70% ethanol after MALDI imaging, and sections were stained with hematoxylin and eosin for histology. Tumor regions with >80% tumor cells were digitally annotated by a pathologist in the SCiLS cloud and transferred into SCiLS Lab software (Version 2019c Pro, Bruker Daltonik GmbH).

4.4. Protein Identification by Electrospray Ionization Tandem Mass Spectrometry

Protein identification for *m/z* values was performed on adjacent tissue (tumor cell-rich regions) sections using a bottom-up nano-liquid chromatography electrospray ionization tandem mass spectrometry approach as previously described [67]. Similar to their preparation for MALDI-MSI, sections were preheated to 80 °C for 15 min before deparaffinization. Paraffin removal, antigen retrieval and tryptic digest were carried out as for MALDI-MSI. After incubation at 50 °C in a humidity chamber saturated with potassium sulfate solution for 2 h, peptides were extracted from tumor cell-rich regions separately from each tissue section into 40 μL of 0.1% trifluoroacetic acid and incubated for 15 min at room temperature. Digests were filtered using a ZipTip® C18 following the manufacturer's instructions, and the eluates were vacuum concentrated (Eppendorf® Concentrator 5301, Eppendorf AG, Hamburg, Germany) and reconstituted separately in 20 μL 0.1% trifluoroacetic acid, from which 2 μL were injected into a NanoHPLC (Dionex UltiMate 3000, Thermo Fisher Scientific) coupled to an ESI-QTOF ultrahigh-resolution mass spectrometer (Impact II™, Bruker Daltonik GmbH, Bremen, Germany). The peptide mixture was loaded onto an Acclaim PepMap™ 100 C18 trap column (100 μm × 2 cm, PN 164564, Thermo Fisher Scientific) and calibrated with 10 mM sodium hypofluorite (flowrate 20 μL/h) before separation in an Acclaim PepMap™ RSLC C18 column (75 μm × 50 cm, PN 164942, Thermo Fisher Scientific) with an increasing acetonitrile gradient 2–35% in 0.1% formic acid (400 nL/min flow rate, 10–800 bar pressure range) for 90 min while the column was kept at 60 °C. Released charged peptides were detected by a tandem mass spectrometer using a full-mass scan (150–2200 *m/z*) at a resolution of 50,000 FWHM. AutoMS/MS InsantExpertise was used to select peaks for fragmentation by collision-induced dissociation. Acquired raw MS/MS spectra were converted into mascot generic files (.mgf) for amino acid sequences using ProteoWizard software [68] and were used to search the human Swiss-Prot database using the Mascot search engine (version 2.4, MatrixScience Inc. Boston, MA, USA) with the significance threshold of $p < 0.05$ and the settings for trypsin as the proteolytic enzyme; a maximum of 1 missed cleavage; 10 ppm peptide tolerance; peptide charges of 2+, 3+ or 4+; oxidation allowed as variable modification; 0.8 Da MS/MS tolerance and a MOWSE score >13 to identify the corresponding protein. MOWSE (for MOlecular Weight SEarch) is a method for identifying proteins from the molecular weight of peptides created by proteolytic digestion and measured with mass spectrometry [47]. The probability-based MOWSE score formed the basis to develop Mascot, a proprietary software for protein identification from mass spectrometry data. Mascot results were exported as.csv files (Table S4). To match aligned *m/z* values from MALDI-MSI (Table S1) with the peptides identified by nanoLC-MS/MS (Table S4), we developed an excel macro in-house (File S1). The macro was applied with settings accommodating previously described parameters [40]. Briefly, the comparison of MALDI-MSI and LC-MS/MS *m/z* values required the identification of >1 peptide (search mass window < 0.3 Da). Only peptides with the smallest mass differences in the mass window and a correlation ratio ≥ 0.30 were counted as a match. The

peptides with highest MOWSE peptide scores and the smallest mass differences between MALDI-MSI and LC-MS/MS data were accepted as correctly identified.

4.5. MALDI-MSI Data Processing for Statistical Analyses

MALDI-MSI raw data were imported into the SciLS Lab software version 2019c Pro (Bruker Daltonik GmbH) using settings preserving the total ion count and without baseline removal and converted into the SciLS base data .sbd file and .slx file. An attribute table was built for sample number, tumor cell-rich regions, tumor INSS stage, *MYCN* amplification status in diagnostic tumor sample, or whether the molecular risk designation was high or other, and on patient age, sex and whether the patient experienced disease recurrence. Attributes were used to divide a dataset into independent datasets from different spatial spectral regions in tissue sections, or samples with different tumor or patient characteristics for analysis. Peak finding and alignment were conducted across a dataset (interval width = 0.3 Da) using a standard segmentation pipeline (SciLS Lab software) in maximal interval processing mode with TIC normalization, medium noise reduction and no smoothing (Sigma: 0.75) [69,70].

4.6. Statistical Analyses

The top-down segmentation using bisecting k-means clustering analysis was performed on the partitioned datasets from tissue sections or from only the regions with >80% tumor cells, as previously described [71], to defined peptide signatures. Both analyses used settings for 0.3 Da interval width, including all individual spectra, medium noise reduction and correlation distance. Discriminative MALDI-MSI *m/z* values from tumor cell-rich regions were identified using supervised ROC analysis on the partitioned datasets from tissue regions with >80% tumor cells. Area under the ROC curve (AUC) varies between 0 and 1, where values close to 0 and 1 indicates peptides to be discriminatory and 0.5 indicates no discriminatory value. Since the number of *m/z* values from the groups to be compared must be similar for this analysis, 35,000 *m/z* values were randomly selected per group. For those peptides with an AUC >0.7 or <0.3, a univariate hypothesis test (Wilcoxon rank sum test) was used to test the statistical significance of *m/z* values. Peptides with *p*-values < 0.001 and a peak correlation ratio ≥ 0.30 were selected as candidate markers. Supervised principal component analysis (PCA) was conducted to define characteristic peptide signatures differentiating between tumor regions with >80% tumor cell content from high or other risk groups. The data were scaled for PCA in a level scaling model. Only *m/z* values with AUC >0.8 or <0.2 and *p* < 0.001 were used as peak intervals for PCA using settings to create five components and use settings to use an interval width of ± 0.3 Da, maximal interval processing mode, normalization to total ion count, and no noise reduction. ROC analysis was also used in validation experiments to identify discriminative *m/z* values (defined in data sets from whole sections) using MALDI-MSI data (2500 *m/z* values randomly selected per group) from arrayed tumor cores. The Wilcoxon rank sum test was used to test the statistical significance of *m/z* values. Peptides with significant differences (*p*-value < 0.001) in the Wilcoxon test with a peak correlation ratio ≥ 0.30 were selected as candidate markers (significant correlations *p* < 0.05; Pearson's correlation analysis [72]). All Figures were created using the SciLS Lab software (Bruker, Bremen, Germany).

5. Conclusions

Molecular intratumor heterogeneity in high-risk neuroblastoma most likely contributes to therapy response and the clinical disease course, and is a challenge for risk assessment at initial tumor diagnosis. This pilot study demonstrates that (1) MALDI-MSI can visualize molecular tumor characteristics on the protein level associated with current risk classification directly in FFPE tumor tissue sections; (2) MALDI-MSI was able to explore spatial proteomic changes and directly identify molecular tumor heterogeneity in tumor sections; and (3) combined with nanoLC-MS/MS, this approach can identify differentially expressed new protein biomarkers in high-risk neuroblastomas (versus lower risk

groups), which might have an important role in neuroblastoma biology and/or progression. We provide proof-of-concept for the usefulness of this innovative technology in assisting risk classification and assessment of tumor heterogeneity on the protein level, as well as identification of new biomarkers with potential relevance for an increased understanding of neuroblastoma biology.

Supplementary Materials: The following are available online at <https://www.mdpi.com/article/10.3390/cancers13133184/s1> are Figure S1: Representative average spectra of whole sections and malignant regions of HR and non-HR neuroblastoma tissue sections. Figure S2: Discriminatory peptide signatures within tumor cell-rich regions in high or other risk groups of neuroblastoma. Figure S3: Ion maps of m/z values for CRMP1 and AHNAK in whole neuroblastoma sections and their validation in selected cores from the tissue microarray. Table S1: Aligned m/z values from cell-rich tumor region in neuroblastoma sections and tumor microarray cores. Table S2: Segmentation map of the tumor cell-rich regions in sections from high-risk neuroblastoma (HR) and neuroblastomas from other risk groups (nHR). Table S3: Identified discriminative MALDI-MSI m/z values by using nanoLC-MS/MS. Table S4: Protein identification by LC-MS of neuroblastoma whole tissue section. File S1: Excel macro codes for linking MALDI-MSI data and LC-MS/MS data.

Author Contributions: O.K., A.E. and J.H.S. designed the study; A.E., J.H.S. and P.H. provided patient samples, patient information, and intellectual input. P.H. and K.S. provided intellectual input and advice on experiments and the manuscript; S.B. and J.H.S. determined tumor content in histological sections. Z.W. performed the MS experiment. Z.W. programmed the excel macro linking MALDI-MS results to LC-MS/MS results. Z.W. and O.K. performed data evaluation, curation and interpretation of results. O.K. student supervision. K.A. provided intellectual input for data presentation and interpretation of results. Z.W., O.K., A.E. and K.A.; manuscript writing and revision. All authors have read and agreed to the published version of the manuscript.

Funding: This research was funded by German Ministry for Education and Research in the SYSMED-NB project (#01ZX1307 and #01ZX1607), MSTAR (#031L0220A) BCRT and the Berlin Institute of Health in the TERMINATE-NB collaborative research project (CRG04).

Institutional Review Board Statement: Ethical approval for use of residual tissue samples in this research was awarded by the local ethics committee of the Charité—Universitätsmedizin Berlin (protocol code, EA2/149/05; 18 August 2005).

Informed Consent Statement: Written informed consent was given by parents or legal guardians of the patients treated according to the BFM-NB-2004 protocol for use of residual tissue samples in research. No individual patients can be identified from data presented in this paper.

Data Availability Statement: Data are contained within the article or supplementary material. The MALDI-MSI data presented in this study are available on request from the corresponding author.

Acknowledgments: The authors thank the patients and their parents for participation in this study, the Core Unit Immunopathologie für Experimentelle Modelle, Charité Universitätsmedizin Berlin for support in immunohistochemistry, Iris Piwonski for crucial tissue assessment and the assistant engineer, Grit Nebrich, for device support. We thank all medical technical assistants from Eggert research group and the Charité Institute of Pathology for processing and sectioning sample blocks. Moreover, we thank Wanja Kassuhn and Hagen Kulbe for supporting the manuscript preparation.

Conflicts of Interest: The authors declare no conflict of interest.

References

1. Husmann, G.; Kaatsch, P.; Katalinic, A.; Bertz, J.; Haberland, J.; Kraywinkel, K.; Wolf, U. *Krebs in Deutschland 2005/2006. Häufigkeiten und Trends*; Robert Koch. Institut: Berlin, Germany, 2010. [\[CrossRef\]](#)
2. Maris, J.M. Recent Advances in Neuroblastoma. *N. Engl. J. Med.* **2010**, *362*, 2202–2211. [\[CrossRef\]](#) [\[PubMed\]](#)
3. Maris, J.M.; Hogarty, M.D.; Bagatell, R.; Cohn, S.L. Neuroblastoma. *Lancet* **2007**, *369*, 2106–2120. [\[CrossRef\]](#)
4. Cheung, N.-K.V.; Dyer, M.A. Neuroblastoma: Developmental biology, cancer genomics and immunotherapy. *Nat. Rev. Cancer* **2013**, *13*, 397–411. [\[CrossRef\]](#)
5. Simon, T.; Hero, B.; Schulte, J.H.; Deubzer, H.; Hundsdorfer, P.; Von Schweinitz, D.; Fuchs, J.; Schmidt, M.; Prasad, V.; Krug, B.; et al. 2017 GPOH Guidelines for Diagnosis and Treatment of Patients with Neuroblastic Tumors. *Klinische Pädiatrie* **2017**, *229*, 147–167. [\[CrossRef\]](#) [\[PubMed\]](#)

6. Cohn, S.L.; Pearson, A.D.J.; London, W.B.; Monclair, T.; Ambros, P.F.; Brodeur, G.M.; Faldum, A.; Hero, B.; Iehara, T.; Machin, D.; et al. The international neuroblastoma risk group (INRG) classification system: An INRG task force report. *J. Clin. Oncol.* **2009**, *27*, 289–297. [[CrossRef](#)]
7. Liang, W.H.; Federico, S.M.; London, W.B.; Naranjo, A.; Irwin, M.S.; Volchenbom, S.L.; Cohn, S.L. Tailoring Therapy for Children With Neuroblastoma on the Basis of Risk Group Classification: Past, Present, and Future. *JCO Clin Cancer Inform* **2020**, *4*, 895–905. [[CrossRef](#)]
8. Øra, I.; Eggert, A. Progress in treatment and risk stratification of neuroblastoma: Impact on future clinical and basic research. *Semin. Cancer Biol.* **2011**, *21*, 217–228. [[CrossRef](#)] [[PubMed](#)]
9. Brodeur, G.M.; Seeger, R.C.; Schwab, M.; E Varmus, H.; Bishop, J.M. Amplification of N-myc in untreated human neuroblastomas correlates with advanced disease stage. *Science* **1984**, *224*, 1121–1124. [[CrossRef](#)] [[PubMed](#)]
10. Campbell, K.; Shyr, D.; Bagatell, R.; Fischer, M.; Nakagawara, A.; Nieto, A.C.; Brodeur, G.M.; Matthay, K.K.; London, W.B.; Dubois, S.G. Comprehensive evaluation of context dependence of the prognostic impact of MYCN amplification in neuroblastoma: A report from the International Neuroblastoma Risk Group (INRG) project. *Pediatr. Blood Cancer* **2019**, *66*, e27819. [[CrossRef](#)]
11. Oberthuer, A.; Juraeva, D.; Hero, B.; Volland, R.; Sterz, C.; Schmidt, R.; Faldum, A.; Kahlert, Y.; Engesser, A.; Asgharzadeh, S.; et al. Revised Risk Estimation and Treatment Stratification of Low- and Intermediate-Risk Neuroblastoma Patients by Integrating Clinical and Molecular Prognostic Markers. *Clin. Cancer Res.* **2015**, *21*, 1904–1915. [[CrossRef](#)]
12. Ackermann, S.; Cartolano, M.; Hero, B.; Welte, A.; Kahlert, Y.; Roderwieser, A.; Bartenhagen, C.; Walter, E.; Gecht, J.; Kerschke, L.; et al. A mechanistic classification of clinical phenotypes in neuroblastoma. *Science* **2018**, *362*, 1165–1170. [[CrossRef](#)]
13. Schramm, A.; Köster, J.; Assenov, Y.; Althoff, K.; Peifer, M.; Mahlow, E.; Odersky, A.; Beisser, D.; Ernst, C.; Henssen, A.; et al. Mutational dynamics between primary and relapse neuroblastomas. *Nat. Genet.* **2015**, *47*, 872–877. [[CrossRef](#)] [[PubMed](#)]
14. Karlsson, J.; Valind, A.; Mengelbier, L.H.; Bredin, S.; Commark, L.; Jansson, C.; Wali, A.; Staaf, J.; Viklund, B.; Øra, I.; et al. Four evolutionary trajectories underlie genetic intratumoral variation in childhood cancer. *Nat. Genet.* **2018**, *50*, 944–950. [[CrossRef](#)]
15. Pugh, T.J.; Morozova, O.; Attiyeh, E.F.; Asgharzadeh, S.; Wei, J.S.; Auclair, D.; Carter, S.L.; Cibulskis, K.; Hanna, M.; Kiezun, A.; et al. The genetic landscape of high-risk neuroblastoma. *Nat. Genet.* **2013**, *45*, 279–284. [[CrossRef](#)] [[PubMed](#)]
16. Eleveld, T.F.; A Oldridge, D.; Bernard, V.; Koster, J.; Daåge, L.C.; Diskin, S.J.; Schild, L.; Bentahar, N.B.; Bellini, A.; Chicard, M.; et al. Relapsed neuroblastomas show frequent RAS-MAPK pathway mutations. *Nat. Genet.* **2015**, *47*, 864–871. [[CrossRef](#)] [[PubMed](#)]
17. Peifer, M.; Hertwig, F.; Roels, F.; Droidax, D.; Gartlgruber, M.; Menon, R.; Krämer, A.; Roncaioli, J.L.; Sand, F.; Heuckmann, J.M.; et al. Telomerase activation by genomic rearrangements in high-risk neuroblastoma. *Nat. Cell Biol.* **2015**, *526*, 700–704. [[CrossRef](#)]
18. Molenaar, J.J.; Koster, J.; Zwijnenburg, D.A.; Van Sluis, P.; Valentijn, L.J.; Van Der Ploeg, I.; Hamdi, M.; Van Nes, J.; Westerman, B.A.; Van Arkel, J.; et al. Sequencing of neuroblastoma identifies chromothripsis and defects in neurogenesis genes. *Nat. Cell Biol.* **2012**, *483*, 589–593. [[CrossRef](#)] [[PubMed](#)]
19. Gröbner, S.N.; Project, I.P.-S.; Worst, B.C.; Weischenfeldt, J.; Buchhalter, I.; Kleinheinz, K.; Rudneva, V.A.; Johann, P.D.; Balasubramanian, G.P.; Segura-Wang, M.; et al. The landscape of genomic alterations across childhood cancers. *Nature* **2018**, *555*, 321–327. [[CrossRef](#)]
20. Brady, S.W.; Liu, Y.; Ma, X.; Gout, A.M.; Hagiwara, K.; Zhou, X.; Wang, J.; Macias, M.; Chen, X.; Easton, J.; et al. Pan-neuroblastoma analysis reveals age- and signature-associated driver alterations. *Nat. Commun.* **2020**, *11*, 1–13. [[CrossRef](#)] [[PubMed](#)]
21. Li, Y.; Ohira, M.; Zhou, Y.; Xiong, T.; Luo, W.; Yang, C.; Li, X.; Gao, Z.; Zhou, R.; Nakamura, Y.; et al. Genomic analysis-integrated whole-exome sequencing of neuroblastomas identifies genetic mutations in axon guidance pathway. *Oncotarget* **2017**, *8*, 56684–56697. [[CrossRef](#)]
22. de Sousa, V.M.L.; Carvalho, L. Heterogeneity in Lung Cancer. *Pathobiology* **2018**, *85*, 96–107. [[CrossRef](#)] [[PubMed](#)]
23. Heijs, B.; Holst-Bernal, S.; De Graaff, M.A.; Bruijn, I.H.B.-D.; Rodriguez-Gironde, M.; Van De Sande, M.A.J.; Wührer, M.; McDonnell, L.A.; Bovée, J.V.M.G. Molecular signatures of tumor progression in myxoid liposarcoma identified by N-glycan mass spectrometry imaging. *Lab. Investig.* **2020**, *100*, 1252–1261. [[CrossRef](#)] [[PubMed](#)]
24. Harris, A.; Roseborough, A.; Mor, R.; Yeung, K.K.-C.; Whitehead, S.N. Ganglioside Detection from Formalin-Fixed Human Brain Tissue Utilizing MALDI Imaging Mass Spectrometry. *J. Am. Soc. Mass Spectrom.* **2020**, *31*, 479–487. [[CrossRef](#)] [[PubMed](#)]
25. Boyle, S.T.; Mittal, P.; Kaur, G.; Hoffmann, P.; Samuel, M.S.; Klingler-Hoffmann, M. Uncovering Tumor–Stroma Inter-relationships Using MALDI Mass Spectrometry Imaging. *J. Proteome Res.* **2020**, *19*, 4093–4103. [[CrossRef](#)]
26. Aichler, M.; Walch, A. MALDI Imaging mass spectrometry: Current frontiers and perspectives in pathology research and practice. *Lab. Investig.* **2015**, *95*, 422–431. [[CrossRef](#)] [[PubMed](#)]
27. Hermann, J.; Noels, H.; Theelen, W.; Lellig, M.; Orth-Alampour, S.; Boor, P.; Jankowski, J.; Jankowski, J. Sample preparation of formalin-fixed paraffin-embedded tissue sections for MALDI-mass spectrometry imaging. *Anal. Bioanal. Chem.* **2020**, *412*, 1263–1275. [[CrossRef](#)]
28. Dilillo, M.; Ait-Belkacem, R.; Esteve, C.; Pellegrini, D.; Nicolardi, S.; Costa, M.; Vannini, E.; de Graaf, E.L.; Caleo, M.; McDonnell, L.A. Ultra-High Mass Resolution MALDI Imaging Mass Spectrometry of Proteins and Metabolites in a Mouse Model of Glioblastoma. *Sci. Rep.* **2017**, *7*, 1–11. [[CrossRef](#)] [[PubMed](#)]
29. Mezger, S.T.P.; Mingels, A.M.A.; Bekers, O.; Heeren, R.M.A.; Cillero-Pastor, B. Mass Spectrometry Spatial-Omics on a Single Conductive Slide. *Anal. Chem.* **2021**, *93*, 2527–2533. [[CrossRef](#)]

30. Spraggins, J.M.; Rizzo, D.G.; Moore, J.L.; Noto, M.J.; Skaar, E.P.; Caprioli, R.M. Next-generation technologies for spatial proteomics: Integrating ultra-high speed MALDI-TOF and high mass resolution MALDI FTICR imaging mass spectrometry for protein analysis. *Proteomics* **2016**, *16*, 1678–1689. [[CrossRef](#)]
31. Kassuhn, W.; Klein, O.; Darb-Esfahani, S.; Lammert, H.; Handzik, S.; Taube, E.; Schmitt, W.; Keunecke, C.; Horst, D.; Dreher, F.; et al. Classification of Molecular Subtypes of High-Grade Serous Ovarian Cancer by MALDI-Imaging. *Cancers* **2021**, *13*, 1512. [[CrossRef](#)]
32. Mascini, N.E.; Teunissen, J.; Noorlag, R.; Willems, S.M.; Heeren, R.M. Tumor classification with MALDI-MSI data of tissue microarrays: A case study. *Methods* **2018**, *151*, 21–27. [[CrossRef](#)] [[PubMed](#)]
33. Klein, O.; Fogt, F.; Hollerbach, S.; Nebrich, G.; Boskamp, T.; Wellmann, A. Classification of Inflammatory Bowel Disease from Formalin-Fixed, Paraffin-Embedded Tissue Biopsies via Imaging Mass Spectrometry. *Proteom. Clin. Appl.* **2020**, *14*, 1900131. [[CrossRef](#)]
34. Neumann, J.M.; Niehaus, K.; Neumann, N.; Knobloch, H.C.; Bremmer, F.; Krafft, U.; Kellner, U.; Nyirády, P.; Szarvas, T.; Bednarz, H.; et al. A new technological approach in diagnostic pathology: Mass spectrometry imaging-based metabolomics for biomarker detection in urachal cancer. *Lab. Investig.* **2021**, 1–8. [[CrossRef](#)]
35. Meding, S.; Nitsche, U.; Balluff, B.; Elsner, M.; Rauser, S.; Schöne, C.; Nipp, M.; Maak, M.; Feith, M.; Ebert, M.P.; et al. Tumor Classification of Six Common Cancer Types Based on Proteomic Profiling by MALDI Imaging. *J. Proteome Res.* **2012**, *11*, 1996–2003. [[CrossRef](#)] [[PubMed](#)]
36. Schwamborn, K.; Krieg, R.C.; Jirak, P.; Ott, G.; Knuchel, R.; Rosenwald, A.; Wellmann, A. Application of MALDI imaging for the diagnosis of classical Hodgkin lymphoma. *J. Cancer Res. Clin. Oncol.* **2010**, *136*, 1651–1655. [[CrossRef](#)]
37. Rauser, S.; Marquardt, C.; Balluff, B.; Deininger, S.-O.; Albers, C.; Belau, E.; Hartmer, R.; Suckau, D.; Specht, K.; Ebert, M.P.; et al. Classification of HER2 Receptor Status in Breast Cancer Tissues by MALDI Imaging Mass Spectrometry. *J. Proteome Res.* **2010**, *9*, 1854–1863. [[CrossRef](#)] [[PubMed](#)]
38. Balluff, B.; Rauser, S.; Meding, S.; Elsner, M.; Schöne, C.; Feuchtinger, A.; Schuhmacher, C.; Novotny, A.; Jütting, U.; Maccarrone, G.; et al. MALDI Imaging Identifies Prognostic Seven-Protein Signature of Novel Tissue Markers in Intestinal-Type Gastric Cancer. *Am. J. Pathol.* **2011**, *179*, 2720–2729. [[CrossRef](#)]
39. Bauer, J.A.; Chakravarthy, A.B.; Rosenbluth, J.M.; Mi, D.; Seeley, E.H.; Granja-Ingram, N.D.M.; Olivares, M.G.; Kelley, M.C.; Mayer, I.A.; Meszoely, I.M.; et al. Identification of Markers of Taxane Sensitivity Using Proteomic and Genomic Analyses of Breast Tumors from Patients Receiving Neoadjuvant Paclitaxel and Radiation. *Clin. Cancer Res.* **2010**, *16*, 681–690. [[CrossRef](#)]
40. Cillero-Pastor, B.; Heeren, R.M.A. Matrix-Assisted Laser Desorption Ionization Mass Spectrometry Imaging for Peptide and Protein Analyses: A Critical Review of On-Tissue Digestion. *J. Proteome Res.* **2013**, *13*, 325–335. [[CrossRef](#)] [[PubMed](#)]
41. Davis, T.; Loos, B.; Engelbrecht, A.-M. AHNAK: The giant jack of all trades. *Cell. Signal.* **2014**, *26*, 2683–2693. [[CrossRef](#)] [[PubMed](#)]
42. Zhang, Z.; Liu, X.; Huang, R.; Liu, X.; Liang, Z.; Liu, T. Upregulation of nucleoprotein AHNAK is associated with poor outcome of pancreatic ductal adenocarcinoma prognosis via mediating epithelial-mesenchymal transition. *J. Cancer* **2019**, *10*, 3860–3870. [[CrossRef](#)]
43. Hartomo, T.B.; Kozaki, A.; Hasegawa, D.; Pham, T.V.H.; Yamamoto, N.; Saitoh, A.; Ishida, T.; Kawasaki, K.; Kosaka, Y.; Ohashi, H.; et al. Minimal residual disease monitoring in neuroblastoma patients based on the expression of a set of real-time RT-PCR markers in tumor-initiating cells. *Oncol. Rep.* **2013**, *29*, 1629–1636. [[CrossRef](#)] [[PubMed](#)]
44. Hirase, S.; Saitoh, A.; Hartomo, T.B.; Kozaki, A.; Yanai, T.; Hasegawa, D.; Kawasaki, K.; Kosaka, Y.; Matsuo, M.; Yamamoto, N.; et al. Early detection of tumor relapse/regrowth by consecutive minimal residual disease monitoring in high-risk neuroblastoma patients. *Oncol. Lett.* **2016**, *12*, 1119–1123. [[CrossRef](#)]
45. Yamamoto, N.; Kozaki, A.; Hartomo, T.B.; Yanai, T.; Hasegawa, D.; Kawasaki, K.; Kosaka, Y.; Matsuo, M.; Hirase, S.; Mori, T.; et al. Differential expression of minimal residual disease markers in peripheral blood and bone marrow samples from high-risk neuroblastoma patients. *Oncol. Lett.* **2015**, *10*, 3228–3232. [[CrossRef](#)] [[PubMed](#)]
46. Thwin, K.K.; Ishida, T.; Uemura, S.; Yamamoto, N.; Lin, K.S.; Tamura, A.; Kozaki, A.; Saito, A.; Kishimoto, K.; Mori, T.; et al. Level of Seven Neuroblastoma-Associated mRNAs Detected by Droplet Digital PCR Is Associated with Tumor Relapse/Regrowth of High-Risk Neuroblastoma Patients. *J. Mol. Diagn.* **2020**, *22*, 236–246. [[CrossRef](#)] [[PubMed](#)]
47. Pappin, D.; Hojrup, P.; Bleasby, A. Rapid identification of proteins by peptide-mass fingerprinting. *Curr. Biol.* **1993**, *3*, 327–332. [[CrossRef](#)]
48. Klein, O.; Kanter, F.; Kulbe, H.; Jank, P.; Denkert, C.; Nebrich, G.; Schmitt, W.D.; Wu, Z.; Kunze, C.A.; Sehoul, J.; et al. MALDI-Imaging for Classification of Epithelial Ovarian Cancer Histotypes from a Tissue Microarray Using Machine Learning Methods. *Proteom. Clin. Appl.* **2019**, *13*, e1700181. [[CrossRef](#)] [[PubMed](#)]
49. Kulbe, H.; Klein, O.; Wu, Z.; Taube, E.; Kassuhn, W.; Horst, D.; Darb-Esfahani, S.; Jank, P.; Abobaker, S.; Ringel, F.; et al. Discovery of Prognostic Markers for Early-Stage High-Grade Serous Ovarian Cancer by Mald-Imaging. *Cancers* **2020**, *12*, 2000. [[CrossRef](#)] [[PubMed](#)]
50. Casadonte, R.; Longuespee, R.; Kriegsmann, J.; Kriegsmann, M. MALDI IMS and Cancer Tissue Microarrays. *Adv. Cancer Res.* **2017**, *134*, 173–200. [[CrossRef](#)] [[PubMed](#)]
51. Kriegsmann, J.; Kriegsmann, M.; Casadonte, R. MALDI TOF imaging mass spectrometry in clinical pathology: A valuable tool for cancer diagnostics (Review). *Int. J. Oncol.* **2014**, *46*, 893–906. [[CrossRef](#)]

52. Longuespee, R.; Baiwir, D.; Mazzucchelli, G.; Smargiasso, N.; De Pauw, E. Laser Microdissection-Based Microproteomics of Formalin-Fixed and Paraffin-Embedded (FFPE) Tissues. *Methods Mol. Biol.* **2018**, *1723*, 19–31. [[CrossRef](#)]
53. Giordano, S.; Zucchetti, M.; Decio, A.; Cesca, M.; Nerini, I.F.; Maiezza, M.; Ferrari, M.; Licandro, S.A.; Frapolli, R.; Giavazzi, R.; et al. Heterogeneity of paclitaxel distribution in different tumor models assessed by MALDI mass spectrometry imaging. *Sci. Rep.* **2016**, *6*, 39284. [[CrossRef](#)] [[PubMed](#)]
54. Schöne, C.; Höfler, H.; Walch, A. MALDI imaging mass spectrometry in cancer research: Combining proteomic profiling and histological evaluation. *Clin. Biochem.* **2013**, *46*, 539–545. [[CrossRef](#)] [[PubMed](#)]
55. McGranahan, N.; Swanton, C. Clonal Heterogeneity and Tumor Evolution: Past, Present, and the Future. *Cell* **2017**, *168*, 613–628. [[CrossRef](#)] [[PubMed](#)]
56. Chen, Q.R.; Song, Y.K.; Yu, L.R.; Wei, J.S.; Chung, J.Y.; Hewitt, S.M.; Veenstra, T.D.; Khan, J. Global genomic and proteomic analysis identifies biological pathways related to high-risk neuroblastoma. *J. Proteome Res.* **2010**, *9*, 373–382. [[CrossRef](#)] [[PubMed](#)]
57. Yu, F.; Zhu, X.; Feng, C.; Wang, T.; Hong, Q.; Liu, Z.; Tang, S. Proteomics-based identification of spontaneous regression-associated proteins in neuroblastoma. *J. Pediatr. Surg.* **2011**, *46*, 1948–1955. [[CrossRef](#)] [[PubMed](#)]
58. Tan, F.; Thiele, C.J.; Li, Z. Collapsin response mediator proteins: Potential diagnostic and prognostic biomarkers in cancers (Review). *Oncol. Lett.* **2014**, *7*, 1333–1340. [[CrossRef](#)]
59. Cheng, F.; Liu, C.; Lin, C.-C.; Zhao, J.; Jia, P.; Li, W.-H.; Zhao, Z. A Gene Gravity Model for the Evolution of Cancer Genomes: A Study of 3,000 Cancer Genomes across 9 Cancer Types. *PLoS Comput. Biol.* **2015**, *11*, e1004497. [[CrossRef](#)]
60. Xiang, X.; Langlois, S.; St-Pierre, M.-E.; Blinder, A.; Charron, P.; Graber, T.E.; Fowler, S.L.; Baird, S.D.; Bennett, S.A.L.; Alain, T.; et al. Identification of pannexin 1-regulated genes, interactome, and pathways in rhabdomyosarcoma and its tumor inhibitory interaction with AHNAK. *Oncogene* **2021**, *40*, 1868–1883. [[CrossRef](#)]
61. Soini, T.; Eloranta, K.; Pihlajoki, M.; Kyrölähti, A.; Akinrinade, O.; Andersson, N.; Lohi, J.; Pakarinen, M.P.; Wilson, D.B.; Heikinheimo, M. Transcription factor GATA4 associates with mesenchymal-like gene expression in human hepatoblastoma cells. *Tumor Biol.* **2018**, *40*, 1010428318785498. [[CrossRef](#)]
62. Jaskiewicz, N.M.; Townson, D.H. Hyper-O-GlcNAcylation promotes epithelial-mesenchymal transition in endometrial cancer cells. *Oncotarget* **2019**, *10*, 2899–2910. [[CrossRef](#)]
63. Sohn, M.; Shin, S.; Yoo, J.Y.; Goh, Y.; Lee, I.H.; Bae, Y.S. Ahnak promotes tumor metastasis through transforming growth factor-beta-mediated epithelial-mesenchymal transition. *Sci. Rep.* **2018**, *8*, 14379. [[CrossRef](#)]
64. Shen, E.; Wang, X.; Liu, X.; Lv, M.; Zhang, L.; Zhu, G.; Sun, Z. MicroRNA-93-5p promotes epithelial-mesenchymal transition in gastric cancer by repressing tumor suppressor AHNAK expression. *Cancer Cell Int.* **2020**, *20*, 76. [[CrossRef](#)]
65. Zhao, Z.; Xiao, S.; Yuan, X.; Yuan, J.; Zhang, C.; Li, H.; Su, J.; Wang, X.; Liu, Q. AHNAK as a Prognosis Factor Suppresses the Tumor Progression in Glioma. *J. Cancer* **2017**, *8*, 2924–2932. [[CrossRef](#)]
66. Cimas, F.J.; Manzano, A.; Balu-Piqué, M.; García-Gil, E.; Pérez-Segura, P.; Nagy, Ádám; Pandiella, A.; Györfy, B.; Ocana, A. Genomic Mapping Identifies Mutations in RYR2 and AHNAK as Associated with Favorable Outcome in Basal-Like Breast Tumors Expressing PD1/PD-L1. *Cancers* **2020**, *12*, 2243. [[CrossRef](#)] [[PubMed](#)]
67. Klein, O.; Strohschein, K.; Nebrich, G.; Oetjen, J.; Trede, D.; Thiele, H.; Alexandrov, T.; Giavalisco, P.; Duda, G.N.; von Roth, P.; et al. MALDI imaging mass spectrometry: Discrimination of pathophysiological regions in traumatized skeletal muscle by characteristic peptide signatures. *Proteomics* **2014**, *14*, 2249–2260. [[CrossRef](#)]
68. Chambers, M.C.; Maclean, B.; Burke, R.; Amodei, D.; Ruderman, D.L.; Neumann, S.; Gatto, L.; Fischer, B.; Pratt, B.; Egertson, J.; et al. A cross-platform toolkit for mass spectrometry and proteomics. *Nat. Biotechnol.* **2012**, *30*, 918–920. [[CrossRef](#)] [[PubMed](#)]
69. Alexandrov, T.; Becker, M.; Deininger, S.-O.; Ernst, G.; Wehder, L.; Grasmair, M.; Von Eggeling, F.; Thiele, H.; Maass, P. Spatial Segmentation of Imaging Mass Spectrometry Data with Edge-Preserving Image Denoising and Clustering. *J. Proteome Res.* **2010**, *9*, 6535–6546. [[CrossRef](#)] [[PubMed](#)]
70. Alexandrov, T.; Becker, M.; Guntinas-Lichius, O.; Ernst, G.; von Eggeling, F. MALDI-imaging segmentation is a powerful tool for spatial functional proteomic analysis of human larynx carcinoma. *J. Cancer Res. Clin. Oncol.* **2013**, *139*, 85–95. [[CrossRef](#)] [[PubMed](#)]
71. Trede, D.; Schiffler, S.; Becker, M.; Wirtz, S.; Steinhilber, K.; Strehlow, J.; Aichler, M.; Kobarg, J.H.; Oetjen, J.; Dyatlov, A.; et al. Exploring Three-Dimensional Matrix-Assisted Laser Desorption/Ionization Imaging Mass Spectrometry Data: Three-Dimensional Spatial Segmentation of Mouse Kidney. *Anal. Chem.* **2012**, *84*, 6079–6087. [[CrossRef](#)]
72. McDonnell, L.A.; van Remoortere, A.; van Zeijl, R.J.M.; Deelder, A.M. Mass spectrometry image correlation: Quantifying colocalization. *J. Proteome Res.* **2008**, *7*, 3619–3627. [[CrossRef](#)] [[PubMed](#)]

Based on the extract from the ISI Web of Knowledge (https://intranet.charite.de/medbib/impact_faktoren_2018_fuer_zeitschriften_nach_fachgebieten/), the journal “Cancers” ranked 31 out of 229 journals in the category “Oncology” with impact factor 6.162 (2018).




Journal Data Filtered By: **Selected JCR Year: 2018** Selected Editions: SCIE, SSCI
 Selected Categories: **“ONCOLOGY”** Selected Category Scheme: WoS
Gesamtanzahl: 229 Journale

Rank	Full Journal Title	Total Cites	Journal Impact Factor	Eigenfactor Score
1	CA-A CANCER JOURNAL FOR CLINICIANS	32.410	223,679	0.077370
2	NATURE REVIEWS CANCER	50.529	51,848	0.074080
3	LANCET ONCOLOGY	48.822	35,386	0.146770
4	Nature Reviews Clinical Oncology	9.626	34,106	0.031890
5	JOURNAL OF CLINICAL ONCOLOGY	154.029	28,245	0.281750
6	Cancer Discovery	13.715	26,370	0.064810
7	CANCER CELL	36.056	23,916	0.091050
8	JAMA Oncology	9.488	22,416	0.048340
9	ANNALS OF ONCOLOGY	40.751	14,196	0.103620
10	Journal of Thoracic Oncology	16.601	12,460	0.038810
11	Molecular Cancer	11.626	10,679	0.021350
12	JNCI-Journal of the National Cancer Institute	36.790	10,211	0.051650
13	NEURO-ONCOLOGY	11.858	10,091	0.029150
14	LEUKEMIA	24.555	9,944	0.054750
15	SEMINARS IN CANCER BIOLOGY	6.992	9,658	0.010730
16	CLINICAL CANCER RESEARCH	78.171	8,911	0.134870
17	Trends in Cancer	1.420	8,884	0.006040
18	Journal of Hematology & Oncology	5.366	8,731	0.013620
19	Journal for ImmunoTherapy of Cancer	2.716	8,676	0.011350
20	Cancer Immunology Research	5.420	8,619	0.025380
21	CANCER RESEARCH	130.932	8,378	0.123870
22	CANCER TREATMENT REVIEWS	8.419	8,332	0.016930
23	Blood Cancer Journal	2.247	7,895	0.009060
24	Journal of the National Comprehensive Cancer Network	5.746	7,570	0.019940
25	BIOCHIMICA ET BIOPHYSICA ACTA-REVIEWS ON CANCER	5.226	6,887	0.008260

26	EUROPEAN JOURNAL OF CANCER	30.731	6,680	0.055220
27	CANCER AND METASTASIS REVIEWS	6.011	6,667	0.006220
28	ONCOGENE	63.249	6,634	0.074600
29	CANCER LETTERS	30.146	6,508	0.043780
30	INTERNATIONAL JOURNAL OF RADIATION ONCOLOGY BIOLOGY PHYSICS	45.833	6,203	0.046810
31	Cancers	5.196	6,162	0.011780
32	CANCER	67.408	6,102	0.071820

Article

Discovery of Prognostic Markers for Early-Stage High-Grade Serous Ovarian Cancer by Maldi-Imaging

Hagen Kulbe ^{1,2,†} , Oliver Klein ^{3,†}, Zhiyang Wu ³, Eliane T. Taube ⁴, Wanja Kassuhn ^{1,2} , David Horst ⁴, Silvia Darb-Esfahani ⁵, Paul Jank ^{4,6} , Salem Abobaker ^{1,2}, Frauke Ringel ^{1,2}, Andreas du Bois ⁷, Florian Heitz ⁷, Jalid Sehouli ^{1,2} and Elena I. Braicu ^{1,2,*}

¹ Tumorbank Ovarian Cancer Network, Charité – Universitätsmedizin Berlin, corporate member of Freie Universität Berlin, Humboldt-Universität zu Berlin, and Berlin Institute of Health, 10117 Berlin, Germany; hagen.kulbe@charite.de (H.K.); wanja.kassuhn@charite.de (W.K.); salem-nuri.abobaker@charite.de (S.A.); frauke.ringel@charite.de (F.R.); Jalid.Sehouli@charite.de (J.S.)

² Department of Gynecology, European Competence Center for Ovarian Cancer, Charité Universitätsmedizin Berlin, corporate member of Freie Universität Berlin, Humboldt-Universität zu Berlin, and Berlin Institute of Health, 10117 Berlin, Germany

³ BIH Center for Regenerative Therapies BCRT, Charité – Universitätsmedizin Berlin, 10117 Berlin, Germany; oliver.klein@charite.de (O.K.); zhiyang.wu@charite.de (Z.W.)

⁴ Institute of Pathology, Charité – Universitätsmedizin Berlin, corporate member of Freie Universität Berlin, Humboldt-Universität zu Berlin, and Berlin Institute of Health, 10117 Berlin, Germany; eliane.taube@charite.de (E.T.T.); david.horst@charite.de (D.H.); paul.jank@uni-marburg.de (P.J.)

⁵ Institute of Pathology Berlin-Spandau and Berlin-Buch, 10117 Berlin, Germany; s.darb-esfahani@ifp-spandau.de

⁶ Institute of Pathology, Philipps-University Marburg, 35032 Marburg, Germany

⁷ Evangelische Kliniken Essen-Mitte Klinik für Gynäkologie und gynäkologische Onkologie, 45136 Essen, Germany; prof.dubois@googlemail.com (A.d.B.); F.Heitz@kem-med.com (F.H.)

* Correspondence: elena.braicu@charite.de; Tel.: +49-(0)30-450-664469

† Authors contributed equally to this work.

Received: 23 June 2020; Accepted: 20 July 2020; Published: 22 July 2020



Abstract: With regard to relapse and survival, early-stage high-grade serous ovarian (HGSOC) patients comprise a heterogeneous group and there is no clear consensus on first-line treatment. Currently, no prognostic markers are available for risk assessment by standard targeted immunohistochemistry and novel approaches are urgently required. Here, we applied MALDI-imaging mass spectrometry (MALDI-IMS), a new method to identify distinct mass profiles including protein signatures on paraffin-embedded tissue sections. In search of prognostic biomarker candidates, we compared proteomic profiles of primary tumor sections from early-stage HGSOC patients with either recurrent (RD) or non-recurrent disease (N = 4; each group) as a proof of concept study. In total, MALDI-IMS analysis resulted in 7537 spectra from the malignant tumor areas. Using receiver operating characteristic (ROC) analysis, 151 peptides were able to discriminate between patients with RD and non-RD (AUC > 0.6 or < 0.4; $p < 0.01$), and 13 of them could be annotated to proteins. Strongest expression levels of specific peptides linked to Keratin type1 and Collagen alpha-2(I) were observed and associated with poor prognosis (AUC > 0.7). These results confirm that in using IMS, we could identify new candidates to predict clinical outcome and treatment extent for patients with early-stage HGSOC.

Keywords: ovarian cancer; early-stage HGSOC; prognostic markers; MALDI-IMS

1. Introduction

Epithelial ovarian cancer (EOC) is the leading cause of death within gynecological cancers in the developed countries (<http://seer.cancer.gov>). Due to the lack of specific symptoms, EOC is often detected at an advanced stage with a five-year survival rate less than 40% [1]. However, 25% of EOC patients are diagnosed in early stage (I-II) as defined by Fédération Internationale de Gynécologie et d'Obstétrique (FIGO), where the disease is often cured by surgery alone, or in combination with platinum-based chemotherapy [2,3]. Even though the prognosis of patients with FIGO stage I-II increases dramatically with treatment, with five-year survival rates between 80–90%, some subgroups of early-stage EOC will relapse and 20–30% of these patients will finally succumb to the disease [4–6]. Older age, greater stage, higher grade and malignant cytology are independent prognostic factors for recurrence [7]. Moreover, the prognosis differs between the histological subtypes with high-grade serous ovarian cancer (HGSOC) being the most common one, accounting for 70–80% of ovarian cancer-related deaths.

According to guidelines of the European Society for Medical Oncology (ESMO), bilateral salpingo-oophorectomy, hysterectomy, omentectomy, peritoneal stripping and lymph node sampling are recommended procedures for stage I and II HGSOC patients (<https://www.esmo.org/guidelines/gynaecological-cancers/newly-diagnosed-and-relapsed-epithelial-ovarian-carcinoma/esmo-esgo-consensus-conference-recommendations-on-ovarian-cancer>) [8,9]. However, fertilization-sparing surgery (FSS) for women of childbearing age could be considered, and be discussed individually [10]. Different criteria for selecting patients have been applied and the debate over FSS in HGSOC is more than controversial as there are limited data on that issue. Preoperative screening methods and comprehensive surgical staging for accurate disease classification are mandatory [11,12]. In this context, one third of presumed stage I ovarian cancers were found to be upstaged by the findings of dissemination in the peritoneal cavity [13]. Patients with high-risk early-stage EOC, defined as stage I, grade 3, stage IC and II, as well as clear cell cancers, will require adjuvant chemotherapy which has been shown to reduce the relapse rate by >60% in stage IC EOC patients [14]. Hence, platinum-based chemotherapy is an important factor in treating these patients with high-risk early-stage EOC with impact on both recurrence-free (RFS) and overall survival (OS). Prognostic markers are needed to stratify patients into low- and high-risk groups in order to select patients who will benefit from chemotherapy. The term EOC refers to at least four different histological subtypes which is an important issue to take into account in the risk assessment of clinical progression. The most aggressive histotype is HGSOC. Nevertheless, the optimal clinical management is still a controversial debate and patients with early-stage high-grade serous EOC might be over-treated which could potentially result in complications after radical surgical management and an increase in toxicity of chemotherapy [15,16]. Hence, it is of utmost importance to identify novel diagnostic markers for this patient cohort in order to improve the risk assessment of tumor recurrence. An optimal evaluation of risk for progression would have the benefit of personalized chemotherapy, and reduced costs and treatment side effects in patients with little risk for progression. Commonly used tissue-based techniques, such as liquid chromatography-based mass spectrometry or gene expression profiling, require large amounts of tissue material. Moreover, these methods do not enable a direct correlation between differentially expressed molecular profiles and the tissue histology [17]. Matrix-assisted laser desorption/ionization (MALDI) imaging mass spectrometry (IMS) has the advantage of combining morphological features with protein expression in tissue. This technique enables spatially resolved tissue assessment via specific molecular signatures (e.g., proteins, peptides, lipids and molecules of cell metabolites) and allows their correlation with alterations in tissue histology [18–20] as well as stages of ovarian cancer [21].

This recently developed diagnostic method of imaging mass spectrometry (MALDI-imaging MS) has also been used for the rapid diagnosis and prognosis of patients [22–24], and to identify peptide profiles spatially resolved directly on the paraffin-embedded tissue to depict and assign to the histological and clinical pathological subtypes of cancer.

Here, we have applied the method to detect a molecular signature of 13 peptides that predicts tumor recurrence in patients with early-stage HGSOE. According to their specific sequence, these peptides were allocated to a signature of proteins for risk stratification in support of clinical management of patients with early-stage HGSOE.

2. Results

2.1. Accumulation of Proteomics Data by MALDI-IMS

The initial proteomic measurements were simultaneously carried out on primary tumor tissue sections of early-stage HGSOE patients ($n = 10$) with either recurrent disease (RD) or non-recurrent disease (non-RD), respectively. Mass spectra of primary tumor tissue sections of early-stage HGSOE were extracted and statistical data analysis was performed by the SCiLS Lab software. In total, 506 aligned m/z values in a mass range between m/z 600 and 3,000 were extracted (Table S1). Average spectra of primary tumor tissue sections of early-stage HGSOE are shown in Figure 1. The unsupervised data analysis of the peptide signatures by probabilistic latent semantic analysis (pLSA) allowed the discrimination of different patient groups via individual mass spectra compound intensity and spatial distribution. Analysis of the peptide signatures by pLSA resulted in the discriminative compounds for HGSOE patients with RD and non-RD. However, a third HGSOE patient group could be identified which showed individual pLSA compounds which did not match to patients with RD nor patients with non-RD (Figure S1).

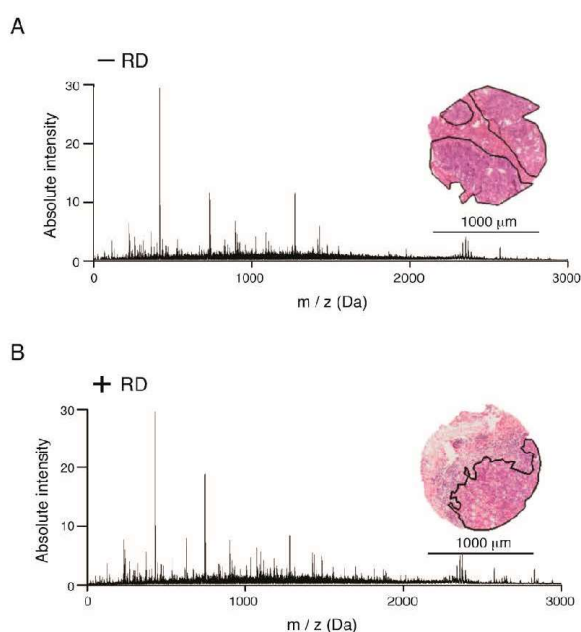


Figure 1. Average spectra of representative MALDI-imaging proteomic profiles of primary tumor sections from either (A) patients without or (B) with recurrent disease. For each group, examples of H&E images with indicated malignant areas measured are included. In total, 506 m/z values in a mass range between m/z 600 and 3000 (signal/noise > 1) were extracted by peak picking from high-grade serous ovarian cancer (HGSOE) at early-stage human tissue. Analyses were performed with 20 biologically independent spots ($N = 10$ each patient group).

Reassessment of the two patients in that subclass group by an experienced gynecological pathologist showed that the previous immunohistological expression pattern in one of the patient biopsies was not conclusive. As in high-grade serous ovarian carcinoma, p53 showed a mutated pattern, but unlike typical high-grade serous carcinoma, CD56 and synaptophysin expressions were evenly and strongly present. Moreover, the morphological picture indicates most likely an undifferentiated non-small cell neuroendocrine carcinoma (NSCNEC) of the ovary. The second patient was re-classified as pT2cG3 and hence not a HGSOc patient diagnosed at early stage. Therefore, samples of these two outlier patients were not considered for further analysis.

Since considerable differences in stroma content occur within the sample cohort, malignant compartments were evaluated in each core of early-stage HGSOc patients ($N = 8$). Mass spectra of malignant areas from both annotated groups ($N = 4$, each group) were obtained and a statistical comparison was performed using the SCIls Lab software. In total, 612 m/z values from a mass range between m/z 800 and 3.500 (threshold 31.42) were identified by peak-picking and used to compare the tissue sections. Average exemplary spectra are shown for primary tumors of early-stage HGSOc patients with RD and non-RD in Figure 1. In total, MALDI-IMS analysis resulted in 7537 spectra from the entire patient cohort.

2.2. Discovery of Discriminative Peptide Signatures

In order to determine specific molecular signatures in HGSOc patients with RD and non-RD, a pLSA based on the peptide signatures was performed and allowed the direct interpretation of score images and loadings. Here, this unsupervised data analysis of the peptide signature enabled the discrimination of both distinct patient groups (Figure 2).

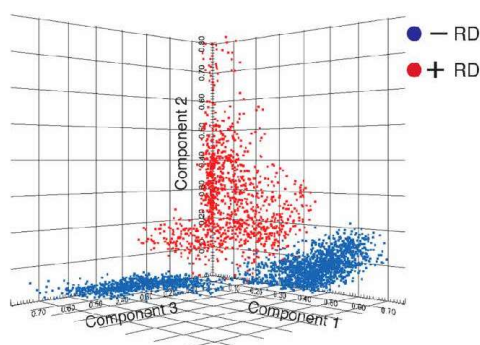


Figure 2. Discrimination of molecular signatures for the groups of HGSOc patients via probabilistic latent semantic analysis (pLSA). Score plots of the first three components from imaging mass spectrometry (IMS) spectra of primary tumors from patients without (–RD, in blue) and with recurrent disease (+RD, in red) are shown.

2.3. Determination of Characteristic m/z Values of HGSOc Patients

The malignant compartments of the tumors were assigned and spectra were compared in a pairwise manner to obtain discriminative peptide values (m/z) using receiver operating characteristic (ROC) analysis. The ROC analysis resulted in 151 peptide values that were able to discriminate between patients with RD and non-RD ($AUC > 0.6$ or < 0.4 ; $p < 0.01$; Table S1). A selection is shown in Figure 3.

For example, the peptide values 840.6 ± 0.2 Da, 1138.5 ± 0.2 Da and 1631.8 ± 0.2 Da denote high spatial intensity distribution in patients with recurrence of tumors, which can be visualized as a heatmap distribution across the tissue section (Figure 3). The peptide value 1631.8 ± 0.2 was associated

with non-RD. The distribution of the most significantly expressed peptides within the groups is shown in Figure 4.

2.4. Identification of Differentially Expressed Proteins

To improve the understanding of the disease progress and provide a method for personalized pathology assessment of early-stage HGSOE, specific localized peptide values were investigated and subsequently identified. Identification of these peptide markers provides important insights into the disease mechanism as well as progression. Since a large number of isobaric ions and the presence of so-called chimera spectra adversely affected the identification of m/z values by MS/MS (direct from tissue section), we performed a corresponding “bottom-up” LC-MS/MS approach (Table S2) with adjacent tissue sections, which enabled the identification of the obtained MALDI-IMS m/z values.

Out of the MALDI-IMS-derived discriminative m/z values between RD and non-RD HGSOE, 18 m/z values could be assigned to 13 proteins (Table 1).

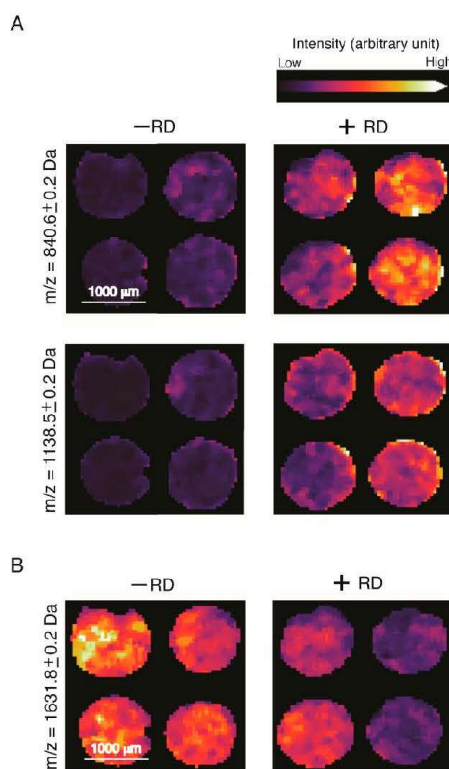


Figure 3. Characteristic peptides for group of patients with recurrence and no recurrence discrimination via individual peak mass spectra intensity and spatial peak distribution. (A) The m/z values 840.6 ± 0.2 and 1138.5 ± 0.2 Da show significantly higher spatial intensities (area under the curve (AUC) > 0.6 ; $p < 0.001$) in patients with recurrent disease (+RD) compared with without recurrence (-RD). (B) In contrast, the 1631.8 ± 0.2 Da peptide, as an example, exhibited significantly higher intensities (AUC < 0.4 ; $p < 0.001$) in patients with no recurrence.

Table 1. Receiver operating characteristic (ROC) curve analysis reveals a prognostic protein signature for early-stage HGSOc. Significantly differentially expressed proteins in primary tumors of patients with recurrent compared with no-recurrent disease are listed (overexpressed, AUC values > 0.6, and underrepresented < 0.4, $p < 0.0001$).

Centroid [m/z]	IMS Mr [m/z] [Da]	Tumor +RD vs -RD (AUC)	LC-MS Mr [Da]	Δ [Da]	Ascension	Protein	HGNC Symbol
2705.026	2704.0181	0.7547	2704.1538	0.1358	K1C9_HUMAN	Keratin, type I cytoskeletal 9	KRT9
1791.698	1790.6901	0.6250	1790.7204	0.0304	K1C9_HUMAN	Keratin, type I cytoskeletal 9	KRT9
644.336	643.3281	0.7470	643.3653	0.0373	ACTB_HUMAN	Actin, cytoplasmic 1	ACTB
840.564	839.5561	0.7407	839.4613	0.0947	COL1A2_HUMAN	Collagen alpha-2(I) chain	COL1A2
868.467	867.4591	0.7331	867.4563	0.0028	COL1A2_HUMAN	Collagen alpha-2(I) chain	COL1A2
2027.831	2026.8231	0.7008	2026.0093	0.8138	COL1A2_HUMAN	Collagen alpha-2(I) chain	COL1A2
1562.765	1561.7571	0.6930	1561.7849	0.0278	COL1A2_HUMAN	Collagen alpha-2(I) chain	COL1A2
1223.417	1222.4091	0.6262	1222.6054	0.1964	COL1A2_HUMAN	Collagen alpha-2(I) chain	COL1A2
700.444	699.4361	0.6388	699.4643	0.0282	RL37A_HUMAN	60S ribosomal protein L37a	RPL37A
1790.797	1789.7891	0.6253	1789.8846	0.0956	ACTB_HUMAN	Actin, cytoplasmic 1	ACTB
1743.691	1742.6831	0.6055	1742.8120	0.1290	H2B1N_HUMAN	Histone H2B type 1-N	HIST1H2BN
1550.764	1549.7561	0.6016	1549.8100	0.0540	ANXA1_HUMAN	Annexin A1	ANXA1
858.566	857.5581	0.3975	857.4607	0.0974	CALD1_HUMAN	Caldesmon	CALD1
1157.708	1156.7001	0.3782	1156.6200	0.0800	APOA1_HUMAN	Apolipoprotein A-I	APOA1
1631.775	1630.7671	0.3682	1630.8236	0.0566	TBB5_HUMAN	Tubulin beta chain	TUBB
1751.792	1750.7841	0.3554	1750.0353	0.7488	H2B1K_HUMAN	Histone H2B type 1-K	HIST1H2BK
1055.394	1054.3861	0.3460	1054.5196	0.1335	4_HUMAN	Histone H4	HIST1H4A
1752.992	1751.9841	0.3159	1751.8551	0.1290	LMNA_HUMAN	Prelamin-A/C	LMNA

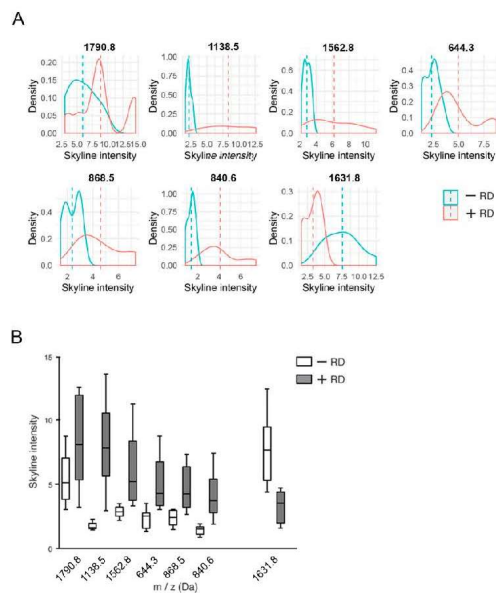


Figure 4. Examples of peptide distribution within groups of patients with (+RD) and without recurrent disease (−RD) by mass spectrometry intensity. (A) Density plot of skyline intensities over a continuous interval. Dashed lines indicate the distributions’ mean values. (B) Boxplot.

More than one m/z value with similar discrimination characteristics was identified from Keratin type 1 and Collagen alpha-2(I) and was assigned to the observed m/z values from the MALDI-IMS experiment, hence correctly recognized (Table 1).

2.5. Relatedness between Patients with RD and between Patients without RD

The analysis was expanded and the peptide signature (discriminative m/z values) was applied to three additional early-stage patients with high-grade endometrioid ovarian cancer (HGEC), two of them with RD; one non-RD, and showed comparable peptide intensities in samples of HGSOC patients. A principal component analysis (PCA) was performed overlaying covariate influences onto the principal component space (Figure 5).

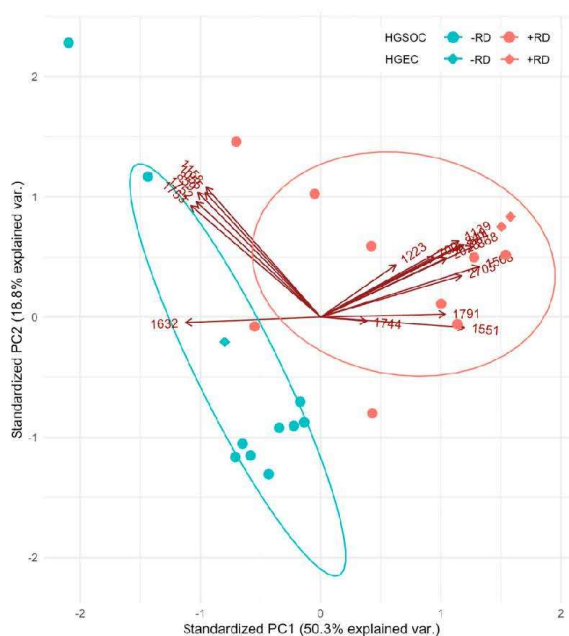


Figure 5. A biplot showing included samples of early-stage HGSOC patients as points. Additionally, three patients with high-grade endometrioid ovarian cancer (HGEC) were included in the analysis and marked with diamonds. Biplot axes indicate the influence of each peptide in the principal component space. The principal component analysis (PCA) shows a discrimination of patients with (+RD) and without recurrent disease (−RD).

PCA confirmed the closer relatedness between patients with RD and between patients without RD. Inclusion of three early-stage HGEC patients showed similar relatedness. The variable markers cluster in two groups indicating correlated variables. The higher correlated group A comprises 1157.7 ± 0.2 , 858.6 ± 0.2 , 1751.8 ± 0.2 , 1753.0 ± 0.2 and 1055.4 ± 0.2 Da. The less correlated group B comprises the remaining peptides with 1631.8 ± 0.2 Da being negatively correlated (Figure 4A,B). The high proportion of variability explained by the two-dimensional principal subspace provides solid grounds for these correlations.

3. Discussion

In general, HGSOc patients diagnosed at early-stage have an excellent prognosis and concern arises that some of the early-stage HGSOcs are over-treated. Hence, there has been a debate about the optimal duration and chemotherapy treatment strategy, e.g., Carboplatin only, or combination regimens, four cycles vs. six cycles. However, a subgroup of patients will relapse and need therapies that are more intensive at time of diagnosis. It is therefore of great importance to identify these high-risk patients in order to improve their clinical outcome.

Currently, there are no reliable markers at hand for standard immunohistochemical assessment of this subpopulation. Here, we have used a novel approach using MALDI-IMS technology to screen for a prognostic peptide signature to support the clinical management of these patients. For this purpose, standardized protocols for MALDI-IMS sample preparation have been developed [25,26], which are intended to enable reliable exploration of molecular signatures as biomarkers and has been shown to provide valuable diagnostic and risk assessment capabilities for other diagnostically challenging neoplasms [27]. Our recently published data, showed that IMS can reliably detect the histological subtypes of ovarian cancer [20]. In this presented study, proteomic analysis results 151 discriminative m/z values between early-stage HGSOc patients with either RD or non-RD. In order to identify MALDI-IMS-derived m/z values, the “bottom-up”-nano liquid chromatography (nLC)-MS/MS approach was performed on adjacent tissue sections. According to the IMS guidelines [28], the mass difference between MALDI-IMS and LC-MS/MS m/z values should be less than 0.9 Da and requires the identification of more than one peptide.

Specific peptides linked to Keratin type1, Actin, cytoplasmic 1 and Collagen alpha-2(I) were observed to have the strongest expression levels in primary tumors from early-stage HGSOc patients with RD and indicated greatest prognostic values (AUC > 0.7). A published reference database of MALDI-IMS-derived peptide and protein values in various and in particular for ovarian cancer FFPE tissue [29] was intended as support for the verification of protein identifications. The observed m/z values 1562.8 ± 0.2 from Collagen alpha-2(I) and 1790.9 ± 0.2 Da from Actin, cytoplasmic 1 were also determined and identified in MALDI-IMS studies of biopsies from lung tumor patients [30]. Through regulation of various signaling pathways in cancer cells, Keratins, the epithelial-predominant members of the intermediate filament superfamily, are involved in a number of processes in tumor progression [31]. KRT9 is one of the most common contaminants in proteomic mass spectrometry analyses, both in ESI and MALDI mass spectrometry methods (see also reference [32]). These contaminations may rarely have their source in the sample material (randomly distributed), but are more often introduced during sample preparation (e.g., contamination from the environment like dust in solvents, buffers or matrix) [32]. However, the difference with MALDI imaging experiments is that the m/z values can be represented spatially in the tissue, such that contaminations would be evenly distributed over the whole sample material. Therefore, the tissue microarrays (TMAs) are randomized and a control area outside the tissue is measured as a control to exclude such contamination. No peptides (Isotopic pattern) and salt adducts were detected in the control area. Only singles from alpha -Cyano-4-hydroxycinnamic acid matrix clusters could be found with no influence on the data evaluation.

Moreover, both patient groups' cores were included and randomly distributed on the same cover slip. Therefore, it is unlikely to detect any significant differences. Furthermore, MALDI imaging experiments predominantly address structural proteins, such as ECM molecules, since methodically an enzymatic surface digestion of the tissue sections is performed. Excluding cytoskeleton proteins from the analysis would be premature, especially since KRT9 is a cellular component of the cytoskeleton, cytosol, extracellular region or membrane (see <https://www.uniprot.org/uniprot/P35527---subcellular> location). Furthermore, a query of the kmplot.com (<https://kmplot.com/analysis/>) database showed a significant decrease in overall survival ($p < 0.0052$) associated with high expression of KRT9 considering only stage I EOC including HGSOc ($p < 0.0028$) patients (Figure S2). Therefore, our KRT9 MALDI-IMS measurement is unlikely a result of contamination.

The major sources of collagen expression are stromal cells with increased collagen production and disposition in the stromal compartment has been shown to be associated with breast cancer development and progression [33,34]. Nevertheless, it was also demonstrated that expression of collagen by ovarian cancer cells, including Collagen alpha-2(I), could increase drug resistance by inhibiting the penetration of the drug into the cancer tissue as well as increase resistance to apoptosis [35].

The analysis of three additional early-stage HGEC patients (two with RD; one without RD) showed comparable measured peptide intensities to the HGSOC patients. A multivariate regression was not feasible due to an insufficient number of observations [36]. However, reduction in covariates (dimension reduction), such as in a PCA, showed the discriminative capacity of the proposed prognostic marker candidates for patients with early-stage of either HGEC or HGSOC (Figure 5). Peptide markers separated into two distinct groups based on the correlation between them.

Even though the utilized sample size of four patients for each group is not sufficient for clinical validation, the purpose of this proof of concept study is to identify prognostic marker candidates. Consequently, validation of applicability of the proposed prognostic marker candidates, including for endometrioid carcinomas, necessitates subsequent high-sample size follow-up studies.

Moreover, changes in the tumor microenvironment in response to malignant transformation have been neglected in the past and need to be considered as a suitable compartment for biomarker discovery. So far, a major limitation of dissecting the stromal signature has been a lack of suitable methods. IMS is able to provide spatial information of protein signatures in both compartments. Unfortunately, the quality of the adjacent stroma in the majority of cores from the tumor tissue was not suitable for further assessment but should be included and subject of future prognostic biomarker research for early-stage HGSOC patients.

Eventually, a profound understanding of the biology in early-stage HGSOC might result in a redefinition of high-risk early-stage EOC to develop novel therapeutic approaches. However, this will need molecular characterization supported by RNA-Seq and high-resolution proteomics data from micro-dissected malignant and adjacent stroma compartments. Nevertheless, the identification of the subpopulation of patients developing recurrent tumors is an unmet clinical need. Here, we show that MALDI-IMS technology has the potential to make a meaningful impact for risk assessment and, hence, patient outcome.

4. Materials and Methods

4.1. Clinicopathological Parameters of Patient Cohort

All samples were collected at Charité, Department for Gynecology at surgery after patients gave their informed consent. Sample collection was permitted by the local ethics committee of the Charité Medical University Berlin (AVD-No. 2004-000034) and conducted according to the Declaration of Helsinki. All patients were of white caucasian background and received an accurate staging via laparotomy, including lymph node sampling. Diagnosis of the early-stage of the high-grade serous subtype of EOC was confirmed by an experienced gynecological pathologist. Adjuvant chemotherapy regime was applied to all patients based on carboplatin in combination with paclitaxel. Detailed descriptions of clinicopathological parameters of patients are shown in Table 2.

4.2. Procedure of MALDI-Imaging

Tissue microarrays (TMAs) of formalin-fixed paraffin-embedded tissue of patients diagnosed at early-stage HGSOC were designed and prepared at the Institute of Pathology, Charité Medical University Berlin. For MALDI-imaging, a 6 µm section was prepared from a paraffin block on a microtome and transferred onto Indium-Tin-Oxide slides (Bruker Daltonik, Bremen, Germany) through decreasing concentrations of ethanol (modified by Caprioli et al.) [37] and antigen retrieval was performed (modified by Gustafsson et al.) [38]. Trypsin and matrix solutions (α -Cyano-4-hydroxycinnamic acid) were deposited by an automated spraying device (HTX Sprayer).

An amount of 550 μ L trypsin solution (20 μ g, 20mM ammonium bicarbonate) was applied onto the section. After tissue incubation (2 h at 50 °C; moist chamber), matrix solution (1 mL 7g/L α -cyano-4-hydroxycinnamic acid in 50% acetonitrile and 1% trifluoroacetic acid) was applied using a HTX Sprayer (75 °C, estimate cycle 1.80).

Table 2. Clinicopathological characteristics of patients. All patients received adjuvant chemotherapy for numbers of cycles as indicated in the table. Follow-ups of patients were performed for at least 5 years, if no relapse occurred, or till development of recurrent disease (RD).

Patients (–RD)				
Age	68	60	68	67
FIGO stage	IA	IC	IA	IC
Grade	G3	G2	G3	G3
Presence of ascites	<500 mL	<500 mL	<500 mL	no
Number of cycles	6	6	4	6
Recurrence (months)	NA	NA	NA	NA
Patients (+RD)				
Age	44	52	67	57
FIGO stage	IIB	IIA	IA	IIA
Grade	G3	G3	G3	G3
Presence of ascites	>500 mL	no	No	no
Number of cycles	6	9	6	6
Recurrence (months)	13	12	54	16

4.3. MALDI Imaging Analysis

Analyses were performed on 10 biologically independent cores of biopsies for each patient group. MALDI-IMS data acquisition was executed in reflector mode, detection range of m/z 800–3200, 500 laser shots per spot, sampling rate of 1.25 GS/s and raster width of 50 μ m on Rapiflex MALDI-TOF/ using flexControl 3.0 and flexImaging 3.0 (Bruker Daltonik). External calibration was performed using a peptide calibration standard (Bruker Daltonik) and spectra processed in flexAnalysis 3.0 (Bruker Daltonik). In order to exclude potential contamination like sodium adducts or peptides, control areas outside the tissue were also analyzed. After MALDI-imaging experiments, the matrix was removed with 70% ethanol and the tissue sections were stained with hematoxylin and eosin (H&E) as histological overview staining [37].

4.4. Data Processing

Statistical data analysis was performed using the SCiLS Lab software (Version2015b, SCiLS GmbH, Bremen, Germany). MALDI-IMS raw data were imported into the SCiLS Lab software and converted to the SCiLS Lab file format. Simultaneous preprocessing of all data sets was carried out to ensure better comparability between the sample sets. Imported data were pre-processed by convolution baseline removal (width: 20) and total ion count (TIC) normalization. Segmentation pipelines as published previously were performed for peak-finding and alignment [19,39,40]. Peaks were selected using the orthogonal matching pursuit (OMP) algorithm [41] and top down segmentations were performed by bisecting k-means clustering, ± 0.156 Da interval width, mean interval processing and medium smoothing strength [39–41]. For convolutional neural networks evaluation, raw data from region spots and m/z values were exported from SCiLS Lab SW as csv format. Two approaches based on different principles were performed: first, an unsupervised approach, probabilistic latent semantic analysis (pLSA), to discriminate both groups, and another supervised approach, receiver operating characteristic

(ROC) analysis, to detect characteristic peptide values. To define common molecular features among the sample sets, unsupervised multivariate classification methods for mass spectra were applied: probabilistic latent semantic analysis (pLSA) was performed as previously described [42,43]. pLSA was performed with five components and the following settings: (i) interval width of ± 0.156 Da, and (ii) individual spectra and deterministic initialization. Receiver operating characteristic analysis (ROC) was used to assess the quality of all m/z values within specific ROIs to discriminate between recurrent and non-recurrent HGSOC tumor tissue. For this method, the number of spectra in the ROIs of both groups should be approximately the same. If that was not the case, 1500 randomly selected spectra per ROI/group were used. To determine statistical significance, discriminating m/z values (peaks) with an AUC < 0.35 or > 0.65 were subsequently analyzed using the Wilcoxon rank sum test. m/z values with delta peak intensities of > 0.7 and < 0.3 ($p < 0.001$) were assumed as potential markers. Figures were created using the SCiLS Lab software (Bruker, Bremen, Germany) and R packages “ggplot2” and “ggbiplot”.

4.5. Identification of Peptides by “Bottom-Up”-Nhlpc Mass Spectrometry

To identify m/z values, complementary protein identification was performed on adjacent tissue sections by a “bottom-up”-nano liquid chromatography (nLC)-MS/MS approach as published previously [19]. Briefly, tissue digestion (20 μ g trypsin, 20 mM ammonium bicarbonate/acetonitrile 9:1) was performed via ImagePrep (Bruker Daltonik). Peptides for nUPLC-MS/MS analysis were extracted directly from adjacent tissue sections into 40 μ L of 0.1% trifluoroacetic acid (TFA; 15 min incubation at room temperature). Peptides were separated (60% acetonitrile/ in 0.1% formic acid) using an analytical UPLC System (Thermo Dionex Ultimate 3000, Acclaim PepMap RSLC C18 column 75 μ m x 15 cm; flow rate 200 nL/min, 70 min) and analyzed via Impact II (QTOF-MS, Bruker Daltonik). All raw spectra from the MS/MS measurement were converted to mascot generic files (.mgf) using the ProteinScape software [44]. Mass spectra were analyzed using the Mascot search engine (version 2.4, MatrixScience; UK) searching the UniPort database. The search was performed with the following set of parameters: (i) taxonomy: human; (ii) proteolytic enzyme: trypsin; (iii) peptide tolerance: 10ppm; (iv) maximum of accepted missed cleavages: 1; (v) peptide charge: 2+, 3+, 4+; (vi) variable modification: oxidation (M); (vii) MS/MS tolerance: 0.8Da; and (viii) MOWSE score > 25 . Identification of MALDI-IMS m/z values by using an LC-MS/MS reference list requires the accordance of more than one peptide (mass differences < 0.9 Da) to subsequently correctly assign the corresponding protein [45]. Peptides with lowest mass difference to the LC-MS/MS reference list value were assumed as a match.

5. Conclusions

Epithelial ovarian cancer (EOC) has the highest mortality rate of the gynecological malignancies worldwide, with HGSOC representing the most common and aggressive histological subtype. Even though HGSOC patients diagnosed at early-stage have an excellent prognosis, a subgroup of patients will relapse and need therapies that are more intensive at time of diagnosis. It is therefore of great importance to identify these high-risk patients in order to improve their clinical outcome. In this proof of concept study, we have applied a novel approach using MALDI-IMS technology to identify a candidate prognostic peptide signature to support the clinical management of these patients. However, there is still a need for a robust validation of our candidate signature based on a higher-size patient cohort that should be addressed in the future. This includes implementing the identified and validated prognostic peptide signature as part of prospective studies in the clinical routine.

Supplementary Materials: The following are available online at <http://www.mdpi.com/2072-6694/12/8/2000/s1>, Figure S1: Discrimination of molecular signatures for groups of HGSOC patients via probabilistic latent semantic analysis (pLSA), Figure S2: Kaplan–Meier curves displaying the estimated overall survival probability of EOC patients with regard KRT9 expression, Table S1: m/z values from IMS and the corresponding identification and AUC values, Table S2: LC-MS reference list of ovarian cancer tissue.

Author Contributions: H.K. and E.I.B. designed research; Z.W., O.K. and S.A. performed the experiments; O.K. design M.S. analyses and perform data evaluation; Z.W. and W.K. analyzed data; E.T.T. and P.J. helped us setting up some crucial experiments; D.H., A.d.B. and F.H. provided patient samples, patient information and intellectual input. S.D.-E. and J.S. provided intellectual input and advice on experiments. F.R. helped with manuscript editing and generation of figures. O.K., W.K. and H.K. wrote the paper. All authors have read and agreed to the published version of the manuscript.

Funding: This research received no external funding.

Acknowledgments: We would like to thank our patients for participation in this study. Moreover, we express our sincerest gratitude to Robin Soper for proofreading the manuscript. For the useful discussion, we also would like to especially thank Grit Nebrich.

Conflicts of Interest: The authors declare no conflict of interest.

References

- Vaughan, S.; Coward, J.I.; Bast, R.C., Jr.; Berchuck, A.; Berek, J.S.; Brenton, J.D.; Coukos, G.; Crum, C.C.; Drapkin, R.; Etemadmoghadam, D.; et al. Rethinking ovarian cancer: Recommendations for improving outcomes. *Nat. Rev. Cancer* **2011**, *11*, 719–725. [[CrossRef](#)] [[PubMed](#)]
- Siegel, R.L.; Miller, K.D.; Jemal, A. Cancer statistics, 2016. *CA A cancer J. Clin.* **2016**, *66*, 7–30. [[CrossRef](#)] [[PubMed](#)]
- Prat, J.; FIGO Committee on Gynecologic Oncology. Staging classification for cancer of the ovary, fallopian tube, and peritoneum. *Int. J. Gynaecol. Obstet.* **2014**, *124*, 1–5. [[CrossRef](#)] [[PubMed](#)]
- Ahmed, F.Y.; Wiltshaw, E.; A'Hern, R.P.; Nicol, B.; Shepherd, J.; Blake, P.; Fisher, C.; Gore, M.E. Natural history and prognosis of untreated stage I epithelial ovarian carcinoma. *J. Clin. Oncol.* **1996**, *14*, 2968–2975. [[CrossRef](#)] [[PubMed](#)]
- Duggan, M.A.; Anderson, W.F.; Altekruse, S.; Penberthy, L.; Sherman, M.E. The Surveillance, Epidemiology, and End Results (SEER) Program and Pathology: Toward Strengthening the Critical Relationship. *Am. J. Surg. Pathol.* **2016**, *40*, e94–e102. [[CrossRef](#)]
- Hoskins, P.J.; Swenerton, K.D.; Manji, M.; Wong, F.; O'Reilly, S.E.; McMurtrie, E.J.; Le, N.; Acker, B.; Le Richer, J. 'Moderate-risk' ovarian cancer (stage I, grade 2; stage II, grade 1 or 2) treated with cisplatin chemotherapy (single agent or combination) and pelvi-abdominal irradiation. *Int. J. Gynecol. Cancer* **1994**, *4*, 272–278. [[CrossRef](#)]
- Chan, J.K.; Tian, C.; Monk, B.J.; Herzog, T.; Kapp, D.S.; Bell, J.; Young, R.C.; Gynecologic Oncology, G. Prognostic factors for high-risk early-stage epithelial ovarian cancer: A Gynecologic Oncology Group study. *Cancer* **2008**, *112*, 2202–2210. [[CrossRef](#)]
- Colombo, N.; Peiretti, M.; Parma, G.; Lapresa, M.; Mancari, R.; Carinelli, S.; Sessa, C.; Castiglione, M.; Group, E.G.W. Newly diagnosed and relapsed epithelial ovarian carcinoma: ESMO Clinical Practice Guidelines for diagnosis, treatment and follow-up. *Ann. Oncol.* **2010**, *21*, v23–v30. [[CrossRef](#)]
- Morice, P.; Denschlag, D.; Rodolakis, A.; Reed, N.; Schneider, A.; Kesic, V.; Colombo, N.; Fertility Task Force of the European Society of Gynecologic Oncology. Recommendations of the Fertility Task Force of the European Society of Gynecologic Oncology about the conservative management of ovarian malignant tumors. *Int. J. Gynecol. Cancer* **2011**, *21*, 951–963. [[CrossRef](#)]
- Fruscio, R.; Corso, S.; Ceppi, L.; Garavaglia, D.; Garbi, A.; Floriani, I.; Franchi, D.; Cantu, M.G.; Bonazzi, C.M.; Milani, R.; et al. Conservative management of early-stage epithelial ovarian cancer: Results of a large retrospective series. *Ann. Oncol.* **2013**, *24*, 138–144. [[CrossRef](#)]
- Lee, C.L.; Kusunoki, S.; Huang, C.Y.; Wu, K.Y.; Lee, P.S.; Huang, K.G. Surgical and survival outcomes of laparoscopic staging surgery for patients with stage I ovarian cancer. *Taiwan J. Obstet. Gynecol.* **2018**, *57*, 7–12. [[CrossRef](#)]
- Wei, W.; Li, N.; Sun, Y.; Li, B.; Xu, L.; Wu, L. Clinical outcome and prognostic factors of patients with early-stage epithelial ovarian cancer. *Oncotarget* **2017**, *8*, 23862–23870. [[CrossRef](#)] [[PubMed](#)]
- Leblanc, E.; Querleu, D.; Narducci, F.; Chauvet, M.P.; Chevalier, A.; Lesoin, A.; Vennin, P.; Taieb, S. Surgical staging of early invasive epithelial ovarian tumors. *Semin. Surg. Oncol.* **2000**, *19*, 36–41. [[CrossRef](#)]

14. Bolis, G.; Colombo, N.; Pecorelli, S.; Torri, V.; Marsoni, S.; Bonazzi, C.; Chiari, S.; Favalli, G.; Mangili, G.; Presti, M.; et al. Adjuvant treatment for early epithelial ovarian cancer: Results of two randomised clinical trials comparing cisplatin to no further treatment or chronic phosphate (32P). G.I.C.O.G.: Gruppo Interregionale Collaborativo in Ginecologia Oncologica. *Ann. Oncol.* **1995**, *6*, 887–893. [[CrossRef](#)] [[PubMed](#)]
15. Vergote, I.B.; Vergote-De Vos, L.N.; Abeler, V.M.; Aas, M.; Lindegaard, M.W.; Kjorstad, K.E.; Trope, C.G. Randomized trial comparing cisplatin with radioactive phosphorus or whole-abdomen irradiation as adjuvant treatment of ovarian cancer. *Cancer* **1992**, *69*, 741–749. [[CrossRef](#)]
16. Chen, C.A.; Chiang, C.J.; Chen, Y.Y.; You, S.L.; Hsieh, S.F.; Tang, C.H.; Cheng, W.F. Survival benefit of patients with early-stage ovarian carcinoma treated with paclitaxel chemotherapeutic regimens. *J. Gynecol. Oncol.* **2018**, *29*, e16. [[CrossRef](#)]
17. Meding, S.; Nitsche, U.; Balluff, B.; Elsner, M.; Rauser, S.; Schone, C.; Nipp, M.; Maak, M.; Feith, M.; Ebert, M.P.; et al. Tumor classification of six common cancer types based on proteomic profiling by MALDI imaging. *J. Proteome Res.* **2012**, *11*, 1996–2003. [[CrossRef](#)]
18. Walch, A.; Rauser, S.; Deininger, S.O.; Hofler, H. MALDI imaging mass spectrometry for direct tissue analysis: A new frontier for molecular histology. *Histochem. Cell Biol.* **2008**, *130*, 421–434. [[CrossRef](#)]
19. Klein, O.; Strohschein, K.; Nebrich, G.; Oetjen, J.; Trede, D.; Thiele, H.; Alexandrov, T.; Giavalisco, P.; Duda, G.N.; von Roth, P.; et al. MALDI imaging mass spectrometry: Discrimination of pathophysiological regions in traumatized skeletal muscle by characteristic peptide signatures. *Proteomics* **2014**, *14*, 2249–2260. [[CrossRef](#)]
20. Klein, O.; Kanter, F.; Kulbe, H.; Jank, P.; Denkert, C.; Nebrich, G.; Schmitt, W.D.; Wu, Z.; Kunze, C.A.; Sehoul, J.; et al. MALDI-Imaging for Classification of Epithelial Ovarian Cancer Histotypes from a Tissue Microarray Using Machine Learning Methods. *Proteomics Clin. Appl.* **2019**, *13*, e1700181. [[CrossRef](#)]
21. Longuespee, R.; Boyon, C.; Castellier, C.; Jacquet, A.; Desmons, A.; Kerdraon, O.; Vinatier, D.; Fournier, I.; Day, R.; Salzet, M. The C-terminal fragment of the immunoproteasome PA28S (Reg alpha) as an early diagnosis and tumor-relapse biomarker: Evidence from mass spectrometry profiling. *Histochem. Cell Biol.* **2012**, *138*, 141–154. [[CrossRef](#)] [[PubMed](#)]
22. Mainini, V.; Angel, P.M.; Magni, F.; Caprioli, R.M. Detergent enhancement of on-tissue protein analysis by matrix-assisted laser desorption/ionization imaging mass spectrometry. *Rapid Commun. Mass Spectrom* **2011**, *25*, 199–204. [[CrossRef](#)] [[PubMed](#)]
23. Gustafsson, J.O.; Oehler, M.K.; McColl, S.R.; Hoffmann, P. Citric acid antigen retrieval (CAAR) for tryptic peptide imaging directly on archived formalin-fixed paraffin-embedded tissue. *J. Proteome Res.* **2010**, *9*, 4315–4328. [[CrossRef](#)] [[PubMed](#)]
24. Aichler, M.; Walch, A. MALDI Imaging mass spectrometry: Current frontiers and perspectives in pathology research and practice. *Lab. Invest.* **2015**, *95*, 422–431. [[CrossRef](#)] [[PubMed](#)]
25. Ly, A.; Longuespee, R.; Casadonte, R.; Wandernoth, P.; Schwamborn, K.; Bollwein, C.; Marsching, C.; Kriegsmann, K.; Hopf, C.; Weichert, W.; et al. Site-to-Site Reproducibility and Spatial Resolution in MALDI-MSI of Peptides from Formalin-Fixed Paraffin-Embedded Samples. *Proteomics Clin. Appl.* **2019**, *13*, e1800029. [[CrossRef](#)]
26. Hermann, J.; Noels, H.; Theelen, W.; Lellig, M.; Orth-Alampour, S.; Boor, P.; Jankowski, V.; Jankowski, J. Sample preparation of formalin-fixed paraffin-embedded tissue sections for MALDI-mass spectrometry imaging. *Anal. Bioanal. Chem.* **2020**, *412*, 1263–1275. [[CrossRef](#)]
27. Lazova, R.; Seeley, E.H.; Kutzner, H.; Scolyer, R.A.; Scott, G.; Cerroni, L.; Fried, I.; Kozovska, M.E.; Rosenberg, A.S.; Prieto, V.G.; et al. Imaging mass spectrometry assists in the classification of diagnostically challenging atypical Spitzoid neoplasms. *J. Am. Acad. Dermatol.* **2016**, *75*, 1176–1186. [[CrossRef](#)]
28. McDonnell, L.A.; Rompp, A.; Balluff, B.; Heeren, R.M.; Albar, J.P.; Andren, P.E.; Corthals, G.L.; Walch, A.; Stoeckli, M. Discussion point: Reporting guidelines for mass spectrometry imaging. *Anal. Bioanal. Chem.* **2015**, *407*, 2035–2045. [[CrossRef](#)]
29. Meding, S.; Martin, K.; Gustafsson, O.J.; Eddes, J.S.; Hack, S.; Oehler, M.K.; Hoffmann, P. Tryptic peptide reference data sets for MALDI imaging mass spectrometry on formalin-fixed ovarian cancer tissues. *J. Proteome Res.* **2013**, *12*, 308–315. [[CrossRef](#)]
30. Groseclose, M.R.; Massion, P.P.; Chaurand, P.; Caprioli, R.M. High-throughput proteomic analysis of formalin-fixed paraffin-embedded tissue microarrays using MALDI imaging mass spectrometry. *Proteomics* **2008**, *8*, 3715–3724. [[CrossRef](#)]

31. Dmello, C.; Srivastava, S.S.; Tiwari, R.; Chaudhari, P.R.; Sawant, S.; Vaidya, M.M. Multifaceted role of keratins in epithelial cell differentiation and transformation. *J. Biosci.* **2019**, *44*, 33. [[CrossRef](#)] [[PubMed](#)]
32. Keller, B.O.; Sui, J.; Young, A.B.; Whittall, R.M. Interferences and contaminants encountered in modern mass spectrometry. *Anal. Chim. Acta* **2008**, *627*, 71–81. [[CrossRef](#)] [[PubMed](#)]
33. Kang, S.; Maeng, H.; Kim, B.G.; Qing, G.M.; Choi, Y.P.; Kim, H.Y.; Kim, P.S.; Kim, Y.; Kim, Y.H.; Choi, Y.D.; et al. In situ identification and localization of IGHA2 in the breast tumor microenvironment by mass spectrometry. *J. Proteome Res.* **2012**, *11*, 4567–4574. [[CrossRef](#)] [[PubMed](#)]
34. Angel, P.M.; Schwamborn, K.; Comte-Walters, S.; Clift, C.L.; Ball, L.E.; Mehta, A.S.; Drake, R.R. Extracellular Matrix Imaging of Breast Tissue Pathologies by MALDI-Imaging Mass Spectrometry. *Proteomics Clin. Appl.* **2019**, *13*, e1700152. [[CrossRef](#)]
35. Januchowski, R.; Swierczewska, M.; Sterzynska, K.; Wojtowicz, K.; Nowicki, M.; Zabel, M. Increased Expression of Several Collagen Genes is Associated with Drug Resistance in Ovarian Cancer Cell Lines. *J. Cancer* **2016**, *7*, 1295–1310. [[CrossRef](#)] [[PubMed](#)]
36. Harrel, F.E. *Regression Modeling Strategies*; Springer: New York, NY, USA, 2001.
37. Casadonte, R.; Caprioli, R.M. Proteomic analysis of formalin-fixed paraffin-embedded tissue by MALDI imaging mass spectrometry. *Nat. Protoc.* **2011**, *6*, 1695–1709. [[CrossRef](#)]
38. Gustafsson, O.J.; Briggs, M.T.; Condina, M.R.; Winderbaum, L.J.; Pelzing, M.; McColl, S.R.; Everest-Dass, A.V.; Packer, N.H.; Hoffmann, P. MALDI imaging mass spectrometry of N-linked glycans on formalin-fixed paraffin-embedded murine kidney. *Anal. Bioanal. Chem.* **2015**, *407*, 2127–2139. [[CrossRef](#)]
39. Alexandrov, T.; Becker, M.; Guntinas-Lichius, O.; Ernst, G.; von Eggeling, F. MALDI-imaging segmentation is a powerful tool for spatial functional proteomic analysis of human larynx carcinoma. *J. Cancer Res. Clin. Oncol.* **2013**, *139*, 85–95. [[CrossRef](#)]
40. Alexandrov, T.; Becker, M.; Deininger, S.O.; Ernst, G.; Wehder, L.; Grasmair, M.; von Eggeling, F.; Thiele, H.; Maass, P. Spatial segmentation of imaging mass spectrometry data with edge-preserving image denoising and clustering. *J. proteome Res.* **2010**, *9*, 6535–6546. [[CrossRef](#)]
41. Trede, D.; Schiffler, S.; Becker, M.; Wirtz, S.; Steinhorst, K.; Strehlow, J.; Aichler, M.; Kobarg, J.H.; Oetjen, J.; Dyatlov, A.; et al. Exploring three-dimensional matrix-assisted laser desorption/ionization imaging mass spectrometry data: Three-dimensional spatial segmentation of mouse kidney. *Anal. Chem.* **2012**, *84*, 6079–6087. [[CrossRef](#)]
42. Hanselmann, M.; Kirchner, M.; Renard, B.Y.; Amstalden, E.R.; Glunde, K.; Heeren, R.M.; Hamprecht, F.A. Concise representation of mass spectrometry images by probabilistic latent semantic analysis. *Anal. Chem.* **2008**, *80*, 9649–9658. [[CrossRef](#)] [[PubMed](#)]
43. Klerk, L.A.; Dankers, P.Y.; Popa, E.R.; Bosman, A.W.; Sanders, M.E.; Reedquist, K.A.; Heeren, R.M. TOF-secondary ion mass spectrometry imaging of polymeric scaffolds with surrounding tissue after in vivo implantation. *Anal. Chem.* **2010**, *82*, 4337–4343. [[CrossRef](#)] [[PubMed](#)]
44. Chambers, M.C.; Maclean, B.; Burke, R.; Amodei, D.; Ruderman, D.L.; Neumann, S.; Gatto, L.; Fischer, B.; Pratt, B.; Egertson, J.; et al. A cross-platform toolkit for mass spectrometry and proteomics. *Nat. Biotechnol.* **2012**, *30*, 918–920. [[CrossRef](#)] [[PubMed](#)]
45. Cillero-Pastor, B.; Heeren, R.M. Matrix-Assisted Laser Desorption Ionization Mass Spectrometry Imaging for Peptide and Protein Analyses: A Critical Review of On-Tissue Digestion. *J. proteome res.* **2013**, *13*, 325–335. [[CrossRef](#)]



© 2020 by the authors. Licensee MDPI, Basel, Switzerland. This article is an open access article distributed under the terms and conditions of the Creative Commons Attribution (CC BY) license (<http://creativecommons.org/licenses/by/4.0/>).

11 Curriculum Vitae

"Mein Lebenslauf wird aus datenschutzrechtlichen Gründen in der elektronischen Version meiner Arbeit nicht veröffentlicht."

12 Complete list of publications

Wu Z, Hundsdoerfer P, Schulte JH, Astrahantseff K, Boral S, Schmelz K, Eggert A, Klein O. Discovery of Spatial Peptide Signatures for Neuroblastoma Risk Assessment by MALDI Mass Spectrometry Imaging. *Cancers (Basel)*. 2021 Jun 25;13(13):3184. doi: 10.3390/cancers13133184.

IF: 6.126, Platz 37/244 Journal Summary List "ONCOLOGY" (2019)

Kulbe H, Klein O, Wu Z, Taube ET, Kassuhn W, Horst D, Darb-Esfahani S, Jank P, Abobaker S, Ringel F, du Bois A, Heitz F, Sehouli J, Braicu EI. Discovery of Prognostic Markers for Early-Stage High-Grade Serous Ovarian Cancer by Maldi-Imaging. *Cancers (Basel)*. 2020 Jul 22;12(8):2000. doi: 10.3390/cancers12082000.

IF: 6.162, Platz 31/229 Journal Summary List "ONCOLOGY" (2018)

Klein O, Kanter F, Kulbe H, Jank P, Denkert C, Nebrich G, Schmitt WD, Wu Z, Kunze CA, Sehouli J, Darb-Esfahani S, Braicu I, Lellmann J, Thiele H, Taube ET. MALDI-Imaging for Classification of Epithelial Ovarian Cancer Histotypes from a Tissue Microarray Using Machine Learning Methods. *Proteomics Clin Appl*. 2019 Jan;13(1):e1700181. doi: 10.1002/prca.201700181.

IF: 1.933, Platz 19/77 Journal Summary List "BIOCHEMICAL RESEARCH METHODS" (2016)

13 Acknowledgments

First and foremost, I would like to express my deepest gratitude to my supervisor **Prof. Dr. Hans-Dieter Volk**, who offered me an excellent scientific platform, patient guidance and encouragement, and supported me during the whole process of my doctoral thesis. Also, I would like to express my deepest heartfelt appreciation to my mentor, **Dr. Oliver Klein**, I have been lucky to have a patient mentor who responded to my questions, opened to discuss new ideas, supported my presentation in each annual meeting of The German Society for Mass Spectrometry. I would also like to take this opportunity to thank the excellent technical assistance and advice of Grit Nebrich, Angelika Krajewski and Sylwia Handzik. Your generosity has been one of the valuable contributions for this thesis. I would like to thank Dr. Elina Taube who taught me basic knowledges about ovarian carcinoma, offered close cooperation and showed me clinical routine as an oncological pathologist. I would like thank Dr. Hagen Kulbe and Wanja Kassuhn for close cooperation and patient help for proof-reading of the manuscript. I would like to express heartfelt appreciation to Prof. Dr. Angelika Eggert and PD Dr. Patrick Hundsdörfer, they organized and realized this pilot study about neuroblastoma. They are always helpful and friendly in answering all questions of this project. I am also grateful to Dr. Karin Schmelz and Dr. Sengül Boral for sample preparation, pathological expertise sharing and close cooperation. I would like to give my special thank to Dr. Kathy Astrahantseff, who gave me a private lesson about scientific writing and provided intellectual input for data presentation and interpretation of results of the manuscript. I would like to thank Fredrick Kanter for statistical help about deep-learning algorithms. I am grateful to all current and past members of the Core Unit Tissue Typing, AG Eggert and AG Volk. Finally, my heartfelt thanks to my supportive wonderful, loving parents Hualing Wu and Meiping Yu, my husband Dominik Wieland, my parents-in-law Ulrich and Gabrielle Wieland and aunt Kiki Odenwald.